Cellular basis underlying the intolerance to haploidy in vertebrates

(脊椎動物における一倍体細胞の性質)

Kan Yaguchi

Laboratory of Cell Machinery Science
Graduate School of Life Science
Hokkaido University

2021. 3.

Content

Introduction

Poor tolerance of vertebrates to somatic haploidy

Vertebrates are typically diplontic organisms, consisting of a couple of genome copies in a cell, and generally inviable with alteration of the DNA content from diploidy in somatic phase of their life cycle (Wutz, 2014). Especially haploidy, single set of genome in a cell, has not been seen in nature of vertebrate somatic cells.

As an unnatural case, it has been reported that haploid vertebrates can be experimentally generated through parthenogenesis with chemical activation of egg or *in vitro* fertilization of eggs with UV-irradiated and DNA-inactivated sperm (Hertwig, 1911; Hertwig, 1913). Since the most difficulty in breeding of commercial species was the long generation time, parthenogenesis was thought as an attractive method to rapidly produce homozygous clones. However, those artificially induced haploid individuals were not suitable for the maintenance because of pleiotropic morphological abnormalities and embryonic death during early development in haploid embryos. The most obvious morphological abnormalities are dwarfism-like shorter body axis and microcephaly-like shrunk size of brain and eye (Ellinger and Murphy, 1980; Hamilton, 1963). These developmental defects have been confirmed also in haploid mammals (Graham, 1970), and further studies have reported novel organogenesis defects, including edema formation and weak heart beating (Menon and Nair, 2018; Purdom, 1969; Uwa, 1965).

Importantly, those pleiotropic developmental defects could be moderated through artificially altering the ploidy of haploid embryos into diploidy at early developmental stage by such as cold bath incubation, by which mitotic process of embryonic cells is perturbed and DNA content is doubled from haploidy (Miller et al., 1994; Streisinger et al., 1981). Additionally, surgical transplantation of diploid tissues or cells into haploid embryos could attenuate the haploid-linked abnormalities in the haploid-diploid chimeric animals (Tanaka et al., 2004; Thorne et al., 1987; Yamaki et al., 1999). Those proceeding findings indicate that haploidy perturbs vertebrate developmental mechanism, and suggest that the certain systems relying

on diploid state. This feature of vertebrates highlights the sharp contrast with insect, yeast and plant, which can normally propagate even in haploid state, arising the possibility that some cellular processes are specifically affected in haploid vertebrates. However, there is no knowledge about the determinant accountable for the difference in the allowable ploidy between vertebrate and non-vertebrate species.

Centrosome loss in mammalian haploidy

I recently found that, in both our systems of parthenogenetic mouse embryos and human somatic cells, >20% of haploid cells lose centrosomes (Yaguchi et al., 2018b), an organelle playing a central role for cell division in vertebrate species but not essential for plants or yeasts (Kilmartin, 2014; Smirnova and Bajer, 1992). Centrosome duplication requires tight regulation in a cell cycle dependent manner to precisely control the centrosome number for faithful mitosis in normal diploid cells during proliferation (Stearns, 2001). However, haploid somatic cells could not complete to duplicate their centrosomes before mitosis, indicative of uncoupling centrosome duplication with cell cycle progression (Yaguchi et al., 2018b). The centrosome loss in haploid cells ultimately resulted in delaying mitotic duration.

It's noteworthy that mutations in genes associated with centrosome duplication cause dwarfism and microcephaly due to cellular proliferation defects through the prolonged mitosis during development of vertebrate species (Bazzi and Anderson, 2014; Insolera et al., 2014; Martin et al., 2014), whose morphological abnormalities is very similar to what has been observed in haploid embryos. Although this raises the possible involvement of centrosome loss in haploid-linked developmental defects, whether haploid vertebrate embryos indeed lose their centrosomes and its effect on subsequent cellular fate during development are completely unknown.

Ploidy-linked changes in cell growth control

In addition to parthenogenetic embryos, non-diploid somatic cells can arise through the large-scale alteration of chromosome number during tumorigenesis (Dewhurst et al., 2014; Olaharski et al., 2006). Alteration of chromosome number from diploidy is a hallmark of broad cancer types (Carter et al., 2012). While tetraploidy, whose chromosomal number is doubled from diploidy by cytokinesis failure, is well characterized to contribute to malignancy (Castillo et al., 2007; Fujiwara et al., 2005), the involvement of haploidy on cancer progression is poorly understood. Near-haploid cells generated during tumorigenesis show drastic genome instability and easily convert into diploid state within few weeks *in vivo* and *vitro* (Kotecki et al., 1999; Oshimura et al., 1977; Safavi and Paulsson, 2017). Once converted into diploid state from haploids, they are nearly indistinguishable from canonical diploid cells by conventional karyotype diagnose, arising the possibility that much more cancer cell types than currently recognized may have passed through near-haploid phase in their history of tumorigenesis.

Therefore, an understanding of ploidy-dependent alteration in gene regulation would provide critical information for both of developing new cancer therapeutic strategies and finding bio-marker of ploidy alteration. Recent transcriptome and proteome analysis between isogenic diploid and tetraploid cells revealed that expression of G1/S cyclin, cyclin D is commonly upregulated in several tetraploid cell lines (Crockford et al., 2017; Potapova et al., 2016; Vigano et al., 2018). Cyclin D mediates entry into the cell cycle through activation of its binding partner cyclin dependent kinase 4/6 (cdk4/6), and was proposed to be required for overriding p53-mediated cell cycle arrest and suppression of proliferation in tetraploid cells (Crockford et al., 2017). Whereas the accumulated evidence suggests that the suppression of proliferation in tetraploid cells is bypassed through the compensation of cell cycle regulation and growth signals, it remains largely unknown how haploidy effects whole gene regulation.

Instability of haploid state

While haploidy is well known as abnormal ploidy in vertebrate species, it has been recognized also as a powerful tool for genetics because of only one allele required for gene editing to induce loss-of-function phenotypes. Though mammalian haploid cell currently became something attempted for forward genetic screening, the maintenance of haploid cells is tricky due to the rapid haploid-diploid conversion from haploid state. Therefore, an understanding of mechanisms underlying the haploid instability is now required for establishing the stable maintenance system for haploidy.

Recent our works have elucidated that some population of haploid cells with unduplicated centrosome resulted in doubling their chromosome number through evoking cell division failure by the centrosome loss (Yaguchi et al., 2018b). Importantly, when the duration of S phase was extended to artificially re-couple the centrosome duplication cycle to cell cycle in haploid cells, haploid state in culture was dramatically stabilized (Yoshizawa et al., 2020). Whereas our proceeding findings proved that the cellular diploidization by centrosome loss is the primary cause of the trigger for haploid-diploid conversion at single cell level, another group has reported that there is also a growth bias between haploid and diploid somatic cells that leads to the dilution of haploid population in culture (Olbrich et al., 2017). Taken together, those evidence suggest that, after cellular diploidization of haploid cells due centrosome loss, the diploidized cells outcompete haploid population. However, it is still unclear what exact cellular processes are the determinant for different in the growth rate between haploidy and diploidy.

An apparent feature of haploid cells is their halved cellular volume to diploids with the halving of total protein content (Yaguchi et al., 2018b). Although this feature possibly alters multiple bioprocesses, such as intracellular metabolism, and potentially have profound influence on the stability of cellular homeostasis in haploid cells, it’s largely unknown what aspects of the intracellular process is altered in haploid cells and how these changes associate with haploid instability.

The aim

This study aimed to elucidate the poorly understood haploid-associated defects and understand its effects on development and cellular processes in vertebrate life cycle. For that purpose, I established and made full use of the direct comparison system between haploidy and diploidy in both of zebrafish embryos and human somatic cells.

Material and Methods

Zebrafish culture

Adult *Danio rerio* were obtained from RIKEN (Saitama, Japan) and home centers near Hokkaido University, and were maintained in a recirculating system at 28.5°C under 14 h light and 11 h dark conditions. For collecting the normally fertilized embryos to test centrosomal antibodies, one female and one male were placed in 2 L mating tanks in the evening before experiments. In the next lighting interval, eggs were collected and cultured with E3 buffer (5 mM NaCl, 0.17 mM KCl, 0.33 mM $CaCl_2$, 0.33 mM $MgSO_4$ and 10^{-5}% Methylene Blue) at 28.5°C until use. In experiments using normally fertilized embryos, the time point of 0 h post fertilization (HPF) is set as 30 min after the light turned on.

In vitro fertilization of zebrafish embryo

Whole testes were harvested into 1 mL cold-Hank's buffer (0.137 M NaCl, 5.4 mM KCl, 0.25 mM Na_2HPO_4, 0.44 mM KH_2PO_4, 1.3 mM $CaCl_2$, 1.0 mM $MgSO_4$ and 4.2 mM $NaHCO_3$). For inactivating DNA of sperm, the sperm solution was irradiated for 1 min with UV light of 254 nm (LUV-6, ASONE) from a distance of 30 cm with gentle pipetting every 30 sec. For generating haploid or diploid embryos, ~200 uL of the irradiated or non-irradiated sperm solution was applied to ~200 eggs extruded from females anesthetized by Ethyl 3-aminobenzoate methanesulfonate (A5040, Sigma-Aldrich) on a dry petri dish, respectively. About 1 min after fertilization, embryos were flooded with E3 buffer and cultured at 28℃ until use.

Immunofluorescence (IF) staining

For IF staining of centrosomal proteins and mitotic spindles, embryos were fixed with 100% methanol at −20°C for 10 min, followed by treatment with 0.5% Triton X-100 over night.

For IF of incorporated BrdU, cells were prefixed with 100% methanol at −20°C for 10 min, postfixed with 3.7% PFA in DPBS for 15 min at 25°C, and treated with 1% Triton X-100 in 4 N HCl for 5 min at 25°C. For Fixed samples were treated with BSA blocking buffer (150 mM NaCl, 10 mM Tris-HCl, pH 7.5, 5% BSA, and 0.1% Tween 20) for 30 min at 25°C, incubated with primary antibodies overnight at 4°C, and incubated with secondary antibodies for 1 h at 37°C or overnight at 4°C. After each treatment, samples were washed two to three times with DPBS or DPBS-G. For staining embryos, 0.1% Triton X-100 was continuously added into the buffer. Stained embryos or cells were mounted with mounting medium (90% [vol/vol] glycerol; 100 mM Tris-HCl, pH 8.0, and 0.5% [wt/vol] N-propyl gallate).

Microscopy

For the observation of centriolar or centrosomal proteins, fixed embryos were observed at 25°C under a C2 microscope (Nikon) equipped with a × 100 1.49 numeric aperture (NA) Apo TIRF 100H objective lens (Nikon), a LU-N4 laser unit (Nikon), and a C2-DU3 spectrum detector unit (Nikon).

Flow cytometry

For flowcytometric analysis of zebrafish embryos, single cell suspension was made by digestion of de-chorionated and de-yolked embryos with ice-cold trypsin (0.25% trypsin [27250-018, Gibco] in 0.14 M NaCl, 5 mM KCl, 5 mM glucose, 7 mM NaHCO3, 0.7 mM EDTA buffer, pH 7.2). Digested embryonic cells were obtained from ~40 embryos for each analysis and collected by centrifugation at 1000 rpm for ~10 min, then treated with 3.7% PFA in PBS for 10 min and 0.5% triton X-100 for 5 min. For analysis of DNA content and mitotic index in zebrafish embryos, fixed cells were collected with centrifugation and stained with Hoechst 33342 (Dojindo; 1:1000) and anti phospho-Histone H3 (S10) conjugate with Alexa Fluor 488 (3465, Cell signaling technology; 1:100) for ~30 min at room temperature, respectively. For analysis of DNA content and proapoptotic population in culture cells, cells

were suspended with 0.05% trypsin solution (Wako) or Accutase solution (C-41310, Promo cell), followed by staining with Hoechst 33342 (Dojindo; 1:100) and Annexin V-FITC (4700-100, MBL; 1:100) for ~15 min at 37°C. The fluorescence intensity was analyzed using a JSAN desktop cell sorter (Bay bioscience).

Cell culture

The HAP1 cell line (Haplogen) was cultured in Iscove's modified Dulbecco's medium (IMDM; Wako) or DMEM (Wako; for cell viability assay) supplemented with 10% FBS and 1× antibiotic-antimycotic (1× AA; Sigma-Aldrich) on culture dishes coated with rat tail type-I collagen (Corning). Haploid HAP1 cells were purified by sorting based on forward scatter (FSC) intensity using a JSAN desktop cell sorter (Bay bioscience). For each sorting, ~10^6 cells were collected. Sorted cells were cultured for a further 6-7 d to reach subconfluence on 15-cm dishes (Nippon Genetics) and then stored in freezing medium (Bambanker; Lymphotec) as 5-6 aliquots in vials (Corning) at −80°C or −196°C. Every cell culture lot was checked for DNA content as described above. Haploid-enriched cells were used within 7 d after recovery from frozen stocks for all experiments to minimize the effects of spontaneous diploidization.

RNA-seq and differentially expressed gene (DEG) analysis

Total RNA was isolated from asynchronous cell culture using NucleoSpin RNA kit (Macherey-Nagel) according to the manufacturer's instruction. Library preparation, sequencing and analysis were performed by Macrogen Inc. (Seoul Korea) as previously described. Briefly, integrity of total RNA was checked using an Agilent 2100 Bioanalyzer. cDNA libraries were constructed using TruSeq RNA Sample Prep Kit v2 (Illumina), and quantified using 2100 Bioanalyzer. One hundred-base paired end sequencing was conducted on the Illumina HiSeq 2000. Overall reads' quality, total bases, total reads, GC (%) and basic statistics were calculated by FastQC program version 0.10.0, and adapter sequences and low

quality reads removed by Trimmomatic program version 0.32. The trimmed reads were mapped to UCSC hg19 human genome with HopHat version 2.0.13. Then, -G option of Cufflinks version 2.2.1 was used to assemble transcripts from aligned reads and calculate expression profiles of assembled transcripts. Expression profiles were expressed as the fragments per kilobase of transcript per million mapped reads (FPKM). To facilitate the statistical analysis with a balanced data distribution, 1 was added to the raw signals (FPKMs) and transformed the data to log 2. After log transformation, in order to reduce systematic bias, quantile normalization was used with preprocessCore' R library. Statistical analysis was performed using fold change per comparison pair. The significant results were selected on conditions of $|fc| \geq 2$.

RNAi

The siRNA sequences used in this study are 5′-CGAUGCCUCUUUGAAUAAA-3' (Anillin), and 5′-CGUACGCGGAAUACUUCGA-3' (Luciferase). siRNA transfection was performed using Lipofectamine RNAiMAX (Thermo Fisher Scientific).

Immunoprecipitation and immunoblotting

For immunoprecipitation, cells were extracted with HB100 buffer (50 mM Hepes-KOH, pH 7.6, 100 mM NaCl, 1 mM $MgCl_2$, 1 mM EGTA, 1% Triton X-100 and protein inhibitor cocktail (04693116001, Complete, Roche)) or RIPA buffer (50 mM Tris, 150 mM NaCl, 1% NP-40, 0.5% Sodium Deoxycholate and 0.1% SDS) for 10 min on ice and incubated with protein beads for 3 h at 4℃. For SDS-PAGE, the immunoprecipitants were washed three times and subjected to SDS-PAGE sample buffer, and boiled for 5 min. For immunoblotting, extracted proteins separated by SDS-PAGE were transferred to Immun-Blot PVDF membrane (Bio-Rad). Membranes were then blocked with 0.3% skim milk in TTBS (50 mM Tris, 138 mM NaCl, 2.7 mM KCl, and 0.1% Tween 20) incubated with primary antibodies overnight at 4℃ or for 1 h at 37℃ and with secondary antibodies for overnight at 4℃ or 30

min at 37℃. Each step was followed by three washes with TTBS. Signal detection used the ezWestLumi plus ECL Substrate (ATTO) and a LuminoGraph II chemiluminescent imaging system (ATTO). For signal detection, the ezWestLumi plus ECL Substrate (ATTO) and a LuminoGraph II chemiluminescent imaging system (ATTO) were used. Quantification of CBB staining or immunoblotting signals was performed using the Gels tool in ImageJ software (National Institutes of Health).

Cell proliferation assay

For cell proliferation assay, cells were seeded on 96-well plates at 9,000, 4,500, or 2250 cells/well (for haploid, diploid, or tetraploid HAP1 cells, respectively). After 24 h, cells were treated with different concentrations of PD0332991 (PZ0199, Sigma-Aldrich), LY2835219 (HY-16297, MedChemExpress) or doxorubicin hydrochloride (040–21521, Wako). Forty-eight h after addition of the compounds, 5% Cell Counting Kit-8 (Dojindo) was added to culture medium, incubated for 4 h, and absorbance at 450 nm was measured using the Sunrise plate reader (Tecan).

Chemical compounds

Compounds were purchased from suppliers as follows: Pitavastatin (163-24861, Wako); U18666A (10009085, Cayman Chemical); Cholesterol (SLBZ0657, Sigma-Aldrich); FTI-277 (S7465, Selleck); GGTI-298 (S7466, Selleck); tauroursodeoxycholic acid (TUDCA, T1567, Tokyo Chemical Industry); mevalonate (mevalonolactone, M4667, Sigma-Aldrich); tunicamycin (11445, Cayman Chemical).

Cholesterol measurement

For total cholesterol measurement, cells were once washed with DPBS, resuspended in 850 μL DPBS, and lysed by sonication. Fifty μL cell lysis was mixed with 50 μL0.1 M NaOH,

incubated at 60℃ for 2 h, and subjected to total protein measurement using Protein Assay Bicinchoninate kit (06385-00, nacalai tesque). For the cholesterol extraction, the remaining cell lysis was mixed with 1 mL chloroform and 2 mL methanol and incubated at 37℃ for 2 h with vigorous agitation. After adding 1 mL chloroform and 1 mL water, test tubes were centrifuged at 1000×*g* for 5 min, cholesterol extract was collected from the hydrophobic phase. Cholesterol was further extracted from the remaining lysis by repeating the addition of 2 mL chloroform and centrifugation for 3 times. The cholesterol extract was evaporated under a stream of N_2 and dissolved in 100 μL DPBS. The extracted total cholesterol was measured using LabAssay Cholesterol kit (294-65801, Wako) according to the manufacture's instruction. The oxidized and condensated N-Ethyl-N-(2-hydroxy-3-sulfopropyl)-3,5-dimethoxyaniline, sodium salt and 4-Aminoantipyrin were measured with 590 nm wavelength absorbance using iMark microplate reader (BIO-RAD). Cholesterol amount is then normalized to total cellular protein amount for comparison. For visualization of intracellular cholesterol, the Cholesterol Cell-Based Detection Assay Kit (10009779, Cayman Chemical) was used according to the manufacture's instruction.

Long-term cell passage experiments

Freshly purified haploid HAP1 cells were cultured in the presence of different compounds at final concentrations described elsewhere. I conducted cell passage using 0.05% trypsin-EDTA (Wako), typically once two days. To investigate the effect of each compound on the stability of haploid state, we continued passages for ~3 weeks before subjecting cell culture to flow cytometric DNA content analysis. As an exception, I conducted DNA content analysis after ~1-week passages for FTI-277-treated culture because drastic cell death precluded further passages. As an index of haploid cell preservation, we quantified the proportion of haploid cells in the G1 cell cycle phase (haploid G1 proportion) in flow cytometric analysis.

Antibodies

Antibodies were purchased from suppliers and used at the following dilutions: rabbit polyclonal anti-ninein (1:100; ab4447; Abcam), rabbit polyclonal anti-Cep290 (1:100; ab85728; Abcam), rabbit polyclonal anti-Sas-6 (1:100; PA5-31301; Thermo Fisher Science), mouse monoclonal anti-centrin (1:100; 20H5; EMD Millipore), rabbit polyclonal anti-γ-tubulin (1:100; T3559; Sigma-Aldrich), mouse monoclonal anti-γ-tubulin (1:100; GTU88; Sigma-Aldrich), rat monoclonal anti-α-tubulin (1:200; YOL1/34; EMD Millipore), rat monoclonal anti-BrdU (1:50; sc-56258; Santa Cruz), mouse monoclonal anti-β-tubulin (1:1000; 10G10; Wako), mouse monoclonal anti-GAPDH (1:3000; sc-32233; Santa Cruz), rabbit monoclonal anti-cyclin D1 (1:250; EPR2241; Abcam), rabbit monoclonal anti-cyclin D2 (1:1000; D52F9; Cell Signaling Technology), mouse monoclonal anti-cyclin D3 (1:1000; DCS22; Cell Signaling Technology), rabbit polyclonal anti-cyclin E1 (1:100; A301-566A; Bethyl Laboratories), rabbit polyclonal anti-cyclin A2 (1:100; sc-751; Santa Cruz), rabbit polyclonal anti-cdk2 (1:1000 for IB and 1:230 for IP; A301-812A; Bethyl Laboratories), mouse monoclonal anti-Rb (1:1000; 4H1; Cell signaling Technology), rabbit monoclonal anti-phospho-Rb (Ser780) (1:1000; D59B7; Cell Signaling Technology), rabbit polyclonal anti-phospho-Rb (Ser795) (1:1000; 9301; Cell Signaling Technology), rabbit monoclonal anti-p27 (1:500; D69C12; Cell Signaling Technology), goat polyclonal anti-anillin (1:50 for IB; sc-54859; Santa Cruz), rabbit polyclonal anti-anillin (1:230 for IP; A301-405; Bethyl Laboratories), mouse monoclonal anti-glypican3 (1:100; sc-65443; Santa Cruz), rabbit monoclonal anti-ATF4 (1:1000; D48B; Cell signaling Technology), mouse monoclonal anti-CHOP (1:1000; L63F7; Cell Signaling Technology), rabbit monoclonal anti-BiP (1:1000; C50B12; Cell Signaling Technology), rabbit polyclonal anti-Grp94 (1:1000; 2104; Cell Signaling Technology), rabbit polyclonal anti-PARP (1:1000; 9542; Cell Signaling Technology); and fluorescence (1:100~1000; Alexa Fluor 488 or Alexa Fluor 568) or horseradish peroxidase-conjugated secondaries (1:1000; Jackson ImmunoResearch Laboratories).

Result (1)

Centrosome loss and cell death in haploid zebrafish embryos

Optimizing the centriole analysis in zebrafish embryos

Whereas one centrosome normally consists of a pair of the centrioles during mitosis, the failure of centriole duplication in mammalian cells occasionally resulted in one centriole in a centrosome. Analysis of only centrosome is risky to miss the abnormal centriole number and, therefore, centriole visualization is essential to precisely characterizing centrosomes in haploid vertebrate individuals. However, there is limited knowledge about centriole visualization technique in zebrafish study (Lessman, 2012).

For visualizing centrioles with immunofluorescence in zebrafish embryos, I first tested several antibodies that target to centrin, Sas-6, ninein or Cep290, whose targets are confirmed in mammalian culture system. Four h post-fertilization (HPF) normally fertilized embryos were fixed with 4% PFA because of the easy handling at this developmental stage. To verify the antibody signals, γ-tubulin antibody that has been confirmed to target to centrosome in several previous works using zebrafish was used for counter-staining with tested antibodies (Lessman, 2012). In confocal microscopy, signal of all antibodies did not co-localized with γ-tubulin foci, or was too weak to identify centriole positions (Fig. 1A). In mammalian system, chilled-MetOH fixative is commonly used for centriole visualization because of its speedy invasion into intracellular components possibly for preventing diffusion of the inner proteins from centrosome, and the signals are observed as dotty patterns with confocal microscope (Connolly and Kalnins, 1978). Considering the visualization technique in culture cell system, I re-tried centriole visualization using MetOH fixative. As a result, whereas Cep290 signal could not be detected, other antibody signals were co-localized with γ-tubulin foci and dramatically improved compared to when using PFA fixative (Fig. 1B). Ninein signal was observed as aster like structure, indicating that this antibody targets to centrosomal proteins rather than centriole components. On the other hand, the signals of centrin and Sas-6 antibodies were observed as sharp dotty pattern co-localizing with γ-tubulin focus in the embryos, demonstrating that these antibody targets to core of centrosomes. Previous studies have reported that, whereas Sas-6 is recruited to proximal position of mother centriole to duplicate the daughter centriole at S phase onset and mostly diffused from centrioles at the

end of S phase (Fong et al., 2014; Kitagawa et al., 2011), centrin is a stable component of inner centriole structure (Pastrana-Rios et al., 2013). Therefore, I hereafter visualized centrioles in zebrafish embryos using a centrin antibody 20H5, which is an authentic centriole marker in both human and rodents.

When I visualized centrioles in early development of fish embryos, it seemed that the regulation of centriole number at 4 HPF is differed from common vertebrate somatic cells. Even in normally fertilized diploid embryos, I frequently observed more than 4 centrioles in a 4 HPF embryonic cell (Fig. 1C). These extra centrioles in early development had been reported also in rabbit and mouse diploid embryos during early development (Szollosi and Ozil, 1991; Yaguchi et al., 2018a), suggesting that the difference in centriole regulation between early development and somatic cells is common in vertebrate species.

To investigate the time point when centriole number become somatic mode, I also visualized centrioles in 12 HPF embryos at when organogenesis is beginning. When centrioles in somite were visualized at 12 HPF, the centriole number seemed to become mostly between 2 to 4 per cell, indicative of the change in the mode of centriole number before 12 HPF (Fig. 1C). Because it has been reported that haploid embryos are not visually distinguishable to diploid embryos before the organogenesis stage (Ellinger and Murphy, 1980), this data rules out the possible involvement of extra centrioles during early development in the morphological abnormality in haploid embryos. Thus, I chose the developmental stages after 12 HPF for the further investigation on the effects of ploidy alteration.

Haploid zebrafish embryos lose their centriole during developing organs

To investigate the effects of haploidy on vertebrate development based on my own previous finding (Yaguchi et al., 2018b), I analyzed centriole number in haploid and diploid zebrafish embryos, which were generated through *in vitro* fertilization of normal eggs with irradiated sperm or normal sperm, respectively. For this, viable embryos were fixed at 12, 24, 48 and 72 HPF, followed by staining centriole and mitotic spindle for the analysis of centriole number and spindle formation in mitotic cells in head region of embryos including several organs such as brain, eye and skin (Fig. 2A). In diploid embryos, only less than 18.23±4.52% of mitotic cells possessed unduplicated centrioles (< 4 centrioles per cell) and almost of all cells formed bipolar spindle throughout all time points (Fig. 2B). On the other hand, whereas the frequency of centriole loss was same between 12 HPF haploid and diploid embryos, 51.60±7.40% of haploid mitotic cells lost their centrioles at 24 HPF and formed abnormal monopolar spindles (Fig. 2B). The frequency of centriole loss and monopolar spindle formation in haploid embryos was gradually increased to 85.47±5.30% and 60.89±8.64%, respectively, at 72 HPF (Fig. 2B). These results indicate that my own previous finding, haploid linked centriole loss in mammalian somatic cells, is widely conserved in vertebrate species.

To further characterize the centriole loss in haploidy, I categorized the distribution of monopolar spindle formation with centriole loss in each tissue. At 24 HPF, the proportion of < 4 centriolar mitotic cells forming monopolar spindle in haploid embryos was 5.08%, 11.29% and 22.40% in skin, eye and brain, respectively, indicating that brain is one of the most perturbed tissue from haploidy during the early phase of organogenesis (Fig. 2C). Those data demonstrate the magnitude of centriole abnormality caused by ploidy alteration depends on organ type during development.

Centriole duplication is tightly regulated in cell cycle dependent manner in normal diploid cells (Stearns, 2001). Since haploid somatic cells lose their centriole because of the delay in centriole duplication (Yaguchi et al., 2018b), the chance of centriole loss in haploid cells should be increased in more efficiently proliferating cells with shorter cell cycle duration.

Several previous studies have reported that cells in developing neural tissues are more efficiently cycling their cell cycle compared to non-neural tissues (Homem et al., 2015). Supportively, the proportion of < 4 centriolar mitotic cells with monopolar spindles in the all analyzed tissues increased as developing organs, and it reached over 50% at the late developmental stages such as 72 HPF (Fig. 2C). Taken together, the more crucial impact of haploid linked centriole loss especially in brain and eye than non-neural tissues at the initiation of organogenesis might stem from the difference in the cellular proliferation profile of each organ.

Haploidy altered subsequent cellular fate and organ morphology during development

The mutations in centrosomal proteins, such as Plk4 and SAS-6, result in defects of centriole duplication and extends mitotic duration because of disorganized mitotic spindle in vertebrate organisms (Bazzi and Anderson, 2014; Martin et al., 2014). Cells possess surveillance systems for mitotic duration, by which prolonged mitosis triggers p53 activation that evokes caspase-3 dependent apoptosis (Fong et al., 2016; Lambrus et al., 2016; Lambrus et al., 2015). It has been reported that those defects in cellular proliferation due to the deregulation of centrosomal gene ultimately cause microcephaly or dwarfism during embryonic development (Marjanovic et al., 2015; Martin et al., 2014). Importantly, these morphological defects in the centrosome mutants are very similar to what has been observed in haploid embryos (Ellinger and Murphy, 1980).

To address the consequence of haploid individuals losing centrioles, I investigated the cellular destiny in haploid embryos. First, to investigate the distribution of mitotic phase in a cell cycle, I compared mitotic index in haploid and diploid embryos by analyzing the proportion of cells positive for phospho-histone pH3 as a marker of mitotic cells with flow cytometric analysis (Fig. 3A). In diploid embryos, the proportion of mitotic cells was gradually reduced as the developmental stage progressed (Fig. 3A and B), presumably reflecting the change in the mitotic mode in the late developmental stage. On the other hand, haploid embryonic cells did not reduce the mitotic population during the development, resulting in significantly higher mitotic index than diploid cells at 72 HPF (Fig. 3A and B). Because the change in proportion of mitotic cells stems from the distribution of the mitotic duration in cell cycle length, this result suggests the prolonged mitosis in haploid embryos.

Next, to investigate whether apoptosis occurs in haploid embryos, active form of caspase3 was visualized in haploid and diploid embryos at 72 HPF, when mitotic progression presumably delayed in haploid embryos (Fig. 3B and Fig. 4A). As a result, cells positive for active caspase3 were obviously increased in haploid embryos compared to diploid embryos (Fig. 4A). Particularly in neural organs such as eye, in which the haploid-linked centriole loss frequently occurs, the increase in apoptotic cells is more markable in haploid embryos (Fig. 4A and B), suggesting the linkage of haploid-linked centriole loss and the cell death.

Furthermore, to investigate neuronal organogenesis in haploid embryos, I measured retina surface between haploid and diploid embryos during late developmental stages using the fixed embryos (Fig. 2A and Fig. 4C). Whereas diploid embryos dramatically expanded retina surface from 87±4 [$\times 10^2$ μm^2] at 12 HPF to 350±5 [$\times 10^2$ μm^2] at 72 HPF, the size expansion of haploid retina was from 74±6 [$\times 10^2$ μm^2] at 12 HPF to 217±13 [$\times 10^2$ μm^2] at 72 HPF, indicating the slowing down of size expansion in haploid tissue (Fig. 4C). As a result, compared to diploid embryos, haploid retina was significantly smaller at 24, 48 and 72 HPF (Fig. 4C). Taken together, those data suggest that the defect in cellular proliferation by centriole loss induces shrinkage of neuronal organs in haploid embryos.

Result (2)

Ploidy-dependent change in cyclin D2 expression and sensitization to cdk4/6 inhibition in human somatic cells

Ploidy-dependent changes in gene expression between haploid and diploid HAP1 cells

In somatic cells, near-haploidy is observed in some cancer types, and this ploidy state leads to poor diagnosis (Holmfeldt et al., 2013; Safavi and Paulsson, 2017). However, the therapeutic target for cells with abnormal ploidy is largely unknown because of the lack of knowledge in gene expression profile of abnormal ploidies.

To gain insights into haploidy-linked changes in gene expression profiles, I performed comprehensive next generation RNA-seq using near-haploid human leukemic cell line, HAP1 and its isogenic diploid counterpart (Fig. 5A). There were ~70 genes indicated to be up- or down-regulated in haploid cells compared to diploid cells in differentially expressed gene analysis (Fig. 5B). Among them, cyclin D2 or glypican3, whose expression reportedly is up- or down-regulated in tetraploid cells compared to diploid counterpart, respectively, showed opposed changes in gene expression level of haploid cells in this study compared to tetraploid cells in previous studies (Jones and Ravid, 2004; Potapova et al., 2016). These results indicate general linearity in ploidy-dependent changes in regulation of certain genes across hypo- and hyper-diploid states. These two genes were confirmed that the changing in post-tanslational level was also consistent with the result of RNA-seq by immunoblotting (Fig. 5C and D), indicative of the protein pool consistent with the transcriptional level of glypican3 and cyclin D2 in HAP1 cells.

Acute increase in cyclin D2 expression upon diploidization after cell division failure

Since cyclin D is a cell cycle regulator, cell cycle distribution in whole cell population possibly affect the cyclin D level. However, cell cycle distribution of asynchronous haploid HAP1 cells was similar to diploid counterpart (Fig. 5A and B), ruling out the possibility that the expression changing is merely an indirect consequence of altered cell cycle distribution between different ploidies.

Though previous study proposed that elevated cyclin D in tetraploid cells is a result of cyclin D overexpressing cells that spontaneously arise and override tetraploid-associated induction of p53 dependent cell cycle arrest (Potapova et al., 2016), the mechanism of low cyclin D level in haploid cells is still unclear. To further investigate whether ploidy-dependent difference in cyclin D expression between haploid and diploid also arise from the similar selective mechanism, I tested the effect of acute ploidy alteration in haploid cells on cyclin D2 level. For that purpose, an essential cytokinesis regulator anillin was depleted to induce acute doubling of whole genome through cell division failure in haploid and diploid cells (Fig. 6A-D). Depletion of anillin resulted in doubling of DNA content with binucleation, and importantly, lead to a substantial increase in cyclin D2 level in both haploid and diploid cells compared to mock-depleted controls (Fig. 6A and D). Upon the binucleation, a proportion of BrdU-positive cells remained unchanged from controls (Fig. 6D), suggesting that whole genome doubling did not induce cell cycle arrest. Consistently, expression level of p21, which induces cell cycle arrest as a downstream of p53, was also unchanged in anillin depleted cells compared to controls (Fig. 6B and C). These results exclude the possibility that the change of cyclin D2 level arose from cell cycle arrest and from the selective proliferation of cyclin D overexpressing cells. The fact that cyclin D2 expression changes within a few days upon doubling whole genome indicates that ploidy alteration drives the change in cyclin D2 expression, rather than selective or adaptive processes for the change in ploidy level.

Reducing cyclin D pool in haploid cells does not affect cell cycle regulation

The change in the expression of cyclin D potentially affects cell cycle regulatory events including induction of S phase cyclins (Choi and Anders, 2013; Sherr and Roberts, 1999). To test this possibility, I compared time-dependent patterns of expressions of cyclin D2 and other cyclins during G1 and S phases between haploid and diploid cells that were synchronized by nocodazole shake-off (Fig. 7A and B). While there was no obvious time-dependent change in expression level of cyclin D1 and D2 both in haploid and diploid cells, expressions of these cyclins were lowered in haploid cells compared to diploid cells throughout G1/S phase. Cyclin D3 was expressed slightly higher than in diploid ones 4h after nocodazole release, which corresponds to late G1 phase in these cell lines (Yaguchi et al., 2018b). On the other hand, expression level of cyclin E1 and A2, which govern the initiation and the progression of S phase (Grana and Reddy, 1995), was roughly equivalent between haploid and diploid cells throughout G1/S phase. Although cyclin D is required for cell cycle re-entry in tetraploid cells (Crockford et al., 2017), these results indicate that the haploid-linked reduction of cyclin D2 level has minimal effect on cell cycle regulation during G1/S phase.

Besides the induction of other cyclins, cyclin D-cdk4/6 complex potentially phosphorylates retinoblastoma protein (Rb) and suppresses binding of p27 to cdk2 for facilitating the binding of cdk2 to S phase cyclin (Jiang et al., 1998; Kato et al., 1993; Matsushime et al., 1992; Sherr and Roberts, 1999). I verified those downstream possibly effected by decrease in cyclin D2 pool in this cell line (Fig. 8A and C). However, the Rb phosphorylation states and the amount of p27 bound to cdk2 were unchanged between haploid and diploid cells (Fig. 8A-D). These results indicate that haploid cells adapt to the low cyclin D level and can promote G1/S progression as efficiently as diploid cells.

Haploid cells are more susceptible to cdk4/6 inhibition than diploids

Ploidy alteration from diploidy is frequently observed and is recognized a hallmark of several cancer types. Cyclin D is also often deregulated in broad spectrum of tumor cells. Therefore, based on the finding of ploidy dependent difference in cyclin D expression, next I wished to gain the insight of the efficacy of the inhibition of cyclin D associated function in different ploidy states. For this, the viability of haploid, diploid and tetraploid HAP1 cells was compared after treating various concentration of PD-0332991 or LY-2835219, which inhibits cyclin D binding partner cdk4/6 (Fig. 9A and B). As a control of this assay, doxorubicin was treated for those cell lines, which induces DNA double strand break (Fig. 9C). However, in cells treated with cdk4/6 inhibitors, whereas the efficacy between diploid and tetraploid cells was roughly same, these compounds selectively suppressed growth of haploid cells (Fig. 9A and B). Importantly, this ploidy dependent selectivity was not observed in doxorubicin treated cell, demonstrating that ploidy selectivity is a specific property of cdk4/6 inhibitors (Fig. 9C). These results indicate that haploid cells are more susceptible to inhibition of cdk4/6 function than higher ploidy state.

Result (3)

ER stress intolerance destabilizes haploidy in human somatic cells

Pitavastatin destabilizes haploidy in HAP1 cells through the inhibition of mevalonate pathway

In addition to the involvement of haploidy on developmental defects or cancer progression, another notable feature of haploidy is its instability. It has been reported that haploid cells convert into diploid state within few weeks through successive passaged culture (Wutz, 2014; Yilmaz et al., 2016). However, what cellular process underlies the haploid instability is remained unclear.

Since the cell size of haploid cells is halved with the decrease in protein pool compared to diploid cells, which possibly alter the cellular processes, I first tried to increase the volume of cytoplasm in haploid cells. Recent studies revealed that statins, which inhibits the rate limiting enzyme 3-hydroxy-3-methylglutaryl-coemzyme A reductase (HMGCR) for mevalonate metabolism and effects multiple cellular processes such as cholesterol homeostasis or protein prenylation, increase the cell size in different cell types by perturbing mitochondrial functionality through inhibition of protein prenylation (Miettinen and Björklund, 2015).

To induce the alteration of cell size, I treated haploid HAP1 cells with 0.5 μM pitavastatin, a novel member of the medication class of statins, during long-term passages (Fig. 10A). Although I could not observe the change in cell size upon pitavastatin treatment, I unexpectedly found that haploid HAP1 cells treated with pitavastatin more rapidly converted to diploid state compared to non-treated haploid cells (Fig. 10A-C). Another group utilizing chemical screen, in parallel, also reported that other statins accelerated the haploid-diploid conversion (Olbrich et al., 2019). Those evidence indicate the involvement of mevalonate metabolism on haploid stability. To address the mechanism of statin-induced haploid instability, I tested whether supplementation of mevalonate to culture ameliorates haploid stability in the presence of pitavastatin (Fig. 10B and C). Mevalonate supplementation significantly preserved haploid population in pitavastatin-treated culture, indicating that the sufficient amount of mevalonate is required for the maintenance of haploids (Fig. 10B and C).

Cholesterol perturbation is not the cause of ptavastatin-induced destabilization of haploidy

Next, I determined downstream branches of mevalonate pathway crucial for the maintenance of haploid state. Because statins are widely used cholesterol-lowering drugs (Adhyaru and Jacobson, 2018), I addressed the possible involvement of cholesterol branch in haploid stability. For this, I compared content of total cholesterol extracted from control and pitavastatin-treated HAP1 cells using colorimetric method (Fig. 11A). In this assay, I did not observe significant difference in cholesterol content between control and pitavastatin-treated cells. This suggests that, at such a low concentration as 0.5 μM, pitavastatin does not drastically block cholesterol synthesis. To assess the effect statin of pitavastatin on cholesterol homeostasis at the single-cell level, I next visualized intracellular distribution and content of cholesterol in control and pitavastatin-treated HAP1 cells using a cholesterol-binding fluorescent compound filipin (Fig. 11B). In control cells, filipin fluorescence signal distributed throughout the plasma- and intracellular membrane structures, and 0.5 μM pitavastatin modestly, but significantly, reduced the filipin staining intensity (Fig. 11B-D). Therefore, at this final concentration, pitavastatin mildly reduced cholesterol level in HAP1 cells. Next, I addressed whether cholesterol supplementation is sufficient to restore haploid stability in pitavastatin-treated cells. The addition of 10 μM cholesterol to the pitavastatin-treated cell culture fully restored cholesterol level (Fig. 11A-D). However, cholesterol supplementation did not affect the progression of haploid-to-diploid conversion in statin-treated culture (Fig. 11E and F). On the other hand, mevalonate supplementation, which fully restored haploid stability in statin-treated cells (Fig. 10B and C), did not change the cholesterol level in statin-treated cells (Fig. 11A-D). These data demonstrated that lowered cholesterol level was not the cause of haploid destabilization by pitavastatin.

Next, I tested the effect of perturbation of cholesterol homeostasis by a non-statin cholesterol inhibitor on haploid stability. An amphipathic steroid U18666A perturbs the cholesterol-mediated bioprocesses by inhibiting both synthesis and intracellular transport of cholesterol. Treatment with 2.5 μM U18666A resulted in the accumulation of cholesterol in intracellular

vesicles, a typical defect caused by the compound (Fig. 11B). HAP1 cell proliferation was not severely affected by 2.5 μM U18666A, allowing us to test its effect on the long-term haploid stability. In the long-term passages, 2.5 μM U18666A-treated cells underwent haploid-to-diploid conversion at a similar pace as non-treated control (Fig. 11G). This result further ruled out the possible involvement of cholesterol homeostatic control in haploid stability in HAP1 cells.

Inhibition of protein prenylation does not phenocopy haploid destabilization by pitavastatin

Among the mevalonate-derived metabolites, farnesyl pyrophosphate and geranylgeranyl pyrophosphate are used for the posttranslational prenylation of small GTPases that play crucial roles in the regulation of cell cycle and proliferation, as well as cell size control (Berndt et al., 2011; Miettinen and Björklund, 2015; Miettinen and Björklund, 2016). Therefore, I tested the effects of FTI-277 or GGTI-298, which inhibits protein farnesylation or geranylgeranylation, respectively, on the stability of the haploid state in HAP1 cells. Twenty μM FTI-277 treatment caused mitotic progression defects marked by the round-shaped mitotically-arrested cells and abnormally enlarged cells in culture (Fig. 12A). Similar FTI-277-induced mitotic defects have been reported in different cell lines (Holland et al., 2015; Morgan et al., 2001; Moudgil et al., 2015). Consistent with the microscopic observation, FTI-277-treated HAP1 cells were drastically polyploidized within several days with the prominent accumulation of 2, 4, and 8 c peaks in flow cytometric analysis (Fig. 12B). This result suggests that FTI-277 induces whole-genome duplication in HAP1 cells regardless of the ploidy state, which was in contrast to the haploidy-specific induction of whole-genome duplication by pitavastatin. The drastic polyploidization and subsequent cell death precluded us from testing the effects of FTI-277 on ploidy dynamics in a more extended period.

On the other hand, treatment with 2 μM GGTI-298 mildly arrested haploid HAP1 cells at the G1 phase within 24 h, consistent with a previous report in several cell types (Fig. 12C). In prolonged culture for 20 d in the presence of 2 μM GGTI-298, the haploid-to-diploid conversion was considerably slowed down compared to non-treated control, presumably because of the moderate G1 arrest (Fig. 12D). Therefore, the suppression of either protein farnesylation or geranylgeranylation did not phenocopy the pitavastatin-induced haploid destabilization in our long-term experiment.

Pitavastatin destabilizes the haploid state by evoking ER stress

Since statins potentially induce ER stress by suppressing dolichol phosphates biosynthesis and inhibiting protein N-glycosylation (Chojnacki and Dallner, 1988), I next tested the possibility that pitavastatin destabilizes the haploid state through perturbing ER homeostasis. For this, we tested the effect of pitavastatin on ER stress in HAP1 cells using immunoblot analysis of ATF4 or CHOP/GADD153/DDIT3, the unfolded protein response (UPR) components whose expression increases upon the induction of ER stress (Harding et al., 2000; Marciniak et al., 2004; Oyadomari and Mori, 2004). Treatment with 0.5 μM pitavastatin for 3 d significantly increased the expression of both ATF4 and CHOP (Fig. 13A and B). Mevalonate supplementation canceled the ATF4 and CHOP upregulation in pitavastatin-treated cells, demonstrating that pitavastatin evoked ER stress specifically through blocking mevalonate metabolism (Fig. 13A and B).

Finally, we determined whether ER stress induction is the cause of pitavastatin-mediated destabilization of haploid state in HAP1 cells. For this, we tested the effect of an ER stress-reducing chemical chaperone, tauroursodeoxycholic acid (TUDCA) (Ozcan et al., 2006; Yoon et al., 2016), on the haploid stability of HAP1 cells. Co-treatment with TUDCA did not affect ATF4 expression, but substantially blocked CHOP upregulation in pitavastatin-treated cells (Fig. 13A and B), presumably reflecting the complex effects of chemical chaperones on different factors in the UPR pathways (Uppala et al., 2017). In contrast, TUDCA did not change the cholesterol level in pitavastatin-treated cells assessed by filipin staining (Fig. 11B-D). In long-term passages, co-treatment of TUDCA significantly slowed down haploid-to-diploid conversion in pitavastatin-treated cells (Fig. 13C and D). Therefore, restoration of ER homeostasis by TUDCA substantially improved the stability of the haploid state in the presence of pitavastatin, demonstrating that haploid destabilization by pitavastatin is caused through the induction of ER stress.

TUDCA restored haploid population both in the presence and absence of artificial ER stress induction

To further investigate whether general ER stress destabilizes haploidy, HAP1 cells were treated with a common ER stressor tunicamycin, an inhibitor of N-glycosylation as a competitive nucleotide sugar analog (Chang et al., 1987; Olden et al., 1979). When haploid cells were treated with 50 nM tunicamycin for 21 d, haploid-diploid conversion was drastically accelerated as observed in pitavastatin-treated culture (Fig. 10B and C, Fig. 14A and B). To verify the effects of tunicamcyin on haploid stability through evoking ER stress, HAP1 cells were co-treated with TUDCA in the presence of tunicamycin. As a result, TUDCA co-treatment with tunicamycin substantially restored the proportion of haploid cell population compared tunicamycin single treated culture (Fig. 14A and B), indicating that tunicamycin destabilizes haploidy through ER stress induction. Moreover, TUDCA single treatment mildly restored the population of haploid cells compared to non-treated culture, demonstrating that the basal level of ER stress destabilizes haploidy (Fig. 14A and B). Those data suggest that, even in the unperturbed condition, non-artificial ER stress promotes haploid-diploid conversion.

The low magnitude of ER stress induces haploid specific cell death, despite of normal chaperone expression in haploid cells

It has been reported that null allele mutation in *HAC1* gene drastically destabilize the haploid state in *S. cerevisiae* (Lee et al., 2003). *HAC1* encodes a transcriptional activator involved in UPR, which subsequently upregulates the expression of folding chaperones to retain the perturbed ER homeostasis (Mori et al., 1996). The fact that *HAC1* mutation leads to haploid instability demonstrates the requirement of UPR for ploidy maintenance in yeast. To test whether UPR pathway is defective in mammalian haploid cells, the expression level of chaperones and UPR components in haploid and diploid HAP1 cells were detected 24 h after treatment with several concentration of tunicamycin. Both of haploid and diploid cells showed the increase in expression of chaperones and UPR components in a concentration dependent manner (Fig. 15A and B). Importantly, expression of ATF4 and folding chaperones such as Grp78 and Grp94 were roughly equivalent between haploid and diploid cells at all concentration ranges, suggesting that UPR is normally evoked in haploid cells (Fig. 14A and B). On the other hand, another UPR component CHOP, which transcribes sentinel genes for activating proapoptotic pathway when ER stress exceeds folding capacity of UPR in cells (Oyadomari et al., 2002; Zinszner et al., 1998), was sub-significantly upregulated in 50 nM tunicamycin-treated haploid cells compared to diploid counterpart (Fig. 14A and B). Consistently, expression of a proapoptotic marker, cleaved-PARP in haploid cells was also drastically upregulated at the same concentration range (Fig. 14A and B). Taken together, these data indicate that, despite the comparable chaperone expression between haploid and diploid cells, the low magnitude of ER stress is insurmountable enough to induce cell death specifically in haploid cells.

To further verify the cell death in haploid cells induced by the low magnitude of ER stress, I analyzed the frequency of proapoptotic state using annexin V-FITC, which binds to phosphotidylserine that translocates from inner- to outer- plasma cell membrane during the early apoptosis (Koopman et al., 1994). Whereas almost of all diploid cells were negative for annexin V-FITC both in the presence or absence of 50 nM tunicamycin, tunicamycin-treated haploid cells significantly increased the proportion of cells positive for annexin V-FITC

compared to non-treated haploid cells, demonstrating the poor tolerability to ER stress in a lower ploidy state (Fig. 16A and B).

Prolonged ER stress causes cell death in haploid cells

Next, to address how the low magnitude of ER stress activates apoptotic pathway in haploid cells, I traced the time course of changes in expression of chaperones and UPR components in haploid and diploid cells treated with 50 nM tunicamycin. Expression level of chaperones and ATF4 was found to be upregulated in a time dependent manner and the level of those components was unchanged in haploid cells compared to diploid counterparts at all time points (Fig. 17A and B), supportively demonstrating that the UPR pathway in haploid cells is intact. However, whereas diploid cells efficiently suppressed expression of CHOP after upregulation of other UPR component such as at 18 and 24 h after tunicamycin treatment started, haploid cells sustained significantly higher expression of CHOP (Fig. 17A and B). This higher expression of CHOP at the late phase of UPR suggests the unsolved ER stress in haploid cells. Concomitantly with the extended CHOP expression, PARP was more efficiently cleaved in haploid cells in the same time points compared to diploid counterparts (Fig. 17A and B). Those results suggest that, in haploid cells, the extended CHOP expression by unmanageable prolonged ER stress induces cell death.

To further test whether prolonged ER stress is the cause of haploid specific cell death, haploid cells were co-treated TUDCA from at 12 h after tunicamycin treatment started. Although CHOP expression was elevated until at 12 h after ER stress induction as observed in Fig. 17, co-treatment of TUDCA from this time point significantly suppressed expression of both CHOP and cleaved-PARP compared to tuicamycin-single treated haploid cells in later time points. Importantly, the expression of cleaved-PARP in TUDCA co-treated haploid cells was roughly comparable to tunicamycin-single treated diploid cells (Fig. 18A and B). This result indicated that the attenuation of prolonged ER stress in haploid cells sufficiently canceled the proapoptotic pathway regardless of the elevated CHOP expression at the early phase of UPR induction. These data demonstrate that the unsolved prolonged ER stress is the cause of haploid cell death.

Reduction in growth of haploid cells by the poor ER stress tolerability dilutes haploid population in culture.

ER stress-induced haploid cell death arises the possibility that ER stress reduces haploid growth in culture. It has been reported that diploidized cells more efficiently proliferate than haploid cells, suggesting the growth bias between haploid and diploid cells that potentially contributes to the increase in the population of diploidized cells in HAP1 cell culture (Olbrich et al., 2017; Yaguchi et al., 2018b). In order to test whether ER stress destabilized haploidy through promoting the growth bias, I examined the effect of tunicamycin on the relative growth between haploid and diploid cells. Haploid WT cells and diploid cells stably expressing GFP empty vector were mixed with the same population in culture, and then treated with several concentration of tunicamycin for 2 d (Fig. 19A). The proportion of haploid population subsequently decreased within 2 d, indicating that the diploid cells more efficiently proliferate than haploid cells in culture even without artificially induced ER stress (Fig. 19A and B). Treatment with 50 nM tunicamycin substantially promoted the decrease in the haploid population in culture, indicating the reduction of relative growth rate in haploid cells (Fig. 19A and B). This result is consistent with that the expression of CHOP and cleaved-PARP were more upregulated in haploid cells compared to diploid counterparts, when treated with the low concentration range of tunicamycin in immunoblotting (Fig. 15). Altogether, those data demonstrate that the poor ER stress tolerability in haploidy accentuates the growth bias between haploid and diploid cells, which allows diploidized cells to outcompete haploid population.

Discussion

Ploidy is one of the most important quantitative information of organisms. It's thought that, during evolutionally history, vertebrate species mainly maintain diploidy with few whole genome duplication phase but without halving their genome quantity from diploidy (Otto, 2007; Sagi and Benvenisty, 2017; Wutz, 2014), suggesting the intolerance of vertebrates to haploidy. However, why haploidy is not allowable in vertebrate was poorly understood. In this study, I identified the haploid-linked cellular abnormalities that potentially impair developmental system, reduce cellular fitness, and destabilize the genome content in population. Those multilateral findings clearly highlight the importance of diplontic environment in vertebrates. Although I here focused on cellular basis of haploidy, it's also observed that the change of cellular features in tetraploidy was oppose to haploidy compared to dipoidy, indicating the linear relationship between the cellular processes and ploidy level. Thus, those evidence might contribute to further unmasking biological significance of ploidy alteration including polyploidization.

The reason why haploidy is inviable in vertebrate species

Besides ploidy limitation, there is a big difference in cell division mode between vertebrate and non-vertebrate. In plant or fungi, cells lack centrosome, and undergo mitosis independently on centrosome. In some insects, centrosome is not essential for mitotic completion, and individuals that do not possess centrosomes can survive. However, from the early branch of vertebrate, lack of centrosome perturbs development systems. Mutation in centrosomal genes cause organogenesis failure during development, including severe delay in size expansion of brain or other neural tissues, which results in microcephaly or primordial dwarfism (Bazzi and Anderson, 2014; Martin et al., 2014). Importantly, these defects are similar to morphological defects in haploid syndrome.

The current study found monopolar spindle induced by centriole loss in haploid zebrafish. This haploid-linked centriole loss, interestingly, showed tissue dependent appearance. In

neural tissue, such as brain and eye, centrioles in haploid cells disappear earlier than non-neural tissues. This tissue dependency may reflect the difference in cellular proliferation profile of each tissue. Neural tissues require the increase in size by more frequent cell division compared to non-neural tissues (Homem et al., 2015), and it may cause the difference in the chance of monopolar spindle formation in each haploid tissue, because centriole duplication is tightly regulated by cell cycle dependent manner (Stearns, 2001).

Recent studies reported that the mutations on centrosomal genes failed to duplicate centrioles and subsequently delay mitotic duration, which activate p53 and finally induce apoptosis in early development of fish and mice (Bazzi and Anderson, 2014; Martin et al., 2014). Consistent with this, the proportion of mitotic cells and apoptotic cells was increased in haploid zebrafish embryos in my system, indicating the similarity to cell death in centrosomal mutants.

Although we identified centriole loss and the cellular destiny in haploid embryos, it still remained elusive whether centriole loss in zebrafish embryos trigger cellular diploidization, which is observed in wide range of cell types in mammalian culture system (Guo et al., 2017; Olbrich et al., 2017; Yaguchi et al., 2018b). Because haploid embryos are short life after fertilization, we could not trace the effects of diploidized cell on vertebrate development. It's possible that diploidized cells in haploid embryos potentially affects organ functions in certain type of tissues. Karyotype analysis with tissue isolation is required to test whether the diploidized population in haploid embryos is masked in the system of this study.

Cancer therapeutic target based on the ploidy alteration

Regarding the diploidization from haploid state in mammalian somatic cells, more cancer types potentially undergo haploid state. This work identified several genes whose expression level is changed depending on ploidy level. Together with previous studies using tetraploid cell lines, among the up- or down- regulated genes in haploid cells compared to diploid cells, the expression level of cyclin D and glyican3 showed linear relationship with the ploidy level in both transcriptional and translational levels, suggesting the possibility these gene could be

biomarker for ploidy level.

Since cyclin D is one of majorly deregulated gene in broad cancer types, it can be a good target for therapeutic strategies. Whereas upregulation of cyclin D level allows p53-activated and cell cycle-arrested tetraploid cells to proliferate, the lowered cyclin D level in haploid cells seemed not perturb cell cycle regulation with the intact downstream pathway of cyclin D. However, sensitivity to the inhibition of cdk4/6, cyclin D binding partner, in haploid cells was substantially higher than diploid and tetraploid cells. This result may reflect that insufficient cyclin D level in haploid cells reduced the active cdk4/6 which buffer the cytotoxic effects of cdk4/6 inhibitors. Although it's required for further investigation of the mechanism crucial for haploid-linked hyper sensitivity to cdk4/6 inhibitor, these results highlight the possibility that ploidy alteration could be a powerful target for cancer therapy.

Oppositely to cyclin D level, together with one previous study using aorta muscle cells, glypican3 is up- or down-regulated in haploid and tetraploid cells. Although Glypcan3 is also thought as a candidate of oncotarget for hepatocellular carcinoma because of its overexpression in tumor tissue, this is paradoxical because of the higher ploidy level in cancerous hepatocyte with upregulated expression level of glypican3 leads poor prognosis (Bou-Nader et al., 2018; Sung et al., 2003; Zhu et al., 2001). One possible explanation is that, in normal ploypoid tissues, glypican3 expression level is actively suppressed, and the disturbance of the suppression mechanism contributes to progressive cancer. Findings of the current transcriptome based investigation indicate the feasibility of ploidy dependent changing of gene expression in certain genes which might be the main cause of some diseases with abnormal ploidies.

ER stress tolerability correlating with ploidy level

My recent study identified the trigger of cellular diploidization through mitotic slippage with centriole loss. However, the frequency of cellular diploidization from haploid state is very few in culture, and both of haploid and diploid cells have similar cell cycle length and cell cycle distribution. Therefore, how the population of haploid cells is diluted in culture was

entirely unclear.

In this study, my pharmacological approach identified that the tolerability to ER stress falls down in haploid cells. ER stress can be caused through the change of multiple endogenous and exogenous circumstances, including nutriture, temperature or proton concentration, suggesting that the trivial environmental changes even during proper experimental conditions potentially dilute haploid population. In agreement with this idea, chemical chaperon indeed slowed down the time course of haploid-diploid conversion when compared with non-treated counterpart in my long-term passage system (Fig. 14), which may reflect that the basal level of ER stress surfer haploid cells. Consistently, the induction of low magnitude of ER stress activated apoptotic pathway and suppressed growth specifically in haploid cells with minimal effect on diploid cells, which ultimately resulted in dilution of haploid population in co-culture with diploid cells.

Whereas I identified one of the main causes of haploid instability in this study, the determinant of haploid linked-poor tolerability to ER stress is still unclear. Considering that haploid cells are half in cell volume than diploids, the intracellular spatial capacity for organelle structure might be restricted in haploids. It has been demonstrated that the expansion of the ER lumen serves as a mechanism to increase ER capacity to ameliorate ER stress upon the accumulation of unfolded proteins. The lower availability of intracellular space may limit stress-responding ER expansion in haploid cells, hence lower processivity of ER and tolerance to ER stress. High-resolution time-lapse observation of dynamic ER structure would be a powerful tool to elucidate ploidy-linked effects on organelle morphology. The spatial limitation in a lower ploidy state suggests the ploidy dependent ER capability. In agreement with that hepatocyte or lactating mammary cells, whose organs are presumably exposed to higher ER stress, majorly polyploidize (Ovrebo and Edgar, 2018), the linkage between ploidy level and ER stress tolerability might be a clear linear relationship from haploidy to polyploidy.

Reference

Adhyaru, B.B., and Jacobson, T.A. (2018). Safety and efficacy of statin therapy. Nature reviews Cardiology *15*, 757-769.

Bazzi, H., and Anderson, K.V. (2014). Acentriolar mitosis activates a p53-dependent apoptosis pathway in the mouse embryo. Proc Natl Acad Sci U S A *111*, E1491-1500.

Berndt, N., Hamilton, A.D., and Sebti, S.M. (2011). Targeting protein prenylation for cancer therapy. Nature reviews Cancer *11*, 775-791.

Bou-Nader, M., Donne, R., Caruso, S., Calderaro, J., Gentric, G., L'Hermitte, A., Guilbert, T., Klein, C., Couchy, G., Celton-Morizur, S.*, et al.* (2018). Nuclear Polyploidy Profile Is a New Marker of Molecular HCC Tumour Classification. Hepatology *68*, 502a-502a.

Carter, S.L., Cibulskis, K., Helman, E., McKenna, A., Shen, H., Zack, T., Laird, P.W., Onofrio, R.C., Winckler, W., Weir, B.A.*, et al.* (2012). Absolute quantification of somatic DNA alterations in human cancer. Nature biotechnology *30*, 413-421.

Castillo, A., Morse, H.C., 3rd, Godfrey, V.L., Naeem, R., and Justice, M.J. (2007). Overexpression of Eg5 causes genomic instability and tumor formation in mice. Cancer research *67*, 10138-10147.

Chang, S.C., Wooden, S.K., Nakaki, T., Kim, Y.K., Lin, A.Y., Kung, L., Attenello, J.W., and Lee, A.S. (1987). Rat gene encoding the 78-kDa glucose-regulated protein GRP78: its regulatory sequences and the effect of protein glycosylation on its expression. Proc Natl Acad Sci U S A *84*, 680-684.

Choi, Y.J., and Anders, L. (2013). Signaling through cyclin D-dependent kinases. Oncogene *33*, 1890.

Chojnacki, T., and Dallner, G. (1988). The biological role of dolichol. The Biochemical journal *251*, 1-9.

Connolly, J.A., and Kalnins, V.I. (1978). Visualization of Centrioles and Basal Bodies by Fluorescent Staining with Non-Immune Rabbit Sera. Journal of Cell Biology *79*, 526-532.

Crockford, A., Zalmas, L.P., Gronroos, E., Dewhurst, S.M., McGranahan, N., Cuomo, M.E., Encheva, V., Snijders, A.P., Begum, J., Purewal, S.*, et al.* (2017). Cyclin D mediates tolerance of genome-doubling in cancers with functional p53. Annals of oncology : official journal of the European Society for Medical Oncology *28*, 149-156.

Dewhurst, S.M., McGranahan, N., Burrell, R.A., Rowan, A.J., Gronroos, E., Endesfelder, D.,

Joshi, T., Mouradov, D., Gibbs, P., Ward, R.L.*, et al.* (2014). Tolerance of whole-genome doubling propagates chromosomal instability and accelerates cancer genome evolution. Cancer discovery *4*, 175-185.

Ellinger, M.S., and Murphy, J.A. (1980). Cellular morphology in haploid amphibian embryos. J Embryol Exp Morphol *59*, 249-261.

Fong, C.S., Kim, M., Yang, T.T., Liao, J.C., and Tsou, M.F. (2014). SAS-6 assembly templated by the lumen of cartwheel-less centrioles precedes centriole duplication. Dev Cell *30*, 238-245.

Fong, C.S., Mazo, G., Das, T., Goodman, J., Kim, M., O'Rourke, B.P., Izquierdo, D., and Tsou, M.F. (2016). 53BP1 and USP28 mediate p53-dependent cell cycle arrest in response to centrosome loss and prolonged mitosis. Elife *5*.

Fujiwara, T., Bandi, M., Nitta, M., Ivanova, E.V., Bronson, R.T., and Pellman, D. (2005). Cytokinesis failure generating tetraploids promotes tumorigenesis in p53-null cells. Nature *437*, 1043-1047.

Graham, C.F. (1970). Parthenogenetic mouse blastocysts. Nature *226*, 165-167.

Grana, X., and Reddy, E.P. (1995). Cell cycle control in mammalian cells: role of cyclins, cyclin dependent kinases (CDKs), growth suppressor genes and cyclin-dependent kinase inhibitors (CKIs). Oncogene *11*, 211-219.

Guo, A., Huang, S., Yu, J., Wang, H., Li, H., Pei, G., and Shen, L. (2017). Single-Cell Dynamic Analysis of Mitosis in Haploid Embryonic Stem Cells Shows the Prolonged Metaphase and Its Association with Self-diploidization. Stem Cell Reports *8*, 1124-1134.

Hamilton, L. (1963). An experimental analysis of the development of the haploid syndrome in embryos of Xenopus laevis. J Embryol Exp Morphol *11*, 267-278.

Harding, H.P., Novoa, I., Zhang, Y., Zeng, H., Wek, R., Schapira, M., and Ron, D. (2000). Regulated translation initiation controls stress-induced gene expression in mammalian cells. Molecular cell *6*, 1099-1108.

Hertwig, G. (1911). Radium irradiation of unfertilized frog eggs and their development after fertilization by means of normal seeds. Arch Mikrosk Anat *77*, 165-209.

Hertwig, P. (1913). Behaviour of frogs' sperma chromatine which have been radiated with radium. Arch Mikrosk Anat *81*, 173-182.

Holland, A.J., Reis, R.M., Niessen, S., Pereira, C., Andres, D.A., Spielmann, H.P., Cleveland, D.W., Desai, A., and Gassmann, R. (2015). Preventing farnesylation of the dynein adaptor Spindly contributes to the mitotic defects caused by farnesyltransferase inhibitors. Molecular

biology of the cell *26*, 1845-1856.

Holmfeldt, L., Wei, L., Diaz-Flores, E., Walsh, M., Zhang, J., Ding, L., Payne-Turner, D., Churchman, M., Andersson, A., Chen, S.C.*, et al.* (2013). The genomic landscape of hypodiploid acute lymphoblastic leukemia. Nat Genet *45*, 242-252.

Homem, C.C., Repic, M., and Knoblich, J.A. (2015). Proliferation control in neural stem and progenitor cells. Nat Rev Neurosci *16*, 647-659.

Insolera, R., Bazzi, H., Shao, W., Anderson, K.V., and Shi, S.H. (2014). Cortical neurogenesis in the absence of centrioles. Nat Neurosci *17*, 1528-1535.

Jiang, H., Chou, H.S., and Zhu, L. (1998). Requirement of Cyclin E-Cdk2 Inhibition in p16 INK4a -Mediated Growth Suppression. Molecular and Cellular Biology *18*, 5284-5290.

Jones, M.R., and Ravid, K. (2004). Vascular smooth muscle polyploidization as a biomarker for aging and its impact on differential gene expression. The Journal of biological chemistry *279*, 5306-5313.

Kato, J., Matsushime, H., Hiebert, S.W., Ewen, M.E., and Sherr, C.J. (1993). Direct binding of cyclin D to the retinoblastoma gene product (pRb) and pRb phosphorylation by the cyclin D-dependent kinase CDK4. Genes & development *7*, 331-342.

Kilmartin, J.V. (2014). Lessons from yeast: the spindle pole body and the centrosome. Philos Trans R Soc Lond B Biol Sci *369*.

Kitagawa, D., Vakonakis, I., Olieric, N., Hilbert, M., Keller, D., Olieric, V., Bortfeld, M., Erat, M.C., Fluckiger, I., Gonczy, P.*, et al.* (2011). Structural basis of the 9-fold symmetry of centrioles. Cell *144*, 364-375.

Koopman, G., Reutelingsperger, C.P., Kuijten, G.A., Keehnen, R.M., Pals, S.T., and van Oers, M.H. (1994). Annexin V for flow cytometric detection of phosphatidylserine expression on B cells undergoing apoptosis. Blood *84*, 1415-1420.

Kotecki, M., Reddy, P.S., and Cochran, B.H. (1999). Isolation and characterization of a near-haploid human cell line. Experimental cell research *252*, 273-280.

Lambrus, B.G., Daggubati, V., Uetake, Y., Scott, P.M., Clutario, K.M., Sluder, G., and Holland, A.J. (2016). A USP28-53BP1-p53-p21 signaling axis arrests growth after centrosome loss or prolonged mitosis. J Cell Biol *214*, 143-153.

Lambrus, B.G., Uetake, Y., Clutario, K.M., Daggubati, V., Snyder, M., Sluder, G., and Holland, A.J. (2015). p53 protects against genome instability following centriole duplication failure. J Cell Biol *210*, 63-77.

Lee, K., Neigeborn, L., and Kaufman, R.J. (2003). The unfolded protein response is required for haploid tolerance in yeast. The Journal of biological chemistry *278*, 11818-11827.

Lessman, C.A. (2012). Centrosomes in the zebrafish (Danio rerio): a review including the related basal body. Cilia *1*, 9.

Marciniak, S.J., Yun, C.Y., Oyadomari, S., Novoa, I., Zhang, Y., Jungreis, R., Nagata, K., Harding, H.P., and Ron, D. (2004). CHOP induces death by promoting protein synthesis and oxidation in the stressed endoplasmic reticulum. Genes & development *18*, 3066-3077.

Marjanovic, M., Sanchez-Huertas, C., Terre, B., Gomez, R., Scheel, J.F., Pacheco, S., Knobel, P.A., Martinez-Marchal, A., Aivio, S., Palenzuela, L.*, et al.* (2015). CEP63 deficiency promotes p53-dependent microcephaly and reveals a role for the centrosome in meiotic recombination. Nat Commun *6*, 7676.

Martin, C.A., Ahmad, I., Klingseisen, A., Hussain, M.S., Bicknell, L.S., Leitch, A., Nurnberg, G., Toliat, M.R., Murray, J.E., Hunt, D.*, et al.* (2014). Mutations in PLK4, encoding a master regulator of centriole biogenesis, cause microcephaly, growth failure and retinopathy. Nat Genet *46*, 1283-1292.

Matsushime, H., Ewen, M.E., Strom, D.K., Kato, J.Y., Hanks, S.K., Roussel, M.F., and Sherr, C.J. (1992). Identification and properties of an atypical catalytic subunit (p34PSK-J3/cdk4) for mammalian D type G1 cyclins. Cell *71*, 323-334.

Menon, T., and Nair, S. (2018). Transient Window of Resilience During Early Development Minimizes Teratogenic Effects of Heat in Zebrafish Embryos. Dev Dynam *247*, 992-1004.

Miettinen, T.P., and Björklund, M. (2015). Mevalonate Pathway Regulates Cell Size Homeostasis and Proteostasis through Autophagy. Cell Rep *13*, 2610-2620.

Miettinen, T.P., and Björklund, M. (2016). Cellular Allometry of Mitochondrial Functionality Establishes the Optimal Cell Size. Dev Cell *39*, 370-382.

Miller, G.D., Seeb, J.E., Bue, B.G., and Sharr, S. (1994). Saltwater Exposure at Fertilization Induces Ploidy Alterations, Including Mosaicism, in Salmonids. Can J Fish Aquat Sci *51*, 42-49.

Morgan, M.A., Dolp, O., and Reuter, C.W.M. (2001). Cell-cycle‐dependent activation of mitogen-activated protein kinase kinase (MEK-1/2) in myeloid leukemia cell lines and induction of growth inhibition and apoptosis by inhibitors of RAS signaling. Blood *97*, 1823-1834.

Mori, K., Kawahara, T., Yoshida, H., Yanagi, H., and Yura, T. (1996). Signalling from endoplasmic reticulum to nucleus: transcription factor with a basic-leucine zipper motif is required for the unfolded protein-response pathway. Genes Cells *1*, 803-817.

Moudgil, D.K., Westcott, N., Famulski, J.K., Patel, K., Macdonald, D., Hang, H., and Chan, G.K. (2015). A novel role of farnesylation in targeting a mitotic checkpoint protein, human Spindly, to kinetochores. J Cell Biol *208*, 881-896.

Olaharski, A.J., Sotelo, R., Solorza-Luna, G., Gonsebatt, M.E., Guzman, P., Mohar, A., and Eastmond, D.A. (2006). Tetraploidy and chromosomal instability are early events during cervical carcinogenesis. Carcinogenesis *27*, 337-343.

Olbrich, T., Mayor-Ruiz, C., Vega-Sendino, M., Gomez, C., Ortega, S., Ruiz, S., and Fernandez-Capetillo, O. (2017). A p53-dependent response limits the viability of mammalian haploid cells. Proc Natl Acad Sci U S A *114*, 9367-9372.

Olbrich, T., Vega-Sendino, M., Murga, M., de Carcer, G., Malumbres, M., Ortega, S., Ruiz, S., and Fernandez-Capetillo, O. (2019). A Chemical Screen Identifies Compounds Capable of Selecting for Haploidy in Mammalian Cells. Cell Rep *28*, 597-604.e594.

Olden, K., Pratt, R.M., Jaworski, C., and Yamada, K.M. (1979). Evidence for role of glycoprotein carbohydrates in membrane transport: specific inhibition by tunicamycin. Proc Natl Acad Sci U S A *76*, 791-795.

Oshimura, M., Freeman, A.I., and Sandberg, A.A. (1977). Chromosomes and causation of human cancer and leukemia. XXIII. Near-haploidy in acute leukemia. Cancer *40*, 1143-1148.

Otto, S.P. (2007). The evolutionary consequences of polyploidy. Cell *131*, 452-462.

Ovrebo, J.I., and Edgar, B.A. (2018). Polyploidy in tissue homeostasis and regeneration. Development *145*.

Oyadomari, S., Araki, E., and Mori, M. (2002). Endoplasmic reticulum stress-mediated apoptosis in pancreatic beta-cells. Apoptosis *7*, 335-345.

Oyadomari, S., and Mori, M. (2004). Roles of CHOP/GADD153 in endoplasmic reticulum stress. Cell death and differentiation *11*, 381-389.

Ozcan, U., Yilmaz, E., Ozcan, L., Furuhashi, M., Vaillancourt, E., Smith, R.O., Görgün, C.Z., and Hotamisligil, G.S. (2006). Chemical chaperones reduce ER stress and restore glucose homeostasis in a mouse model of type 2 diabetes. Science *313*, 1137-1140.

Pastrana-Rios, B., Reyes, M., De Orbeta, J., Meza, V., Narvaez, D., Gomez, A.M., Rodriguez Nassif, A., Almodovar, R., Diaz Casas, A., Robles, J.*, et al.* (2013). Relative stability of human centrins and its relationship to calcium binding. Biochemistry *52*, 1236-1248.

Potapova, T.A., Seidel, C.W., Box, A.C., Rancati, G., and Li, R. (2016). Transcriptome analysis of tetraploid cells identifies cyclin D2 as a facilitator of adaptation to genome doubling in the presence of p53. Molecular biology of the cell *27*, 3065-3084.

Purdom, C.E. (1969). Radiation-induced gynogenesis and androgenesis in fish. Heredity (Edinb) *24*, 431-444.

Safavi, S., and Paulsson, K. (2017). Near-haploid and low-hypodiploid acute lymphoblastic leukemia: two distinct subtypes with consistently poor prognosis. Blood *129*, 420-423.

Sagi, I., and Benvenisty, N. (2017). Haploidy in Humans: An Evolutionary and Developmental Perspective. Dev Cell *41*, 581-589.

Sherr, C.J., and Roberts, J.M. (1999). CDK inhibitors: positive and negative regulators of G1-phase progression. Genes & development *13*, 1501-1512.

Smirnova, E.A., and Bajer, A.S. (1992). Spindle poles in higher plant mitosis. Cell Motil Cytoskeleton *23*, 1-7.

Stearns, T. (2001). Centrosome duplication. a centriolar pas de deux. Cell *105*, 417-420.

Streisinger, G., Walker, C., Dower, N., Knauber, D., and Singer, F. (1981). Production of clones of homozygous diploid zebra fish (Brachydanio rerio). Nature *291*, 293-296.

Sung, Y.K., Hwang, S.Y., Park, M.K., Farooq, M., Han, I.S., Bae, H.I., Kim, J.C., and Kim, M. (2003). Glypican-3 is overexpressed in human hepatocellular carcinoma. Cancer Sci *94*, 259-262.

Szollosi, D., and Ozil, J.P. (1991). De novo formation of centrioles in parthenogenetically activated, diploidized rabbit embryos. Biol Cell *72*, 61-66.

Tanaka, M., Yamaha, E., and Arai, K. (2004). Survival capacity of haploid-diploid goldfish chimeras. J Exp Zool A Comp Exp Biol *301*, 491-501.

Thorne, M.H., Collins, R.K., and Sheldon, B.L. (1987). Live Haploid-Diploid and Other Unusual Mosaic Chickens (Gallus-Domesticus). Cytogenet Cell Genet *45*, 21-25.

Uppala, J.K., Gani, A.R., and Ramaiah, K.V.A. (2017). Chemical chaperone, TUDCA unlike PBA, mitigates protein aggregation efficiently and resists ER and non-ER stress induced HepG2 cell death. Scientific reports *7*, 3831.

Uwa, H. (1965). Gynogenetic haploid embryos of the medaka (Oryzias latipes). Embryologia (Nagoya) *9*, 40-48.

Vigano, C., von Schubert, C., Ahrne, E., Schmidt, A., Lorber, T., Bubendorf, L., De Vetter, J.R.F., Zaman, G.J.R., Storchova, Z., and Nigg, E.A. (2018). Quantitative proteomic and phosphoproteomic comparison of human colon cancer DLD-1 cells differing in ploidy and chromosome stability. Molecular biology of the cell *29*, 1031-1047.

Wutz, A. (2014). Haploid animal cells. Development *141*, 1423-1426.

Yaguchi, K., Yamamoto, T., Matsui, R., Shimada, M., Shibanuma, A., Kamimura, K., Koda, T., and Uehara, R. (2018a). Tetraploidy-associated centrosome overduplication in mouse early embryos. Commun Integr Biol *11*, e1526605.

Yaguchi, K., Yamamoto, T., Matsui, R., Tsukada, Y., Shibanuma, A., Kamimura, K., Koda, T., and Uehara, R. (2018b). Uncoordinated centrosome cycle underlies the instability of non-diploid somatic cells in mammals. J Cell Biol *217*, 2463-2483.

Yamaki, M., Kawakami, K., Taniura, K., and Arai, K. (1999). Live haploid-diploid mosaic charr Salvelinus leucomaenis. Fisheries Sci *65*, 736-741.

Yilmaz, A., Peretz, M., Sagi, I., and Benvenisty, N. (2016). Haploid Human Embryonic Stem Cells: Half the Genome, Double the Value. Cell Stem Cell *19*, 569-572.

Yoon, Y.M., Lee, J.H., Yun, S.P., Han, Y.S., Yun, C.W., Lee, H.J., Noh, H., Lee, S.J., Han, H.J., and Lee, S.H. (2016). Tauroursodeoxycholic acid reduces ER stress by regulating of Akt-dependent cellular prion protein. Scientific reports *6*, 39838.

Yoshizawa, K., Yaguchi, K., and Uehara, R. (2020). Uncoupling of DNA Replication and Centrosome Duplication Cycles Is a Primary Cause of Haploid Instability in Mammalian Somatic Cells. Front Cell Dev Biol *8*, 721.

Zhu, Z.W., Friess, H., Wang, L., Abou-Shady, M., Zimmermann, A., Lander, A.D., Korc, M., Kleeff, J., and Buchler, M.W. (2001). Enhanced glypican-3 expression differentiates the majority of hepatocellular carcinomas from benign hepatic disorders. Gut *48*, 558-564.

Zinszner, H., Kuroda, M., Wang, X., Batchvarova, N., Lightfoot, R.T., Remotti, H., Stevens, J.L., and Ron, D. (1998). CHOP is implicated in programmed cell death in response to impaired function of the endoplasmic reticulum. Genes & development *12*, 982-995.

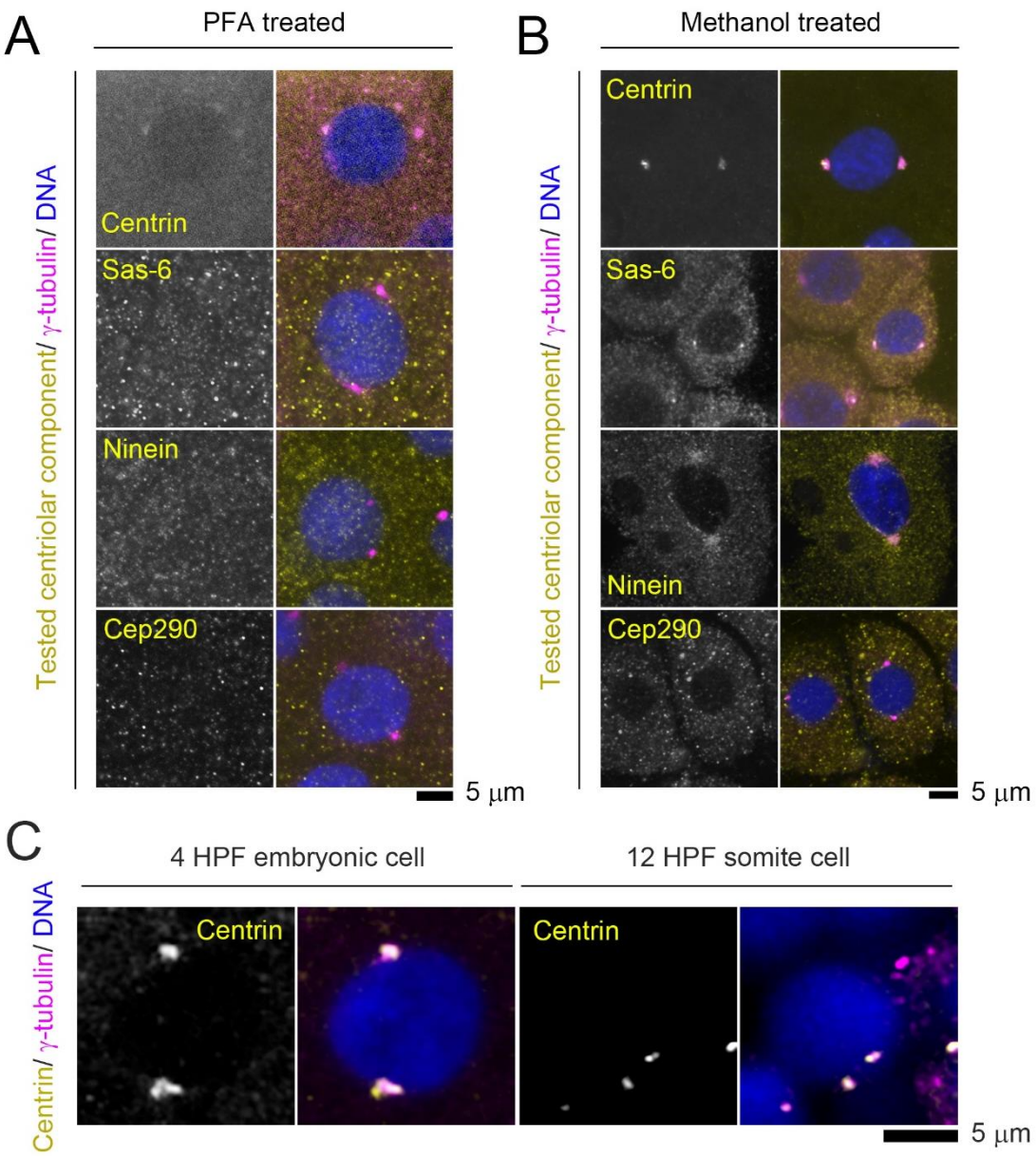

Figure 1. Immunostaining of centriole components in zebrafish embryos

(A, B) Normally fertilized embryos were fixed at 4 h post-fertilization (HPF) with 4 % PFA in PBS at 25℃ for 6 h (A) or chilled-MetOH at –20℃ for 10 min (B), followed by the immunostaining using centriolar protein antibodies. **(C)** Representative image of 4 HPF embryonic cells and 12 HPF somite cells from two independent experiments.

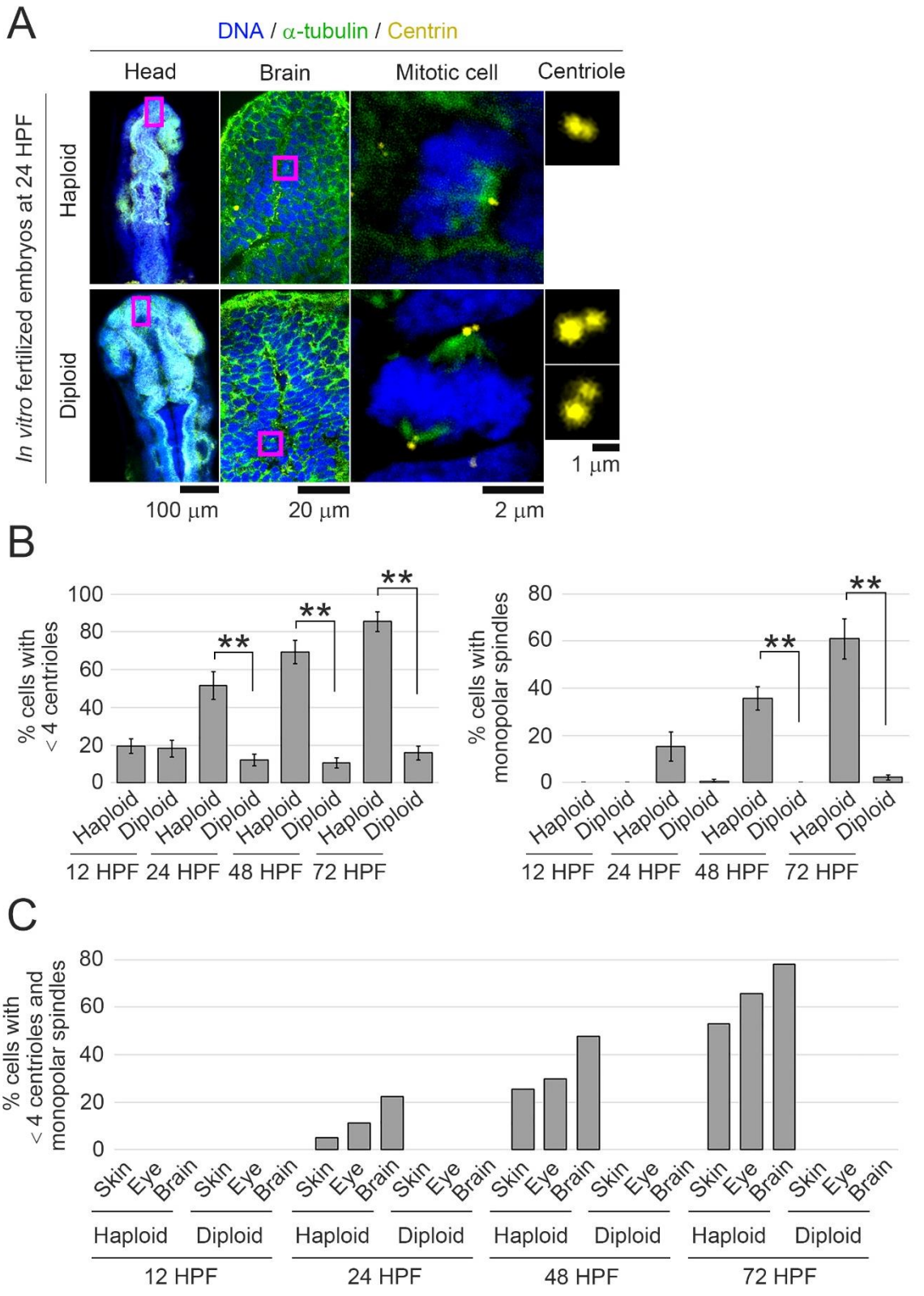
A
DNA / α-tubulin / Centrin
Head
Brain
Mitotic cell
Centriole
In vitro fertilized embryos at 24 HPF
Haploid
Diploid
100 μm
20 μm
2 μm
1 μm
B
% cells with < 4 centrioles
% cells with monopolar spindles
Haploid
Diploid
12 HPF
24 HPF
48 HPF
72 HPF
**
C
% cells with < 4 centrioles and monopolar spindles
Skin
Eye
Brain
Haploid
Diploid
12 HPF
24 HPF
48 HPF
72 HPF

Figure 2. Centriole loss in haploid embryos during late developmental stages

(A) Immunostaining of centrin, α-tubulin and DNA in 24 HPF *in vitro* fertilized haploid and diploid embryos. **(B, C)** Frequency of centriole loss (B) and monopolar spindle formation (C) in head region of haploid and diploid embryos at 12, 24, 48 and 72 HPF. Values represent means ± standard error (SE) of at least 4 embryos. More than 80 cells from at least 2 independent experiments were analyzed at each developmental time point (**, $P < 0.01$, *t* test). **(D)** Frequency of monopolar spindle formation with centriole loss in skin, eye and brain. At least 11 cells from the analysis in (B) and (C) were categorized analyzed for each developing tissue.

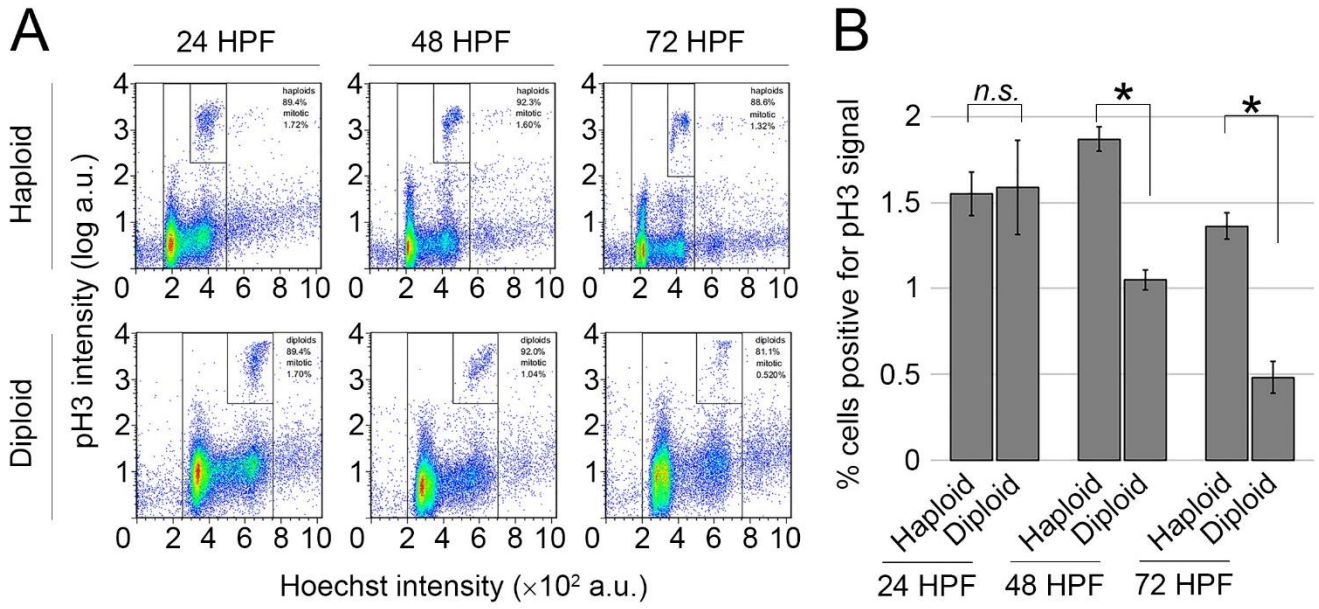

Figure 3. Increase in the proportion of mitotic cells in haploid embryos

(A) Flow cytometric analysis of DNA content and mitotic index in haploid and diploid embryos at 24, 48 and 72 HPF. Co-stained cells with Hoechst and phosphor-histone pH3 antibody were analyzed. Dot plots of the pH3 signal against the Hoechst signal are shown. **(B)** Quantification of the proportion of cells positive for phospho histone pH3 signal in haploid and diploid embryonic cells in (A). Values represent means ± SE of at least three independent experiments for each developmental time point (*, $P < 0.05$, *t* test).

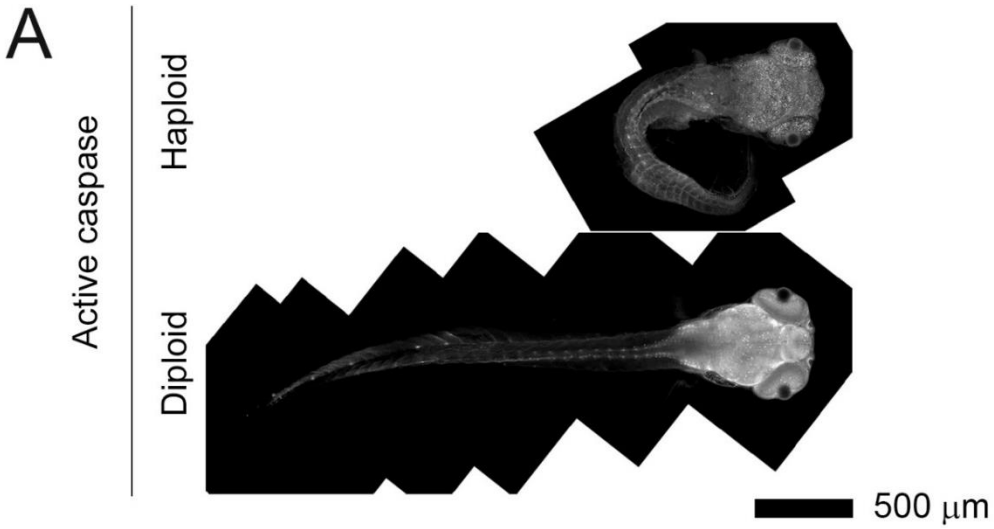
A
Active caspase
Haploid
Diploid
500 μm

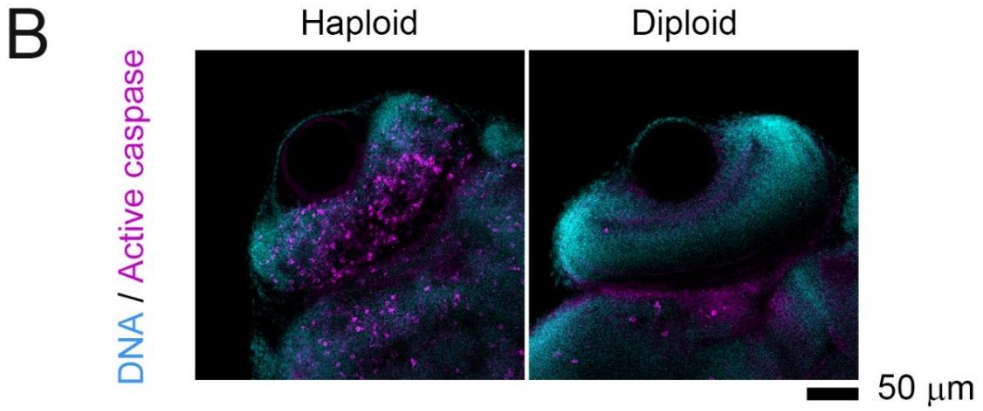
B
Haploid
Diploid
DNA / Active caspase
50 μm

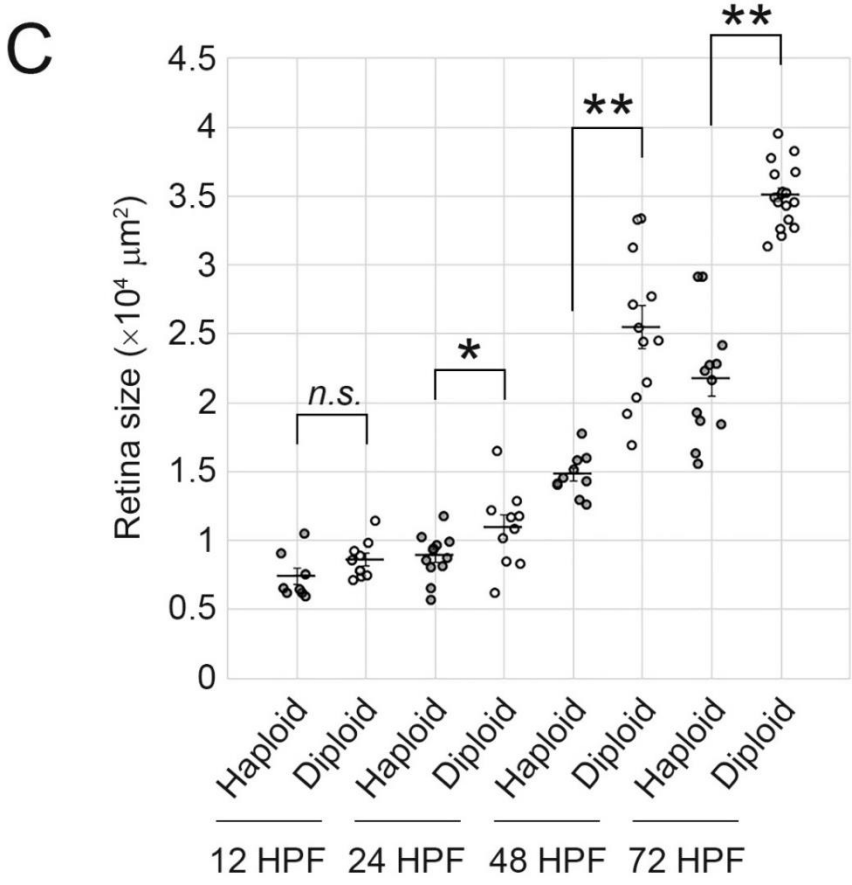
C
Retina size (×10⁴ μm²)
4.5
4
3.5
3
2.5
2
1.5
1
0.5
0
n.s.
*
**
**
Haploid
Diploid
Haploid
Diploid
Haploid
Diploid
Haploid
Diploid
12 HPF
24 HPF
48 HPF
72 HPF

Fig. 4 Apoptosis in neuronal tissues of haploid embryos with the shrinkage of the organ size

(A) Immunostaining of active caspase in 72 HPF haploid and diploid embryos. Representative images from at least two experiments are shown. **(B)** Enlarged retina region of immunostaining of active caspase with DAPI. **(C)** Quantification of eye surface in fixed haploid and diploid embryos at 12, 24, 48 and 72 HPF in Fig. 1. Values represent means ± SE of at least 8 eyes from two independent experiments (*, $P < 0.05$; **, $P < 0.01$, *t* test).

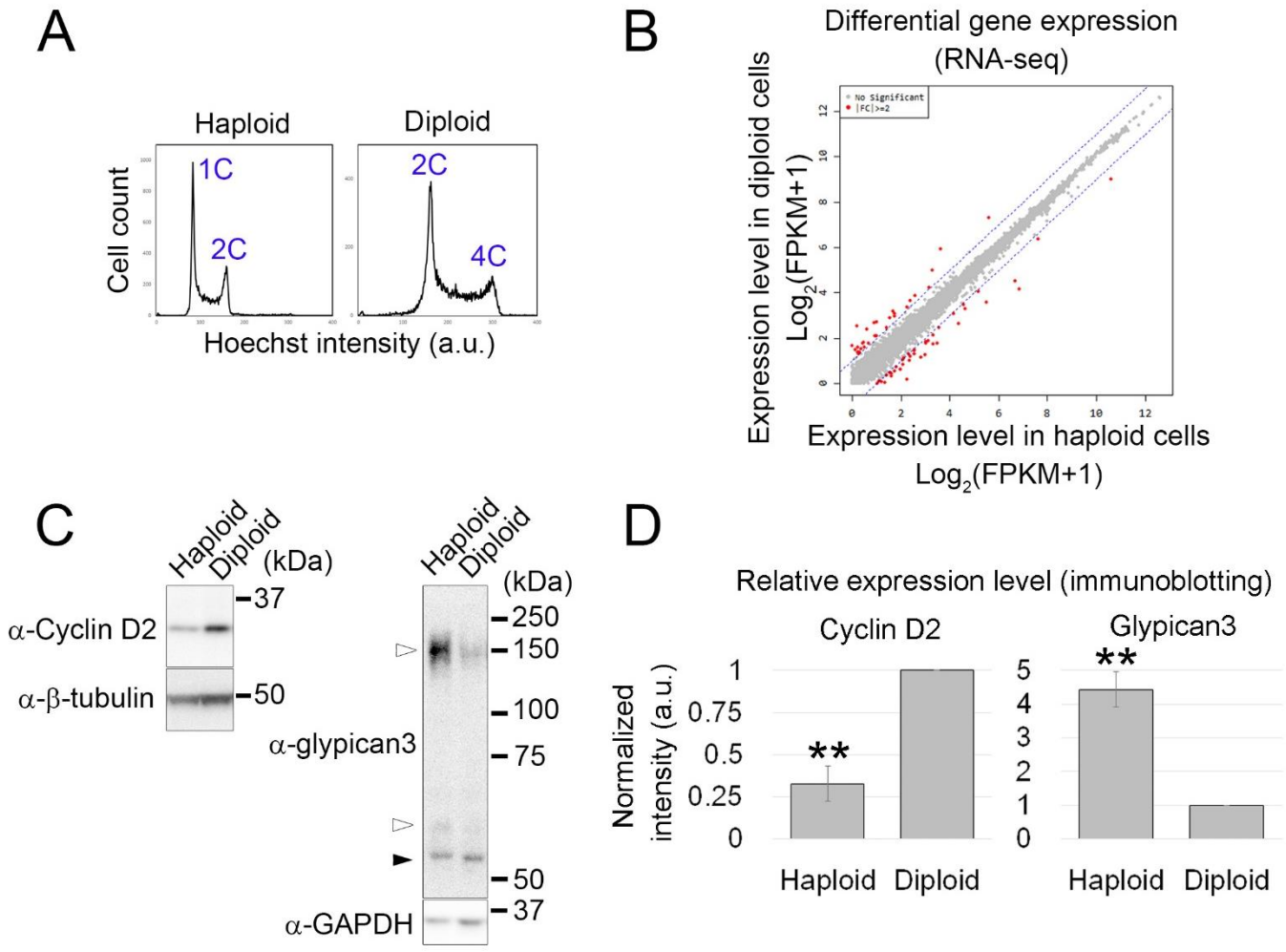

Figure 5. Ploidy-dependent change in gene expression between haploid and diploid HAP1 cells

(A) Flow cytometric analysis of DNA content in Hoechst-stained haploid and diploid HAP1 cells. **(B)** Scatter plot of gene expression level between haploid and diploid HAP1 cells in differentially expressed gene analysis. Genes with more than 2-fold difference in $\log_2$ (FPKM+1) values were indicated in red. **(C)** Immunoblotting of cyclin D2 and glypican3 in haploid and diploid cells. Solid and open arrowhead correspond to unglycosylated and glycosylated forms of glypican3, respectively. Equal total protein amount of sample was loaded to each lane. β-tubulin or GAPDH was detected as a loading control. **(D)**

Quantification of immunoblotting signals in (C). Signal intensities were normalized to those of the loading control. Mean ± SE of 3 independent experiments (**, $P < 0.01$, *t* test).

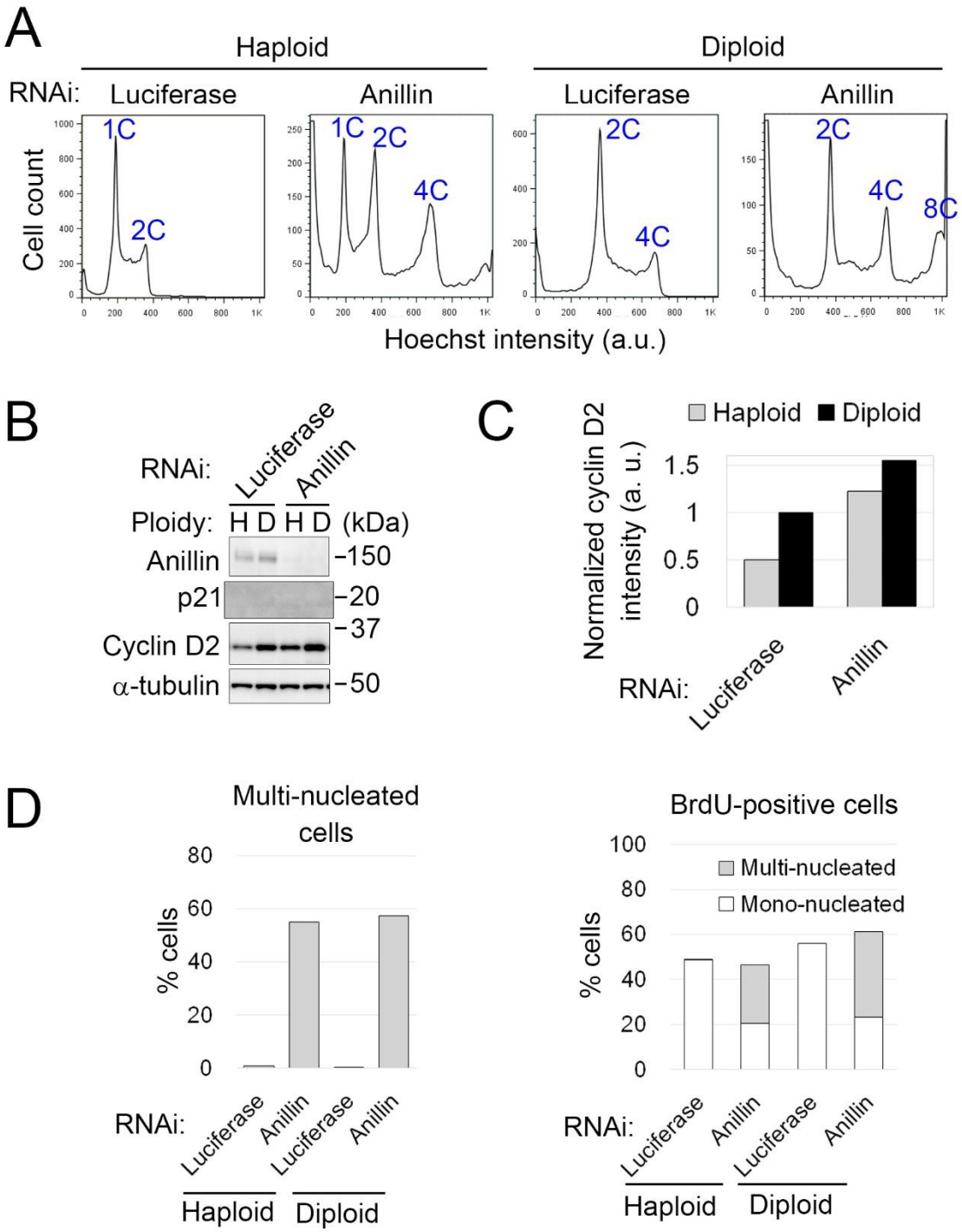

Figure 6. Acute diploidization results in upregulation of cyclin D expression

(A) Flow cytometric analysis of DNA content in RNAi-treated Hoechst-stained haploid and

diploid cells. **(B)** Immunoblotting of anillin, p21 and cyclin D in control and anillin-depleted haploid and diploid HAP1 cells. α-tubulin was detected as a loading control. **(C)** Quantification of immunostaining signals in B. Signal intensities were normalized to those of the loading control, and then to that of diploid mock-depleted cells. Mean of two independent experiments. **(D)** Frequency of multi-nucleated cells (left) or BrdU-incorporated cells population (right) in RNAi-treated haploid or diploid cells. Mean of two independent experiments. At least 393 cells were analyzed for each condition.

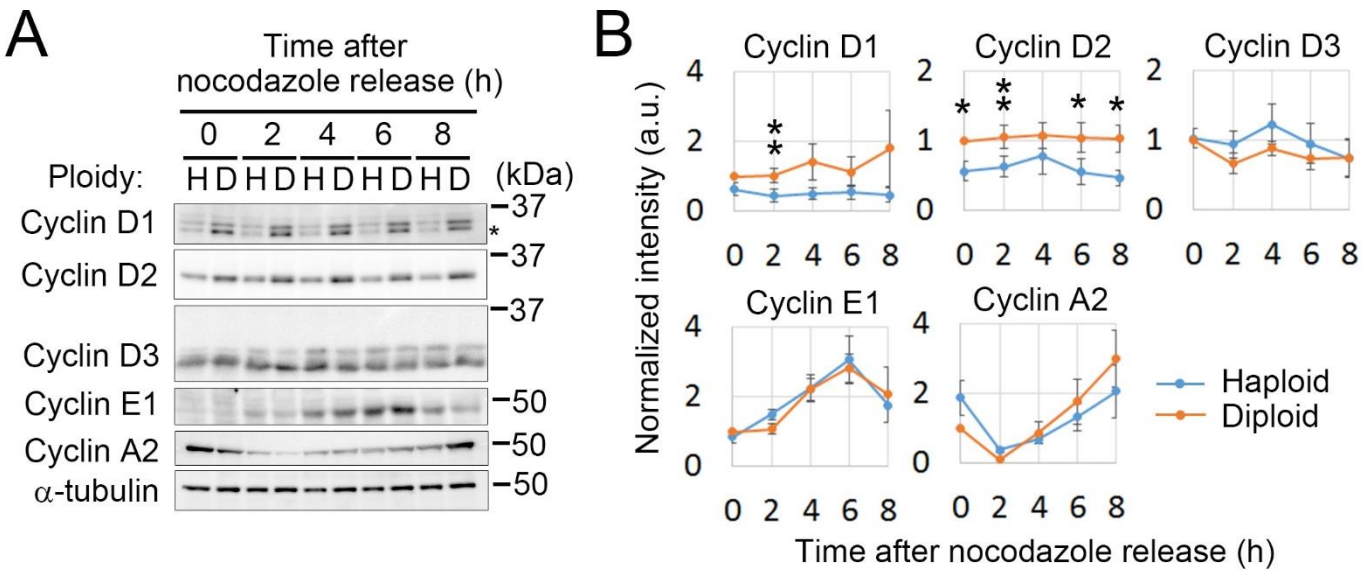

Figure 7. Expression of G1/S cyclins in synchronized haploid and diploid cells

(A) Immunoblotting of G1/S cyclins in synchronized haploid or diploid cells. Equal total protein amount of sample was loaded to each lane. α-tubulin was detected as a loading control. Asterisk indicates cross-reaction of anti-cyclin D1 and cyclin D2. **(B)** Quantification of immunostaining signals in A. Signal intensities were normalized to those of the loading control, and then to that of diploid cells at 0 h after nocodazole release. Mean ± SE of three independent experiments (*, $P < 0.05$; **, $P < 0.01$, *t* test).

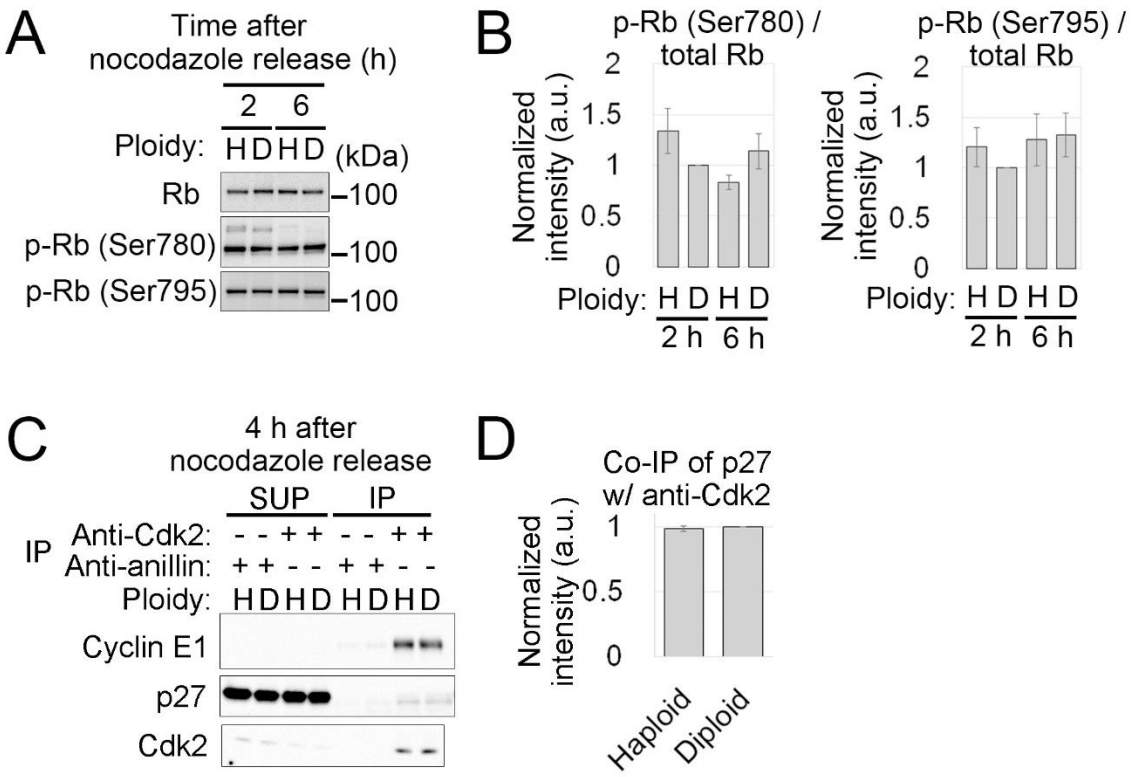

Figure 8. The initiation of S phase is not perturbed in haploid cells

(A) Immunoblotting of G1/S phosphorylated Rb in synchronized haploid or diploid cells. Equal total protein amount of sample was loaded to each lane. **(B)** Quantification of immunostaining signals in A. Signal intensities were normalized to those of the loading control, and then to that of diploid cells at 2 h after nocodazole release. Mean ± SE of three independent experiments. **(C)** Immunoblotting of cyclin E1, p27 and cdk2 in immunoprecipitant obtained using anti-cdk2 antibody from synchronized haploid or diploid cells. Anti-anillin antibody was used as negative control. **(D)** Quantification of p27 co-immunoprecipitated with cdk2 in F. Mean ± SE of three independent experiments.

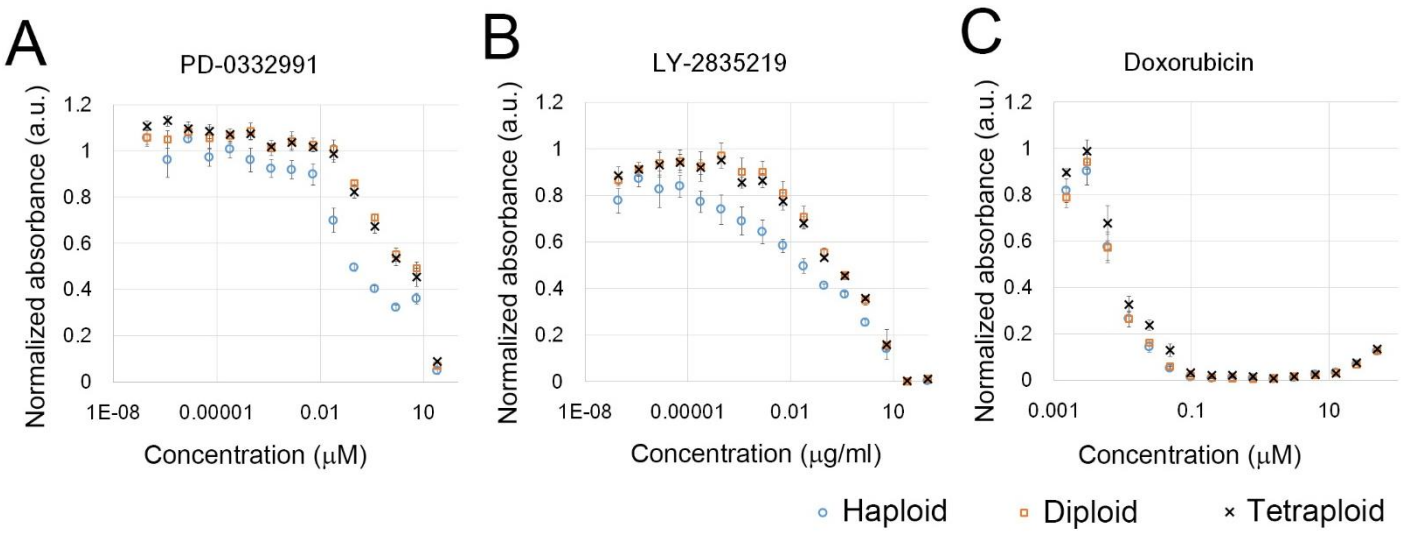

Figure 9. Haploid cells are more susceptible to cdk4/6 inhibitors

(A-C) Effects of PD-332991 (A), LY-2835219 (B), and Doxorubicin (C) on growth of haploid, diploid and tetraploid HAP1 cells. Cells were treated with each compound for 48 h, and their growth was quantified by the CCK-8 assay. Absorbance at 450 nm measured of each sample was normalized to that of non-treated control with the corresponding ploidy. Mean ± SE of four samples from two independent experiments.

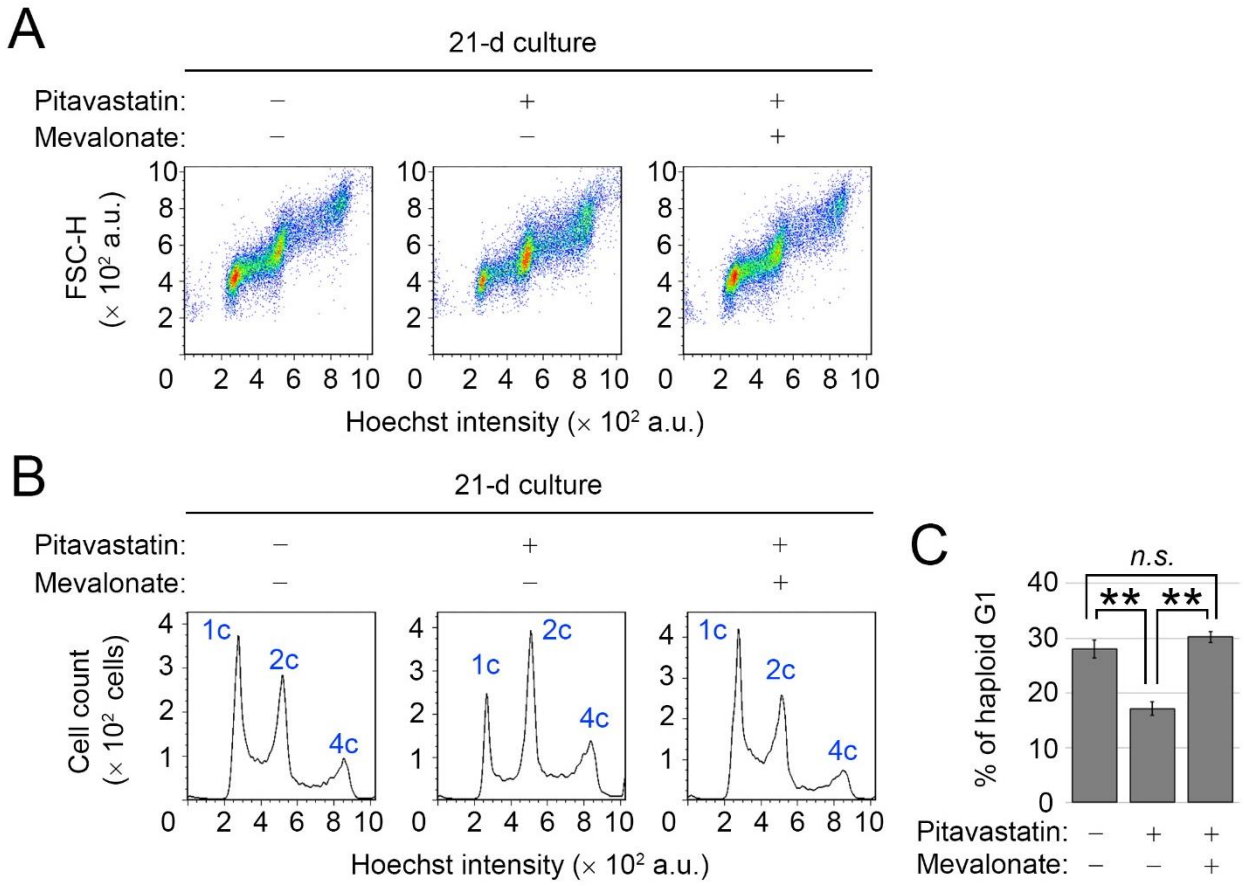

Figure 10. Destabilization of the haploid state by inhibition of the mevalonate pathway in HAP1 cells.

(A, B) Flowcytometric analysis of DNA content in Hoechst-stained cells after 21-d culture. Cells were cultured in the absence or presence of 0.5 μM pitavastatin with or without 20 μM mevalonate supplementation. Dot plots of forward scatter signal (for the judgement of relative cell size) against Hoechst signal (A) and histograms of Hoechst signal (B). **(C)** The proportion of haploid G1 population in B. Mean ± SE of three independent experiments (day 20 or 21 in the long-term passages, **, $P < 0.01$, one-way ANOVA with Tukey post-hos test).

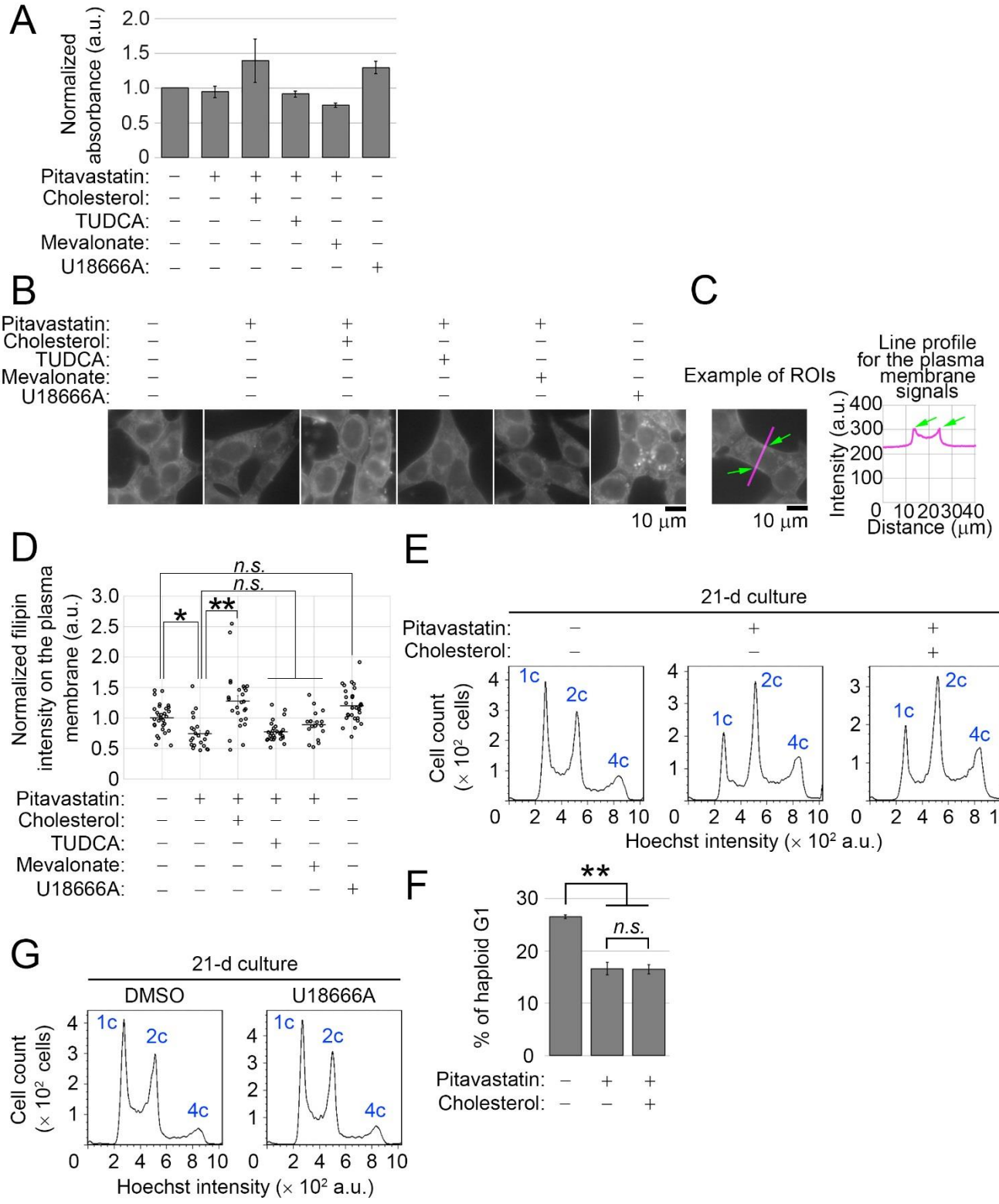
A
Normalized absorbance (a.u.)
2.0
1.5
1.0
0.5
0
Pitavastatin: – + + + + –
Cholesterol: – – + – – –
TUDCA: – – – + – –
Mevalonate: – – – – + –
U18666A: – – – – – +
B
Pitavastatin: – + + + + –
Cholesterol: – – + – – –
TUDCA: – – – + – –
Mevalonate: – – – – + –
U18666A: – – – – – +
10 μm
C
Example of ROIs
10 μm
Line profile for the plasma membrane signals
Intensity (a.u.)
400
300
200
100
0 10 20 30 40
Distance (μm)
D
Normalized filipin intensity on the plasma membrane (a.u.)
n.s.
n.s.
*
**
3.0
2.5
2.0
1.5
1.0
0.5
0
Pitavastatin: – + + + + –
Cholesterol: – – + – – –
TUDCA: – – – + – –
Mevalonate: – – – – + –
U18666A: – – – – – +
E
21-d culture
Pitavastatin: – + +
Cholesterol: – – +
Cell count (× 10² cells)
1c
2c
4c
0 2 4 6 8 10
Hoechst intensity (× 10² a.u.)
F
**
n.s.
% of haploid G1
30
20
10
0
Pitavastatin: – + +
Cholesterol: – – +
G
21-d culture
DMSO
U18666A
Cell count (× 10² cells)
1c
2c
4c
0 2 4 6 8 10
Hoechst intensity (× 10² a.u.)

Figure 11. Ether supplementation or perturbation of cholesterol does not affect haploid stability

(A) Fluorescence microscopy of HAP1 cells stained by filipin after treating the compounds for 1 d. **(B, C)** Quantification of filipin fluorescence intensity on the plasma membrane in A. The fluorescence signals on the plasma membrane were quantified from the line profiles taken across the cells, as shown in B. Mean ± SE of at least 18 cells from two independent experiments (*, $P < 0.05$; **, $P < 0.01$, one-way ANOVA with Tukey post-hos test). **(D)** DNA content analysis after 21-d culture. Cells were cultured in the absence or presence of 0.5 μM pitavastatin with or without 10 μM cholesterol supplementation. **(E)** The proportion of the haploid G1 population in D. Mean ± SE of three independent experiments (day 21 in the long-term passages, **, $P < 0.01$, one-way ANOVA with Tukey post-hos test). **(F)** DNA content analysis after 21-d culture. Cells were cultured in the absence or presence of 2.5 μM U18666A. Representative data from two independent experiments.

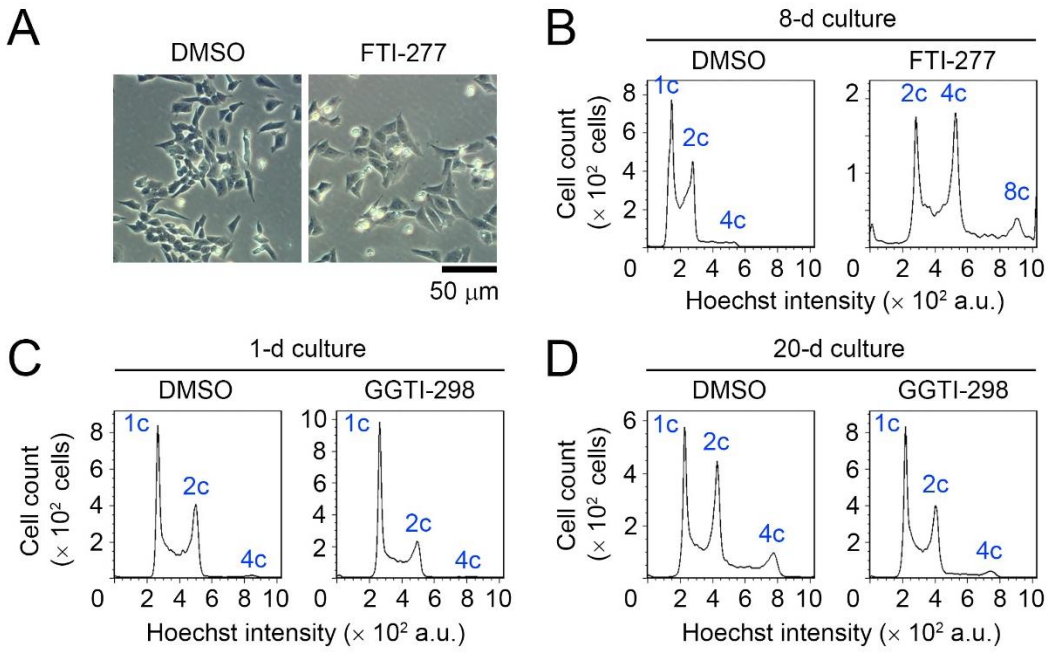

Figure 12. Inhibition of protein prenylation does not phenocopy the statin-induced haploid destabilization

(A) Transparent microscopy of HAP1 cells treated with or without 20 μM FTI-277 for 2 d. Representative data from two independent experiments. **(B-D)** DNA content analysis after 8-d (B), 1-d (C), or 20-d culture (D). Cells were cultured with or without 20 μM FTI-277 (B) or 2 μM GGTI-298 (C, D). Representative data from two independent experiments.

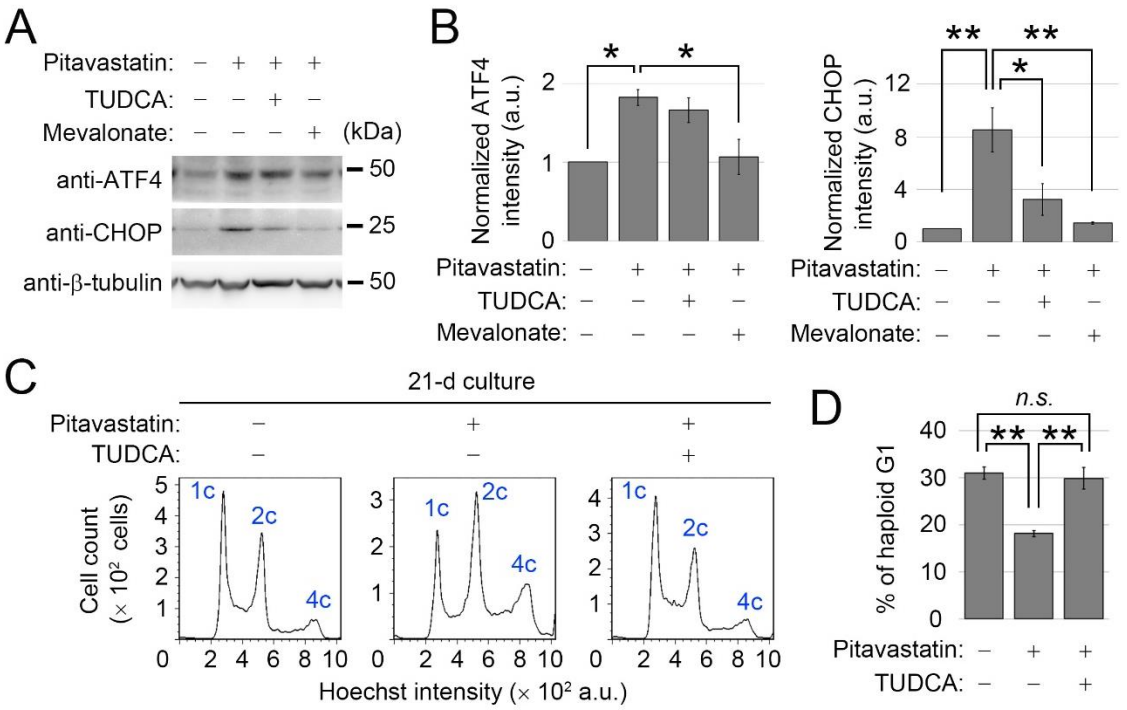

Figure 13. Amelioration of ER stress improves haploid stability in pitavastatin-treated cells

(A) Immunoblotting of ATF4 and CHOP in HAP1 cells treated with the compounds for 3 d. β-tubulin was detected as a loading control. **(B)** Quantification of relative expression of ATF4 and CHOP in A. Mean ± SE of three independent experiments (*, $P < 0.05$; **, $P < 0.01$, one-way ANOVA with Tukey post-hos test). **(C)** DNA content analysis after 21-d culture. Cells were cultured in the absence or presence of 0.5 μM pitavastatin with or without 2.5 mM TUDCA. (D) The proportion of the haploid G1 population in C. Mean ± SE of three independent experiments (day 21 in the long-term passages, **, $P < 0.01$, one-way ANOVA with Tukey post-hos test).

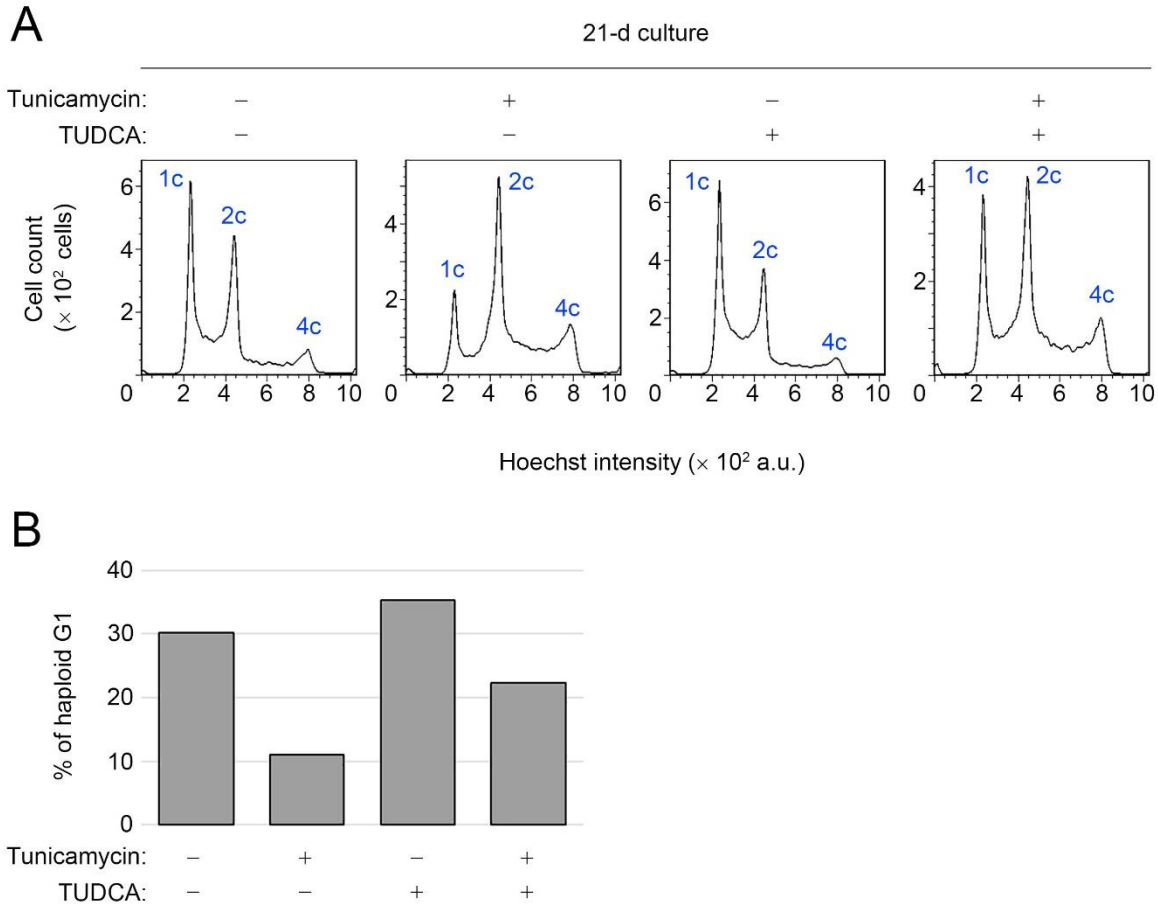

Figure 14. TUDCA stabilized haploidy in the presence and absence of tunicamycin

(A) DNA content analysis after 21-d culture. Cells were cultured in the absence or presence of 50 nM tunicamycin with or without 2.5 mM TUDCA. **(B)** The proportion of haploid G1 population in B. Mean of two independent experiments. (day 21 or 23 in the long-term passages).

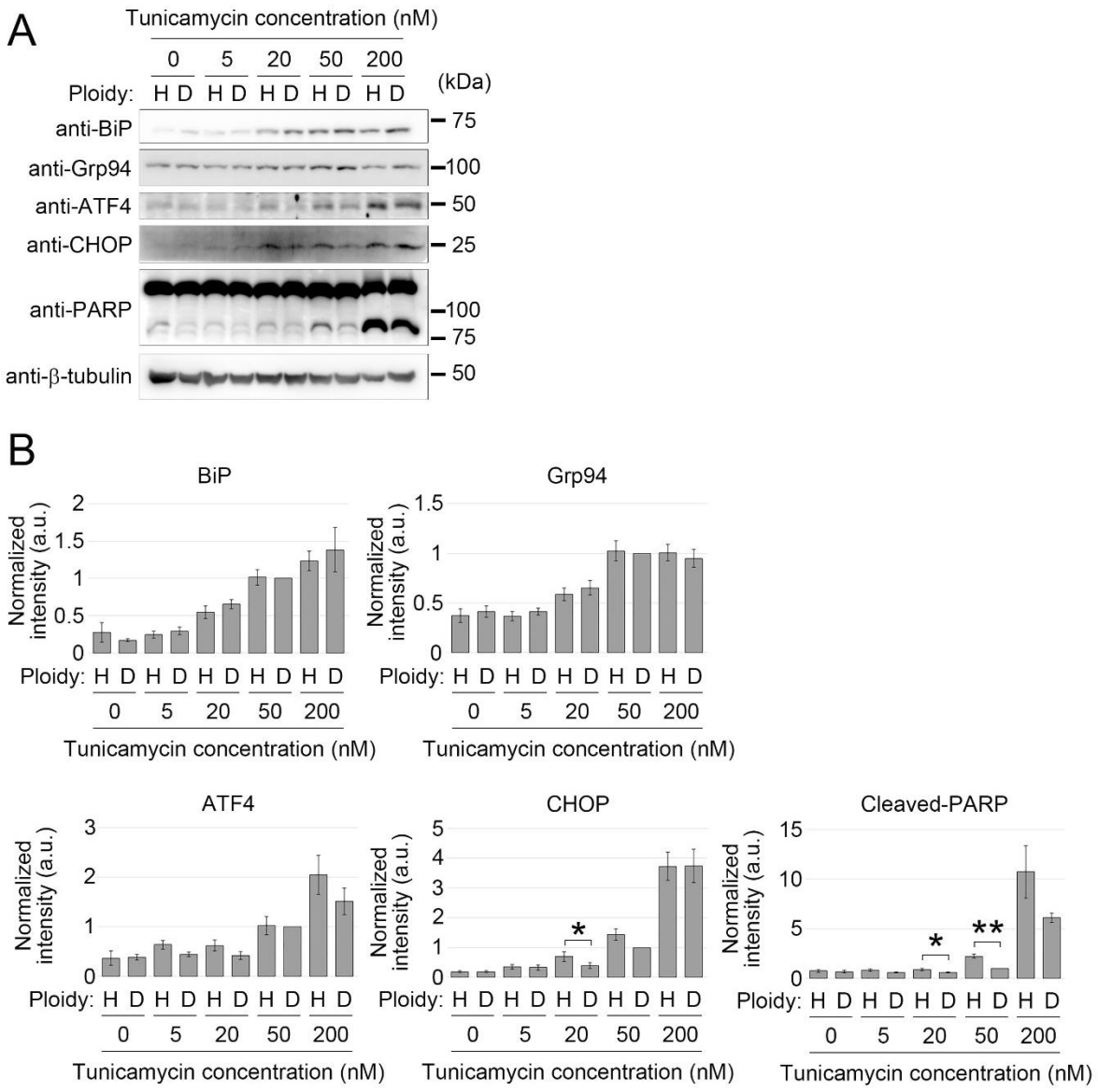

Figure 15. Low magnitude of ER stress induces haploid-specific apoptosis

(A) Immunoblotting of BiP, Grp94, ATF4, CHOP and PARP in HAP1 cells treated with the several concentration of tunicamycin for 1 d. β-tubulin was detected as a loading control. **(B)** Quantification of relative expression of UPR components and cleaved-PARP in A. Mean ± SE of at least five independent experiments (*, $P < 0.05$; **, $P < 0.01$, *t* test).

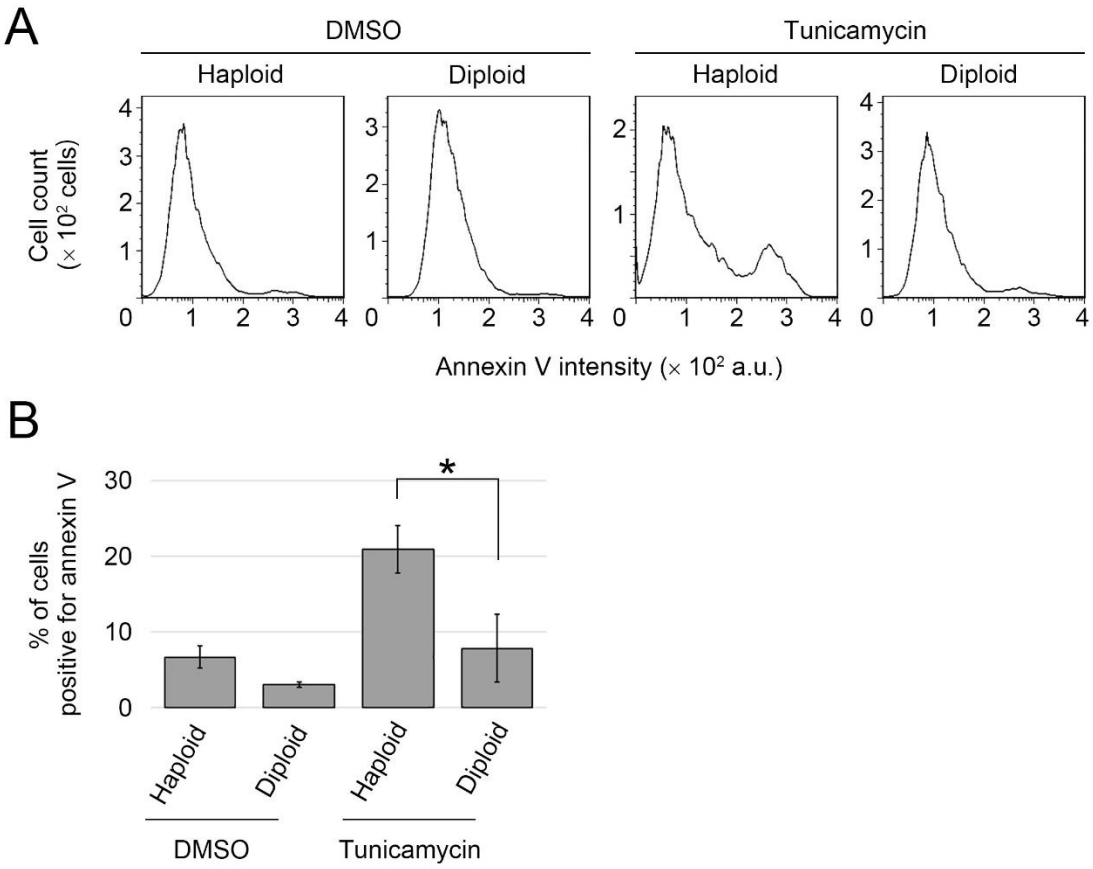

Figure 16. Increase in the apoptotic cells in tunicamycin-treated haploid cells

(A) Flow cytometric analysis of annexin V-FITC intensity after 2-d culture in the presence of 50 nM tunicamycin. **(B)** The proportion of cell population positive for annexin V-FITC in A. Mean ± SE of three independent experiments (*, $P < 0.05$, *t* test).

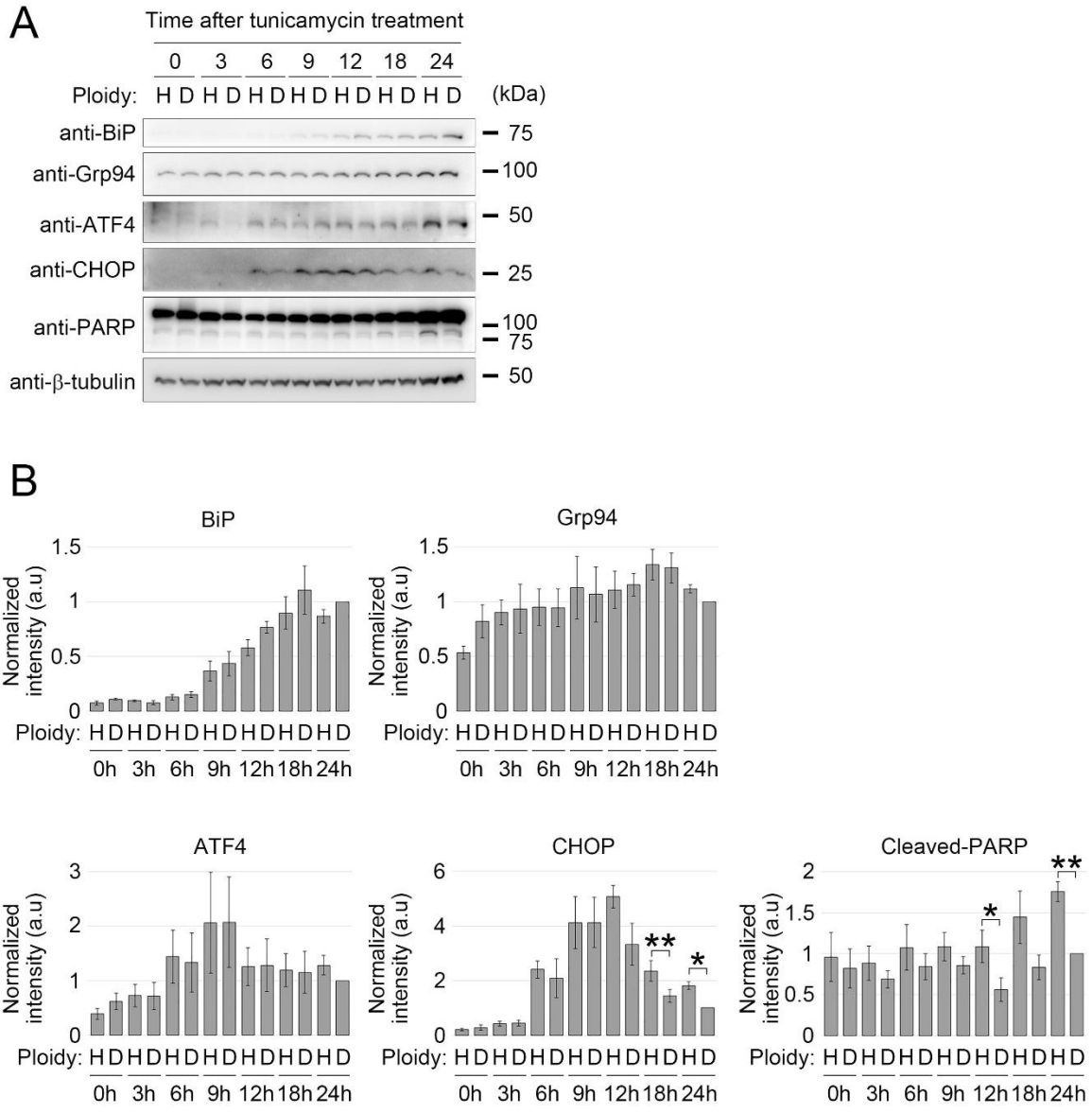

Figure 17. Haploid cells sustaining high CHOP expression activated proapoptotic pathway

(A) Immunoblotting of BiP, Grp94, ATF4, CHOP and PARP in HAP1 cells treated with 50 nM tunicamycin. β-tubulin was detected as a loading control. **(B)** Quantification of relative expression of UPR components and cleaved-PARP in A. Mean ± SE of four independent

experiments (*, $P < 0.05$; **, $P < 0.01$, *t* test).

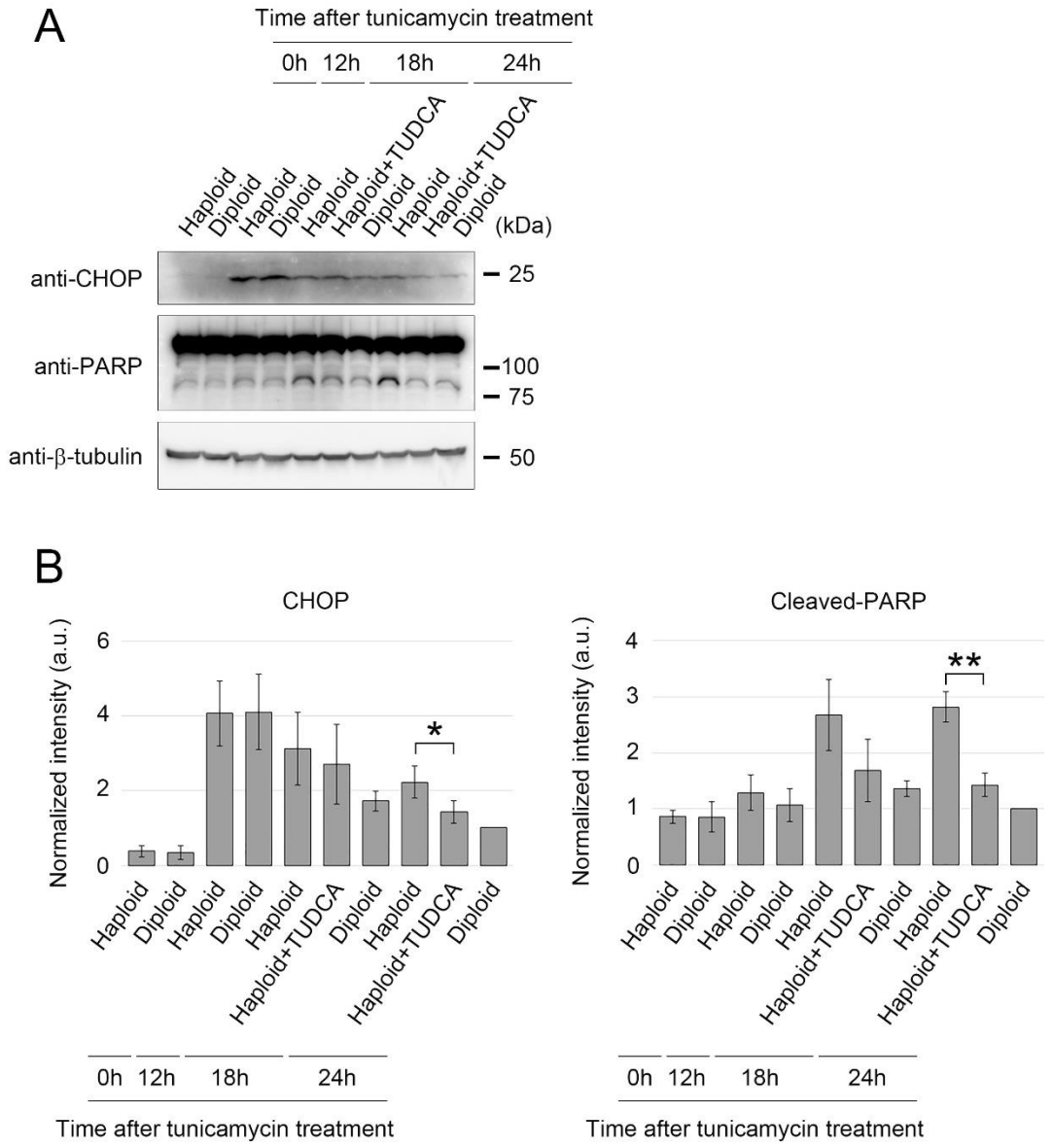

Figure 18. Amelioration of extended ER stress cancels the apoptosis in haploid cells

(A) Immunoblotting of CHOP and PARP in HAP1 cells treated with 50 nM tunicamycin. . β-tubulin was detected as a loading control. **(B)** Quantification of relative expression of UPR components in A. Mean ± SE of four independent experiments (*, $P < 0.05$; **, $P < 0.01$, *t* test).

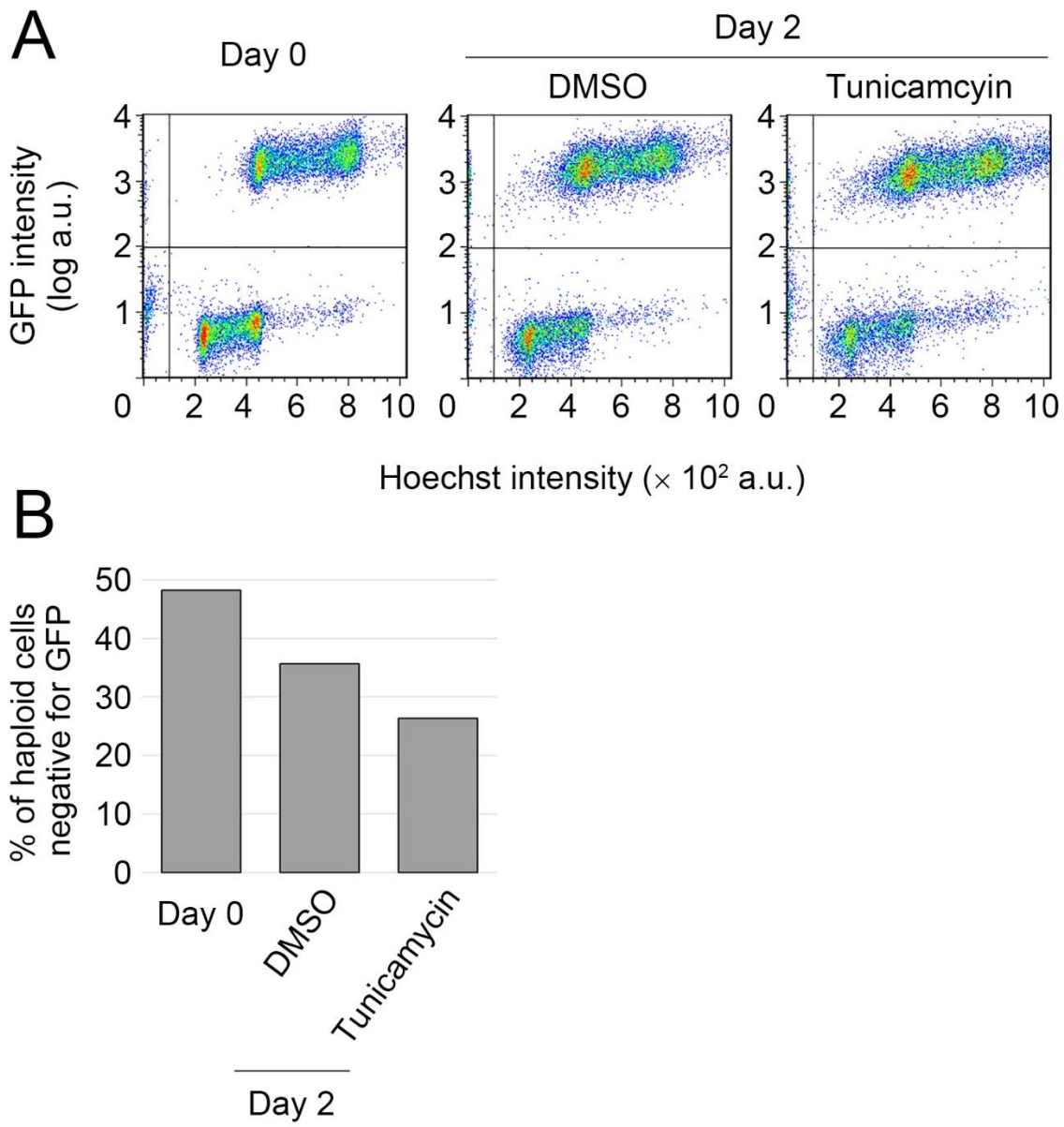

Figure 19. Relative growth efficacy of haploid cells was reduced by the low magnitude of ER stress in the co-culture with diploid cells

(A) The same cell number of haploid WT and diploid stably expressing GFP empty vector were mixed and co-cultured for 2 d in the presence or absence of 50 nM tunicamcyin. Dot plots of GFP intensity (for the judgement of original ploidy of cells) against Hoechst signal.

(B) The proportion of haploid cells negative for GFP signals in A. Mean of two independent experiments.

Acknowledgement

First, I would like to express the deepest gratitude to my supervisor, Dr. Ryota Uehara. His scientific thinking dramatically improved my skills to conduct experiments and to logically construct my work. And all members of Uehara laboratory kindly helped me with scientific discussion whenever.

I gratefully appreciate to Professor Tokiyoshi Ayabe, Professor Hisashi Haga and Professor Hiroshi Hinou for continuing encouragement and giving me valuable advice with brilliant logic, which always conceptually expanded the big pictures in my current research.

I would like to express extensive gratitude to Professor Sreelaja Nair and Dr. Triveni Menon at Tata Institute for Fundamental Research in Mumbai. Thanks to them, I could deepen the concept of developmental biology and develop practical technique for embryology. I would like to express grateful gratitude to Professor Gabor Banhegyi and Dr. Eva Margittai at Semmelweis University in Budapest. I obtained lots of materials and learned the latest knowledge of the metabolism from them. I really appreciate to Dr. Kohei Yuyama and Dr. Daisuke Mikami. They kindly told me how to conduct experiments for cholesterol quantification.

I appreciate the financial support from Research Fellowship of Japan Society for the Promotion of Science (JSPS) for Young Scientists and Scholarship of Japan student Services Organization. This study was supported by JSPS KAKENHI Grant Number 19J12210 from Grant-in-Aid for JSPS Fellow.

Publication

1. Uncoordinated centrosome cycle underlies the instability of non-diploid somatic cells in mammals.
   Yaguchi K, Yamamoto T, Matsui R, Tsukada Y, Shibanuma A, Kamimura K, Koda T, Uehara R.
   J Cell Biol. 2018 Jul 2;217(7):2463-2483

2. Ploidy dependent change in cyclin D2 expression and sensitization to cdk4/6 inhibition in human somatic haploid cells.
   Yaguchi K, Yamamoto T, Shimada M, Sugimoto R, Nakamura K, Ayabe T, Uehara R.
   Biochem Biophys Res Commun. 2018 Sep 26;504(1)231-237

3. Mevalonate pathway-mediated ER homeostasis is required for haploid stability in human somatic cells.
   Yaguchi K, Sato K, Yoshizawa K, Mikami D, Yuyama K, Igarashi Y, Banhegyi G, Margittai E, Uehara R.
   Cell Struct Funct. 2020 Dec 22. Accepted

JCB Journal of Cell Biology

ARTICLE

Uncoordinated centrosome cycle underlies the instability of non-diploid somatic cells in mammals

Kan Yaguchi[1], Takahiro Yamamoto[1*], Ryo Matsui[1*], Yuki Tsukada[2], Atsuko Shibanuma[3], Keiko Kamimura[1], Toshiaki Koda[1,4], and Ryota Uehara[1,3,4]

In animals, somatic cells are usually diploid and are unstable when haploid for unknown reasons. In this study, by comparing isogenic human cell lines with different ploidies, we found frequent centrosome loss specifically in the haploid state, which profoundly contributed to haploid instability through subsequent mitotic defects. We also found that the efficiency of centriole licensing and duplication changes proportionally to ploidy level, whereas that of DNA replication stays constant. This caused gradual loss or frequent overduplication of centrioles in haploid and tetraploid cells, respectively. Centriole licensing efficiency seemed to be modulated by astral microtubules, whose development scaled with ploidy level, and artificial enhancement of aster formation in haploid cells restored centriole licensing efficiency to diploid levels. The ploidy–centrosome link was observed in different mammalian cell types. We propose that incompatibility between the centrosome duplication and DNA replication cycles arising from different scaling properties of these bioprocesses upon ploidy changes underlies the instability of non-diploid somatic cells in mammals.

Introduction

Animal species generally have diplontic life cycles, where somatic cell division occurs only during the diploid phase. Exceptionally, haploid or near-haploid animal somatic cells arise through activation of oocytes without fertilization or because of aberrant chromosome loss during tumorigenesis (Wutz, 2014). However, haploidy in animal somatic cells is generally unstable, and haploid cells in a wide variety of species, including insects, amphibians, and mammals, convert to diploid through doubling of the whole genome during successive culture for several weeks both in vitro and in vivo (Freed, 1962; Kaufman, 1978; Debec, 1984; Kotecki et al., 1999; Elling et al., 2011; Leeb and Wutz, 2011; Yang et al., 2013; Essletzbichler et al., 2014; Li et al., 2014; Sagi et al., 2016). This is in sharp contrast to plants and lower eukaryotic organisms, in which haploid somatic cells can proliferate stably (Mable and Otto, 1998; Forster et al., 2007). This raises the possibility that, specifically in animals, the cell replication mechanism is stringently adapted to the diploid state and becomes compromised in haploid cells; however, the physiological impacts of ploidy differences on animal cell replication processes remain largely unknown.

In animal cells, control of centrosome number is essential for precise cell replication. During mitosis, pairs of centrosomes serve as major microtubule (MT) organizing centers for bipolar spindle formation, and irregular numbers of centrosomes form spindles with abnormal polarities, endangering proper chromosome segregation (Gönczy, 2015). Centrosome number control is achieved through elaborate regulation of the centrosome duplication cycle (Loncarek and Bettencourt-Dias, 2018). Upon exit from mitosis, an engaged pair of centrioles comprising a centrosome separate from one another, producing two centrosomes (Kuriyama and Borisy, 1981). This centriole disengagement process is a prerequisite for "licensing" each preexisting centriole to serve as a template for the formation of a daughter centriole in the subsequent cell cycle (Tsou and Stearns, 2006; Tsou et al., 2009). A scaffold protein, Cep152, accumulates on the licensed preexisting centrioles, subsequently recruiting a key centriole duplication regulator, Polo-like kinase 4 (Plk4; Cizmecioglu et al., 2010; Dzhindzhev et al., 2010; Hatch et al., 2010; Kim et al., 2013; Sonnen et al., 2013; Fu et al., 2016). Plk4, in turn, mediates the recruitment of SAS-6 on the outside wall of the preexisting centrioles to form the procentriolar cartwheel, which founds the basis for the subsequent elongation of daughter centrioles (Bettencourt-Dias et al., 2005; Habedanck et al., 2005; Leidel et al., 2005; Kleylein-Sohn et al., 2007; Nakazawa et al., 2007; Dzhindzhev et al., 2014; Fong et al., 2014; Ohta et al., 2014; Moyer et al., 2015). Importantly, there are striking similarities between

[1]Graduate School of Life Science, Hokkaido University, Sapporo, Japan; [2]Division of Biological Science, Graduate School of Science, Nagoya University, Nagoya, Japan; [3]Creative Research Institution, Hokkaido University, Sapporo, Japan; [4]Faculty of Advanced Life Science, Hokkaido University, Sapporo, Japan.

*T. Yamamoto and R. Matsui contributed equally to this paper; Correspondence to Ryota Uehara: ruehara@sci.hokudai.ac.jp.

https://doi.org/10.1083/jcb.201701151

the molecular mechanisms governing temporal regulation of the centriole duplication cycle and DNA replication cycle. A mitotic kinase, Plk1, and a cysteine endoprotease, separase, cooperatively regulate resolution of the connections of the engaged centrioles or paired sister chromatids during or at the end of mitosis, and cyclin E–cdk2 controls the initiation of both centriole duplication and DNA replication during G1/S phase (Matsumoto et al., 1999; Meraldi et al., 1999; Coverley et al., 2002; Nasmyth, 2002; Sumara et al., 2002; Tsou and Stearns, 2006; Tsou et al., 2009). These regulatory mechanisms ensure precise temporal coordination between these two cellular processes, allowing cells to possess a constant number of centrosomes throughout numerous rounds of cell cycles during proliferation.

To determine the cellular processes affected by ploidy difference and understand the origin of intolerance of somatic haploidy in animal cells, we performed side-by-side comparisons of cell replication in isogenic mammalian somatic cells with different ploidy levels. We found that the efficiency of centrosome cycle progression scales proportionally with ploidy level, which uncouples the progression of the centrosome cycle from that of the DNA cycle and compromises centrosome number control in non-diploid states.

Results

Haploidy-specific mitotic defects in human somatic cells

To investigate the effect of ploidy differences on the cell replication process, we used the near-haploid human cell line, HAP1 (Carette et al., 2011). As previously reported, the haploid state of this cell line was unstable, and almost all cells in haploid-enriched culture diploidized over several weeks of passage (Fig. 1 A; Essletzbichler et al., 2014). Diploidized cells were significantly larger than haploid cells (Fig. 1 B and Fig. S1, A–C); therefore, we could purify the isogenic haploid and diploid cell populations separately for side-by-side comparisons using size-based sorting.

We first compared the progression of the cell cycle and cell division in haploid and diploid cells using live imaging (Fig. 1, C–F; and Videos 1, 2, and 3). Mean cell cycle length was significantly greater in haploid than in diploid cells (806 ± 212 and 714 ± 186 min, respectively; $n > 282$; $P < 10^{-8}$, *t* test; Fig. 1 D). We also found that 72 of 1,181 haploid cells (6.0%) showed a severe mitotic delay, spending >50 min in the mitotic phase (Fig. 1, C, E, and F). Of the mitotically arrested haploid cells, 36 entered anaphase and completed cytokinesis, whereas 20 died during mitosis, and the remaining 7 exited the mitotic phase without chromosome segregation (mitotic slippage; Fig. 1, C and F; and Video 2). Importantly, these defects were scarcely observed in diploid cells (Fig. 1 F and Video 3).

Because mitotic slippage doubles DNA content, it can affect haploid stability, even when it occurs at low frequency. We therefore estimated the potential contribution of haploid-specific mitotic defects to haploid instability using a mathematical cell population transition model (described in Materials and methods; source code files are provided in the online supplemental material). In this model, haploid or diploid cells proliferate exponentially, with respective doubling times corresponding to measured cell cycle lengths. Haploid cells die or diploidize through mitotic death or mitotic slippage, respectively, with empirically observed frequencies (Fig. 1 F). A simulated time course of a haploid population using the model was essentially consistent with the experimentally observed diploidization profiles (Fig. 1 G). In the simulation, mitotic slippage at the observed order of frequency could account solely for ∼40% of haploid population loss during 60 d of culture, and haploid stability was sensitive to small changes in the frequency of mitotic slippage (Figs. 1 G and S1 D). Based on the above experimental and theoretical analyses, we propose the following mechanism for haploid instability: haploid-specific cell division failure drives chronic conversion of haploid cells into diploid, which is accompanied by preferential expansion of the diploid population because of its cell-autonomous growth advantage over haploid cells. Because haploid-specific mitotic defects are likely to contribute profoundly to haploid instability, we decided to investigate the cellular mechanisms underlying them.

Frequent centrosome loss and monopolar spindle formation in haploid human somatic cells

To determine the cause of haploid-specific mitotic defects, we investigated the organization of the mitotic spindle in haploid and diploid cells by α-tubulin immunostaining. Whereas the majority of diploid cells possessed bipolar spindles, ∼25% (n = 3) of haploid cells had monopolar spindles (Fig. 2, A and B). Consistently, whereas the majority of diploid mitotic cells had a pair of centrosomes, each of which consisted of two centrioles, we observed loss of centrosomes and centrioles in >20% of haploid mitotic cells (visualized by γ-tubulin and centrin immunostaining, respectively; Fig. 2, C and D; and Fig. S1 E). Even when 10 individual clonal subpopulations were isolated from haploid cell culture by single-cell sorting, the frequent spindle monopolarization and centrosome loss were observed in all these haploid clones (Fig. S1 F). This suggests that the entire population of haploid cells potentially lose their centrosomes over time. Because these haploid and diploid cells were isogenic, the frequent centrosome loss in haploid cells must be a consequence of haploidy rather than genetic background.

To examine the relationship between spindle disorganization and mitotic defects in haploid cells, we performed live imaging using haploid HAP1 cells stably expressing EGFP-α-tubulin (Fig. 2, E and F; Fig. S1 G; and Videos 4, 5, and 6). Of 1,264 cells that entered mitosis, 118 (9.3%) formed monopolar spindles, and of these monopolar cells, 19 later bipolarized and completed mitosis (Fig. 2 E, arrowhead; and Video 5), 48 died in mitosis, and 9 underwent mitotic slippage (Fig. 2, E and F; and Video 6). Importantly, all mitotic slippage events and the majority of mitotic deaths accompanied spindle monopolarization. These results suggest that spindle disorganization caused by haploid-specific centrosome loss makes a major contribution to the mitotic defects in haploid cells.

Cells are more susceptible to centrosome loss in the haploid state than in the diploid state

In general, animal somatic cells without centrosomes can still form bipolar spindles and complete mitosis, albeit with reduced fidelity (Khodjakov et al., 2000; Khodjakov and Rieder, 2001; Sir et al., 2013). The fact that haploid cells suffer from frequent

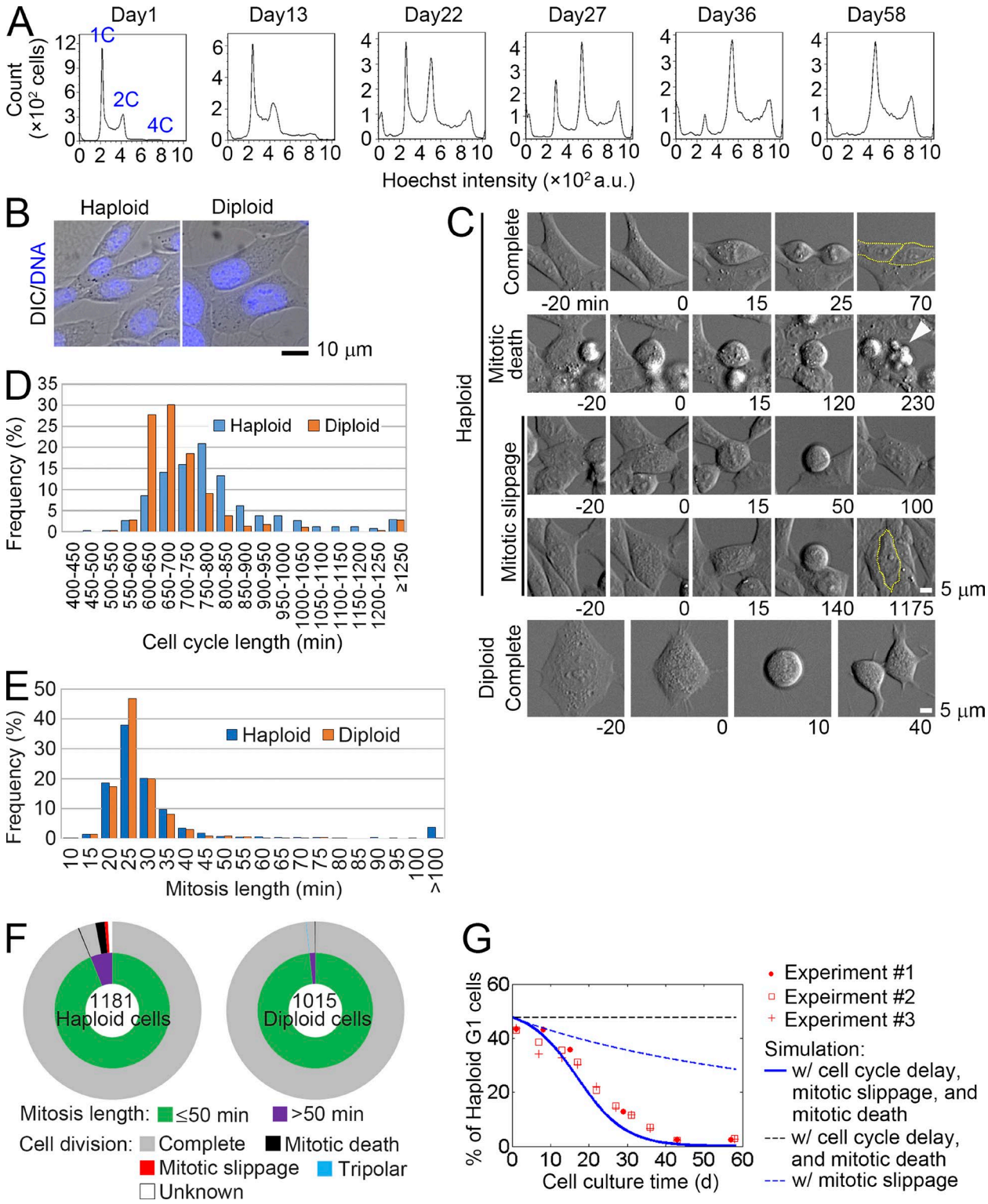

Figure 1. **Haploid-specific mitotic defects and subsequent diploidization in HAP1 cells. (A)** Flow cytometric analysis of DNA content in Hoechst-stained cells during long-term culture. Representative data from three independent experiments are shown. **(B)** Hoechst-stained haploid and diploid cells. **(C)** Live images of haploid and diploid cells taken at 5-min intervals. Nuclear envelope breakdown (NEBD) was set as 0 min. Arrowhead indicates mitotic death. Broken lines mark cell boundaries. **(D and E)** Distribution of cell cycle length (from one NEBD to the next NEBD) or mitotic duration (from NEBD to anaphase onset) quantified from 339 haploid and 285 diploid (D) and 1,180 haploid and 1,015 diploid cells (E), respectively. Data are from at least two independent experiments. **(F)** Classification of mitotic defects (outer circle) sorted by mitotic duration (inner circle) determined based on analysis of 1,181 haploid and 1,015 diploid cells in at least two independent experiments. **(G)** Time course of the haploid G1 fraction during long-term culture of haploid-enriched cells in A. Data from three independent experiments are compared with theoretical model simulations.

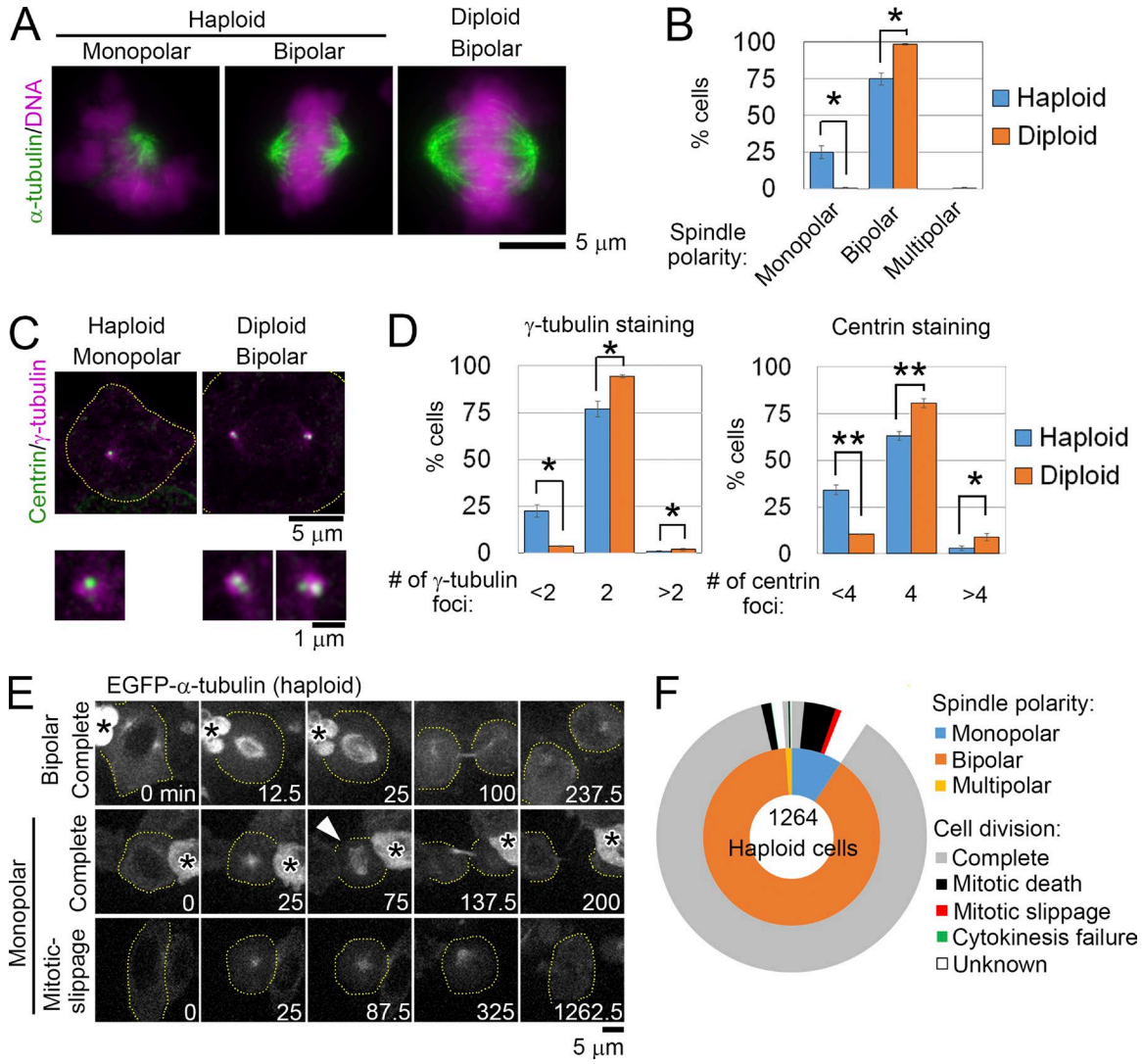

Figure 2. **Centrosome loss and monopolar spindle formation in haploid HAP1 cells. (A and C)** Immunostaining of α-tubulin and chromosomes (stained using DAPI; A), or γ-tubulin and centrin (C) in haploid and diploid mitotic cells. Enlarged images (3×) of centrosomes are shown at bottom in C. **(B and D)** Frequency of spindle polarities (B) and centrosome or centriole numbers (D) in A and C, respectively. Values represent means ± standard error (SE) of three independent experiments (*, $P < 0.05$; **, $P < 0.01$, *t* test). At least 159 (B) or 302 cells (D) were analyzed per condition. **(E)** Live images of haploid EGFP-α-tubulin cells taken at 12.5-min intervals. NEBD was set as 0 min. Arrowhead indicates an acentrosomal pole newly formed from a monopolar spindle. Broken lines show cell boundaries. Asterisks mark neighboring cells. **(F)** Classification of mitotic defects (outer circle) sorted by spindle polarities (inner circle) determined by analysis of 1,264 haploid EGFP-α-tubulin cells from five independent experiments. Cells that moved out of the field of view during the mitotic phase were categorized as unknown.

monopolar spindle formation and mitotic failure upon centrosome loss raises the possibility that cells are particularly susceptible to centrosome loss in the haploid state. To test this possibility, we performed live imaging of haploid and diploid HAP1 cells stably expressing GFP-centrin that were pretreated with a Plk4 inhibitor (centrinone B) for 1 d (Fig. 3, A and B; and Fig. S1 H; Wong et al., 2015). Pretreatment reduced the number of GFP-centrin foci to the same extent (to less than 3) in haploid and diploid cells. Approximately 35% or 11% of centrinone B–treated haploid cells (38 or 12 out of 105 mitotic cells, respectively) showed mitotic death or slippage, respectively. On the contrary, the effect of centrosome loss on mitotic progression was milder in diploid than in haploid cells; ∼18% of the centrinone B–treated diploid cells (20 out of 113 cells) showed mitotic death, which was similar to those reported in other cell lines (Wong et al., 2015), and only 2.6% of these cells (3 out of 113 cells) showed mitotic slippage. We also investigated the impact of the centrinone B–induced centrosome loss on the stability of the haploid or diploid state in HAP1 cells (Fig. 3 C). Interestingly, although DNA content remained almost unchanged after 4 d centrinone B treatment in diploid cells, large populations of haploid cells were converted to the diploid state under the same experimental condition. These results suggest that the haploid state is particularly susceptible to centrosome loss, which, in combination with the haploidy-linked centrosome loss, causes frequent mitotic failure and haploid instability. We observed that diploid HAP1 cells, similar to other cell lines such as HeLa or DLD-1 cells, continued to grow upon chronic centrosome loss after prolonged (>14 d) centrinone B treatment, eliminating

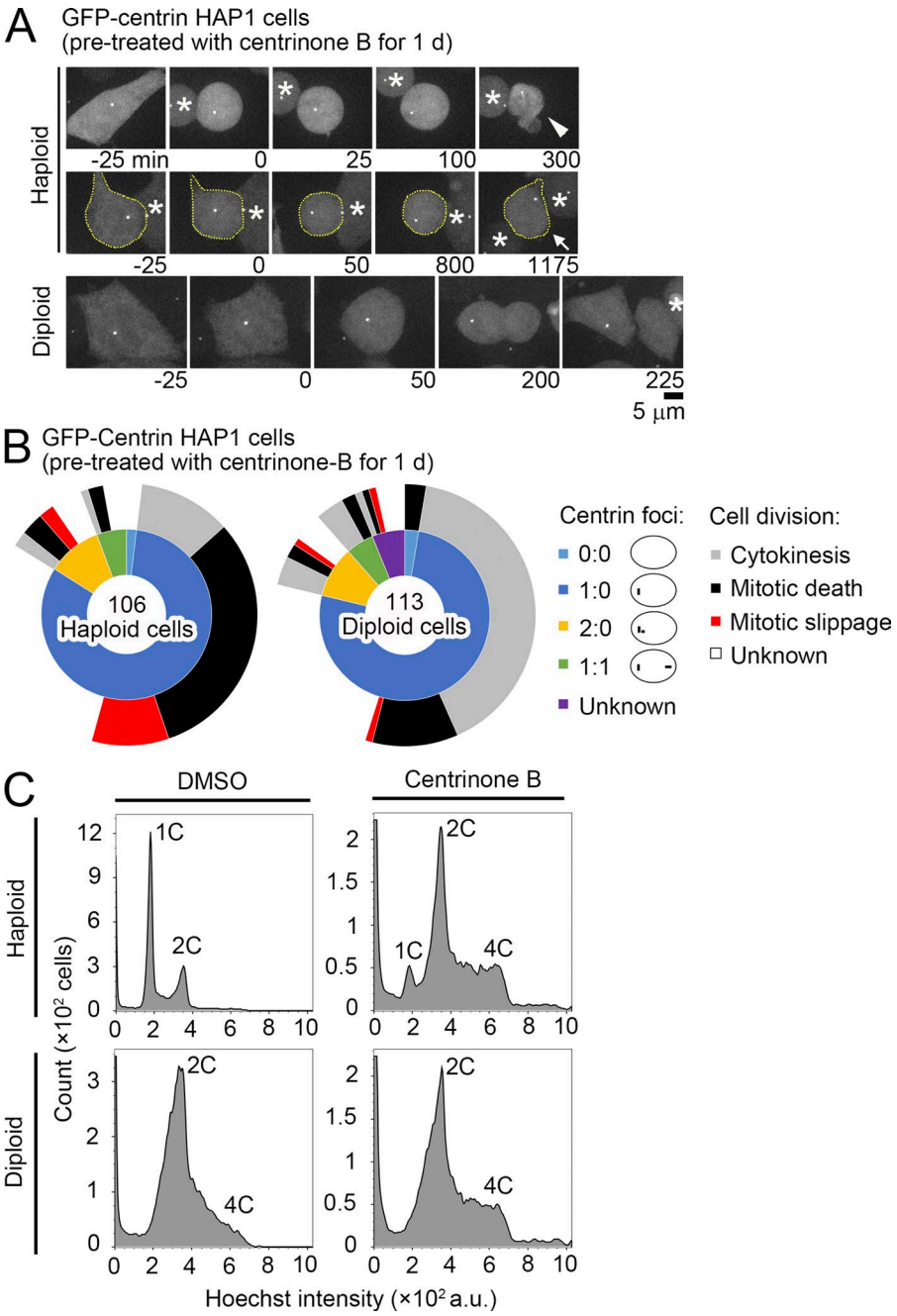

Figure 3. **Haploid cells are more susceptible to centrosome loss than diploid cells. (A)** Live images of haploid or diploid GFP-centrin cells pre-treated with 500 nM centrinone B for 1 d. Images were taken at 25-min intervals. Mitotic entry was set as 0 min. Arrowhead or arrow indicates mitotic death or mitotic slippage, respectively. Broken lines show cell boundaries. Asterisks mark neighboring cells. **(B)** Classification of mitotic defects (outer circle) sorted by centriole content (inner circle) determined by live imaging of GFP-centrin cells in A. Data are from two independent experiments. Mitotic cells that moved out of the field of view or did not exit mitosis by the end of imaging were categorized as unknown. **(C)** Flow cytometric analysis of DNA content in Hoechst-stained cells pretreated with or without 500 nM centrinone B for 4 d. Representative data from two independent experiments are shown.

the possibility that the cell-type–specific background of HAP1 cells renders them particularly vulnerable to centrosome loss (Fig. S1, I and J).

Centriole duplication efficiency scales proportionally with ploidy level

To understand how haploid cells lose their centrosomes, we next tested the progression of centriole duplication in haploid and diploid cells. Cells were synchronized by mitotic shake-off after release from nocodazole arrest, and DNA replication and centriole duplication in the subsequent cell cycle was monitored by BrdU incorporation and counting of immunostained centrin-positive foci, respectively (Fig. 4, A–C; and Fig. S2 A). BrdU incorporation in haploid cells was slightly slower than that in diploids; however, it reached the same maximum level within 8 h of nocodazole release (Fig. 4 A). In contrast, the progression of centriole duplication was drastically delayed in haploid cells relative to that in diploids. Centriole duplication started ∼5 h after nocodazole release, and cells with four centrioles predominated at 8 h after nocodazole release in diploid cells, whereas ∼65% (n = 3) of haploid cells had unduplicated centrioles at that time (Fig. 4, B and C). When the duration of the S phase was extended by thymidine treatment after nocodazole release, the percentage of duplicated pairs of centrioles in haploid cells increased monotonically, reaching a maximum level equivalent to that in diploids within 16 h after the addition of thymidine (Fig. S2 B). Hence, centriole duplication was not completely compromised in haploid cells; rather, it became too inefficient to keep pace with

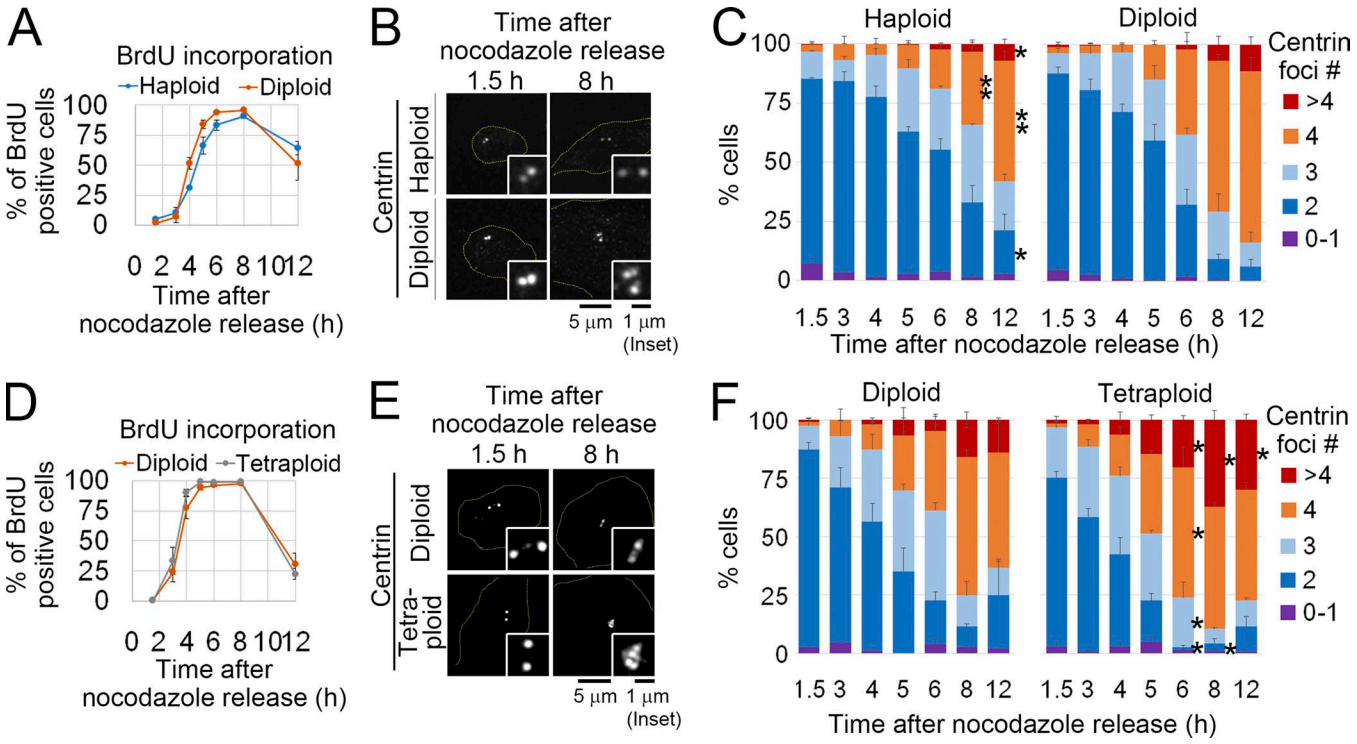

Figure 4. **Centriole duplication efficiency scales to ploidy level in HAP1 cells. (A and D)** BrdU incorporation after nocodazole release in cells with different ploidies. Mean ± SE of three independent experiments. At least 1,258 (A) or 818 cells (D) were analyzed for each data point. **(B and E)** Immunostaining of centrin in synchronized cells with different ploidies. Insets show 3× enlarged images of centrioles. Broken lines show cell boundaries. **(C and F)** Percentages of cells with indicated numbers of centrin foci at each time point after nocodazole release. Values represent means ± SE of three independent experiments (asterisks indicate significant differences from diploid cells; *, $P < 0.05$; **, $P < 0.01$, *t* test). At least 170 (C) or 87 cells (F) were analyzed for each data point. Note that centrin foci number decreased from 8 h to 12 h after nocodazole release in some cases, because some population of cells divided during that time.

the DNA replication cycle, resulting in gradual loss of centrioles in successive cell cycles. The delay in centriole duplication in haploid cells was also observed in the asynchronous condition using correlative live- and fixed-cell imaging (Fig. 8; Materials and methods), thereby eliminating the possibility of side effects of cell synchronization.

Next, we determined whether an increase in ploidy from diploid could also affect centriole duplication efficiency. We established stable tetraploid HAP1 cell lines by doubling the whole genomes of diploid cells (Fig. S2 C; Materials and methods). The majority (~72%, $n = 3$) of tetraploid cells had two mother centrioles when synchronized in the G1 phase, suggesting that excess centrosomes obtained upon tetraploidization were lost during subsequent cloning, as reported for other cell lines (Fig. 4, D–F; Ganem et al., 2009; Potapova et al., 2016). The progression of BrdU incorporation after nocodazole release was similar between diploid and tetraploid cells (Figs. 4 D and S2 D); however, centriole duplication progressed significantly faster in tetraploid cells than that in diploid cells (Fig. 4, E and F). We observed centriole overduplication significantly more often in tetraploid cells than in diploid cells (Fig. 4 F). Up-regulation of centriole duplication and formation of the supernumerary centrioles in tetraploid cells were also observed in the asynchronous cell culture condition in correlative live- and fixed-cell imaging (see Fig. 8). Long-term live imaging using GFP-centrin HAP1 cells demonstrated that a substantial population of tetraploid cells that possessed supernumerary centrioles at mitotic entry completed cell division, resulting in ~8% tetraploid daughter cells entering the next cell cycle with excess numbers of centrioles (Fig. S2, E–G). Consistent with this, the mean centriole number in an asynchronous culture of tetraploid HAP1 cells was significantly higher than that in diploid cells (3.2 ± 0.9 and 2.8 ± 0.9 centrioles per cell, respectively; $n > 87$; $P < 0.01$, *t* test; Fig. S2 H).

These results above indicate that the efficiency of centriole duplication scaled proportionally with ploidy level, whereas that of DNA replication was relatively insensitive to ploidy. This difference in ploidy dependency potentially threatens centrosome homeostasis upon ploidy conversion (either decreasing or increasing) from diploidy, owing to lack of coordination of these biological processes. To gain insight into the ploidy-dependent up-regulation of centriole duplication among other cell types, we established tetraploid lines from two different nearly diploid human cells, DLD-1 and hTERT RPE-1 (Fig. S3 A). The tetraploidy-linked acceleration of centriole duplication was also observed in DLD-1 cells, but not in RPE-1 cells (Fig. S3, B and C). Consistent with this, mean centriole number was significantly increased in tetraploid DLD-1 cells compared with their diploid counterparts (3.5 ± 1.5 and 2.9 ± 1.1 centrioles per cell, respectively; $n > 86$; $P < 0.01$, *t* test), whereas it was similar between diploid and tetraploid RPE-1 cells (2.6 ± 0.9 and 2.8 ± 0.9 centrioles per cell, respectively; $n > 93$; $P = 0.17$, *t* test; Fig. S3 D). Therefore, the link between centriole duplication and ploidy level is present in cell lines with different tissue origins, although a cell-type–specific difference in its conspicuity might also exist.

The efficiency of the recruitment of centriole duplication factors changes according to ploidies

Next, we addressed the molecular mechanism by which ploidy difference affects centriole duplication efficiency. For this, we analyzed recruitment of the key duplication factors Cep152, Plk4, and SAS-6 on the preexisting centrioles in haploid, diploid, or tetraploid HAP1 cells synchronized at G1/S phase by nocodazole shake-off (Fig. 5). At early G1 phase (2 h after nocodazole release), Cep152 had already accumulated to more than 50% ($n = 3$) of preexisting centrioles in all ploidies, which is consistent with previous studies reporting that mother centrioles recruit Cep152 from the previous cell cycle (Fig. 5, A and B; Sonnen et al., 2013; Park et al., 2014; Fu et al., 2016). In diploid cells, the majority of preexisting centrioles recruited Cep152 before entry into S phase, but Cep152 recruitment was drastically delayed in haploid cells, and ∼35% ($n = 3$) centrioles remained devoid of Cep152 signal, even in early S phase (4 h after nocodazole release; Fig. 5 B). In contrast, Cep152 recruitment was accelerated in tetraploid cells compared with that in diploid cells, with a significant increase in the frequency of Cep152-positive centrioles in early S phase. Because Cep152 is required for the hierarchical recruitment of centriole duplication factors (Kim et al., 2013; Sonnen et al., 2013), the ploidy-dependent changes in its recruitment potentially affect the subsequent processes of centriole biogenesis. Indeed, in haploid or tetraploid cells, recruitment of Plk4 and SAS-6 was delayed or hastened, respectively, compared with those in diploid cells (Fig. 5, C–F). The time gaps in the recruitment of these proteins among different ploidies roughly corresponded with those of daughter centriole formation (Fig. 4, C and F), suggesting that the ploidy-linked shifts in the timing of the sequential recruitment of these key duplication factors during G1 and early S phase change the progression of the entire centriole duplication process among different ploidies. Besides the changes in the timing of their recruitment, we also found that amounts of Cep152 and Plk4 at the centrioles during the S phase (6 h after nocodazole release) changed proportionally with ploidy levels (Fig. S2, I and J).

Previous studies have reported that overexpression of Plk4 overrides the regulatory mechanism that limits daughter centriole number, leading to the formation of excess procentrioles (Bettencourt-Dias et al., 2005; Habedanck et al., 2005; Kleylein-Sohn et al., 2007; Peel et al., 2007). We next determined whether ploidy difference also affects the efficiency of the Plk4-dependent centriole overduplication by transiently expressing GFP-tagged Plk4 in HAP1 cells with different ploidies that were arrested at S phase (Fig. 5, G and H; Materials and methods). Interestingly, the number of daughter centrioles induced by Plk4 overexpression increased with ploidy, with drastic suppression of extra centriole formation in the haploid state. Therefore, the ploidy dependency of the centriole duplication mechanism persisted even in the presence of excess Plk4, suggesting that rate-limiting processes other than Plk4 recruitment may determine the efficiency of the centriole duplication cycle in different ploidy states.

Centriole licensing is rate limiting for the centriole duplication process in different ploidies

During mitotic exit, the tightly connected mother and daughter centrioles are disengaged, which "licenses" these centrioles to recruit centriole duplication factors and serve as templates for centriole biogenesis (Tsou and Stearns, 2006; Tsou et al., 2009). Because the centriole licensing through disengagement may potentially be rate limiting for the entire centriole duplication process, we next investigated the effect of ploidy difference on the status of centriole engagement at mitotic exit. For that purpose, a centriole-linking protein, C-Nap1, and centrin were immunostained in asynchronous haploid, diploid, and tetraploid cells (Fig. 6, A and B). Using these markers, engaged centriole pairs are visualized as two adjacent centrin dots flanking a C-Nap1 dot, whereas disengaged pairs are visualized as two centrin dots with two discrete C-Nap1 dots (Tsou and Stearns, 2006). At mitotic exit, during which time two daughter cells were connected by an intercellular bridge after the constriction of the contractile ring, ∼25% ($n = 3$) of diploid cells possessed a disengaged centriole pair (Fig. 6 B). In haploids or tetraploid cells, frequency of centriole disengagement was significantly lower or higher than that in diploids, respectively (Fig. 6 B). The ploidy-dependent increase in the frequency of centriole disengagement at mitotic exit was also observed in DLD-1 cells but was less prominent in RPE-1 cells (Fig. S3, E and F).

Next, we investigated the time course of the resolution of intercentriolar connection during mitotic exit using live imaging of GFP-centrin HAP1 cells with different ploidies (Fig. 6, C–E). With the spatiotemporal resolution of our imaging setting, it was difficult to unambiguously specify the exact timing of centriole disengagement. However, by quantifying the time course of intercentriolar distance during mitotic exit, we were able to follow the process of centriole separation (Fig. 6, D and E). In all ploidy states, pairs of centrioles were located within 0.6 µm of one another at cytokinesis onset (Fig. 6 D), which approximately corresponds to the intercentriolar distance of engaged centriole pairs (Piel et al., 2000). By 30 min after cytokinesis onset, in 50% of diploid cells (6 out of 12 cells), the intercentriolar distance became >0.8 µm (Fig. 6 E), which approximately corresponds to that of disengaged pairs (Piel et al., 2000). In haploid cells, the progression of centriole separation was severely delayed (Fig. 6 D), and intercentriolar distance stayed below 0.8 µm in more than 30% of these cells (4 out of 13 cells), even 140 min after cytokinesis onset (Fig. 6 E). In contrast, in tetraploid cells, the timing of centriole separation was brought forward substantially compared with that in diploids (Fig. 6, D and E). Therefore, consistent with results from the fixed-cell analysis, the efficiency of centriole separation during mitotic exit scaled with ploidy level.

To assess whether the ploidy-dependent change in the efficiency of centriole disengagement is the primary cause for the delay in centriole duplication in haploid cells, we set out to manipulate the efficiency of centriole disengagement. Previous studies have revealed that a particular fraction of pericentriolar material is involved in centriole engagement, and that the removal of a pericentriolar material component, PCNT/pericentrin/kendrin, from the centrosomes is the prerequisite for timely centriole disengagement and subsequent duplication (Lee and Rhee, 2012; Matsuo et al., 2012; Pagan et al., 2015). Therefore, we investigated the effect of PCNT depletion on the progression of centriole separation during mitotic exit in GFP-centrin haploid cells by live

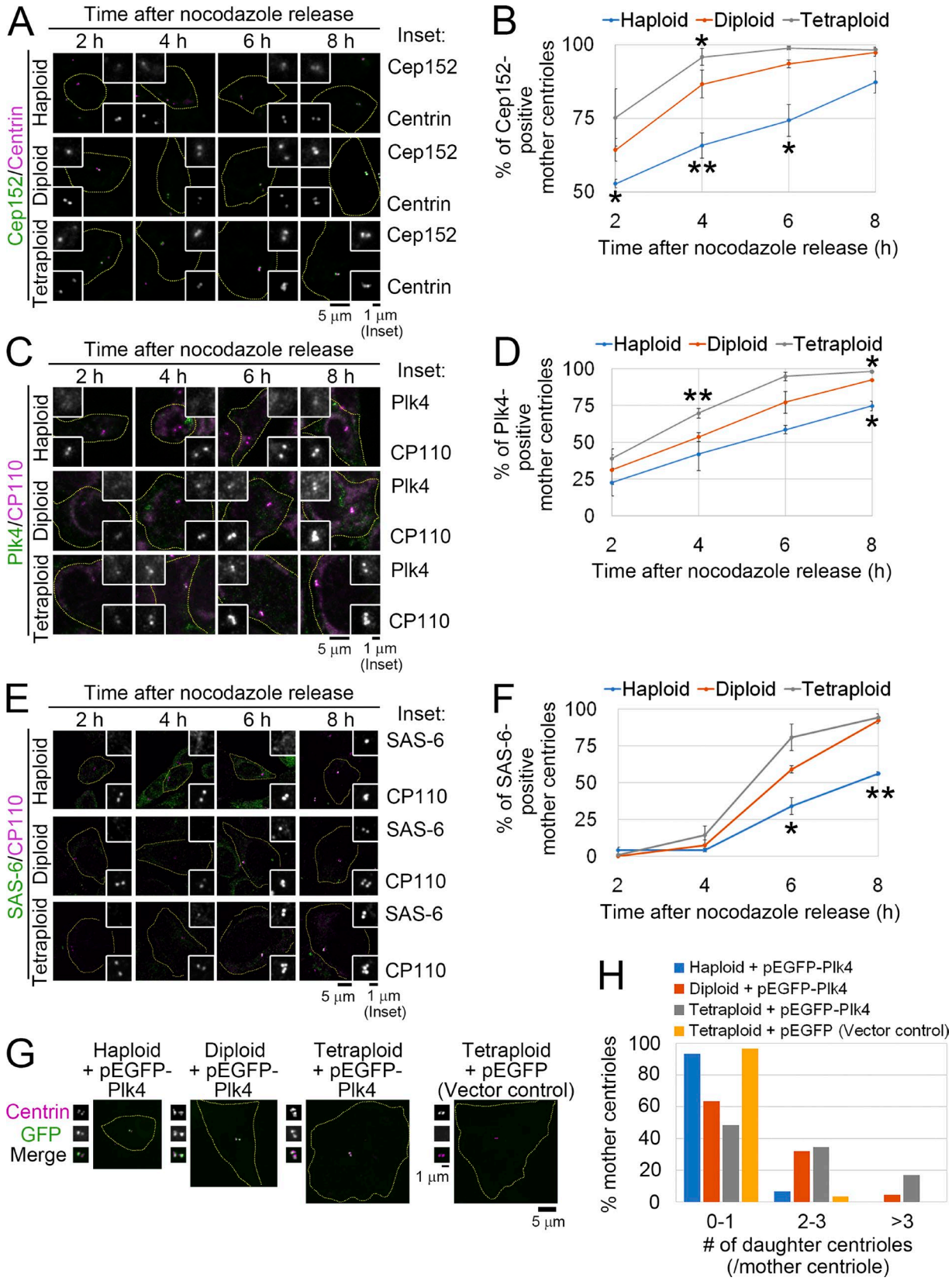

Figure 5. **Recruitment efficiency of centriole duplication factors scales to ploidy level. (A, C, and E)** Immunostaining of Cep152 (A), Plk4 (C), and SAS-6 (E) in synchronized cells with different ploidies. The centrioles were marked by immunostaining of centrin (A) or CP110 (C and E). **(B, D, and F)** Percentages of Cep152-, Plk4-, and SAS-6–positive mother centrioles in A, C, or E. Values represent means ± SE of three independent experiments (asterisks indicate significant differences from diploid cells; *, P < 0.05; ** P < 0.01, *t* test). At least 114 (B), 147 (D), or 250 mother centrioles (F) were analyzed for each data point. **(G)** Immunostaining of centrin in HAP1 cells with different ploidies transiently expressing GFP or GFP-Plk4. Broken lines mark cell boundaries. Insets show

imaging (Fig. 7). Live imaging was conducted 48 h after RNAi treatment, when DNA content in PCNT-depleted haploid cells remained unchanged compared with that in mock-depleted haploid control cells (Fig. 7, A and B). To avoid complexity of interpretation caused by cell division defects or failure, we analyzed only the cells that successfully completed symmetric cell division without mitotic arrest. Depletion of PCNT drastically increased centriole separation efficiency in haploid cells (Fig. 7, C–E), with intercentriolar distance becoming >0.8 µm by 30 min in >70% of PCNT-depleted cells (15 out of 20 cells; Fig. 7 E).

We next determined the effect of PCNT depletion on the progression of centriole duplication in haploid cells using correlative live- and fixed-cell imaging. Asynchronous mock- or PCNT-depleted HAP1 cells were live imaged from the pre- to postmitotic phase, and the progression of centriole duplication after cell division were tested by immunostaining of SAS-6 and CP110 (Fig. 8, A and B). Consistent with the result obtained in the synchronization assay (Figs. 4 C and 5 E), the progression of SAS-6 recruitment and centriole duplication in mock-depleted haploid cells was severely delayed compared with those in the diploid counterpart (Fig. 8, C and D). However, PCNT depletion considerably restored the efficiency of both the progression of SAS-6 recruitment and centriole duplication in haploid cells (Fig. 8, C and D). These results suggest that the delay in centriole disengagement is the primary cause of the delay in the progression of centriole duplication in haploid cells.

Ploidy-dependent difference in astral MT development determines the efficiency of centriole licensing

We next wished to understand the mechanism that changes the efficiency of centriole disengagement in a ploidy-dependent manner. Two mechanisms have been proposed to drive centriole disengagement during mitotic exit, that is, the Plk1- and separase-mediated PCNT degradation or mechanical separation of the engaged centriole pair by astral MT-driven pulling forces (Lee and Rhee, 2012; Matsuo et al., 2012; Cabral et al., 2013; Kim et al., 2015; Seo et al., 2015). Therefore, we tested whether either of these two mechanisms was affected by ploidy difference. We first tested the effect of ploidy difference on the progression of PCNT degradation during mitotic exit. To avoid any potential side effects of MT perturbation by nocodazole treatment, we arrested cells at mitotic phase using a proteasome inhibitor MG132 that blocks anaphase onset without affecting MT organization (Uetake and Sluder, 2010; Fig. S4, A and B). The degradation of PCNT after MG132 washout and mitotic shake-off progressed similarly in all ploidies, suggesting that this process was unaffected by ploidy difference. We next assessed the effect of ploidy difference on astral MT-dependent centriole disengagement. Interestingly, fluorescence microscopy of immunostained α-tubulin and GFP-centrin revealed that during anaphase (when centriole separation is normally initiated), spindle poles in cells with higher ploidies developed more prominent astral MTs than those with lower ploidies regardless of their centriole content (Fig. 9, A and B). Tracings of astral fibers revealed that the number of astral fibers associated with the cell cortex at the polar regions increased more than twofold upon doubling of ploidies (Fig. 9 B). We also compared accumulation of an essential MT organizing center factor, γ-tubulin, at the spindle poles among different ploidies (Fig. 9, C and D). To avoid the complexity arising from the possible influence of abnormal centriole content on γ-tubulin accumulation, we analyzed only the spindle poles with two centrioles. Under this analytical condition, the accumulation of γ-tubulin increased with ploidy levels, which possibly promotes the ploidy-dependent increase in astral MT generation. Ploidy-dependent increase in γ-tubulin accumulation at the spindle poles was also prominent between diploid and tetraploid DLD-1 cells, but was absent in RPE-1 cells (Fig. S3, G and H).

The poor astral MT formation in haploid cells potentially affects the efficiency of astral MT-dependent processes. Indeed, spindle tilting occurred at significantly higher frequency in haploid cells than in diploids, suggesting attenuation of astral MT function in the haploid state (Fig. S4, C and D; McNally, 2013). Therefore, to clarify the causal relationship between poor astral MT development and inefficient centriole duplication cycle in haploid cells, we next assessed whether forced enhancement of astral MTs can circumvent the delay in centriole disengagement and duplication in these cells. Previously, we observed that depletion of a spindle-associated protein complex, augmin, suppressed MT generation within the spindle and instead enhanced development of prominent astral MTs during anaphase in HeLa cells (Uehara et al., 2016). Consistent with this, when an augmin subunit, FAM29A/hDgt6/HAUS6/Aug6, was depleted by RNAi in haploid HAP1 cells, the number of astral fibers associated with the polar cortex significantly increased compared with that in control haploid cells and was similar to that in diploid cells (Fig. 9, E and F; see also Fig. 9 B). Therefore, we tested the effect of HAUS6 depletion on the progression of centriole disengagement, SAS-6 recruitment, and subsequent centriole duplication in haploid HAP1 cells (Figs. 7 and 8). At the time the experiments were conducted (2 d after siRNA transfection), a substantial population of HAUS6-depleted haploid cells remained in the haploid state, whereas mitotic arrest or cell division failure (indicated by the increase in 2C or 4C DNA content, respectively) occurred in a population because of spindle malfunctioning (Uehara et al., 2009; Fig. 7, A and B, FACS data). To avoid the potential side effects of these mitotic defects, we monitored the progression of cell division by live imaging and analyzed only cells with haploid cell size that succeeded in cell division without delay. HAUS6 depletion drastically accelerated the progression of centriole separation in haploid GFP-centrin cells (Fig. 7, C–E), and the efficiency of SAS-6 recruitment and centriole duplication in HAUS6-depleted cells was similar to that of control diploid cells in the correlative live- and fixed-cell imaging assay (Fig. 8, B–D). The

2× (A, C, and G) or 3× (E) enlarged images of the centrioles. **(H)** Quantification of daughter centrioles generated by each mother centriole in G. At least 88 mother centrioles from two (vector control) or three (others) independent experiments were analyzed for each condition. The numbers of supernumerary centrioles were significantly different between haploid and diploid or diploid and tetraploid GFP-Plk4–expressing cells ($P < 10^{-7}$ or $P < 0.01$, *t* test, respectively).

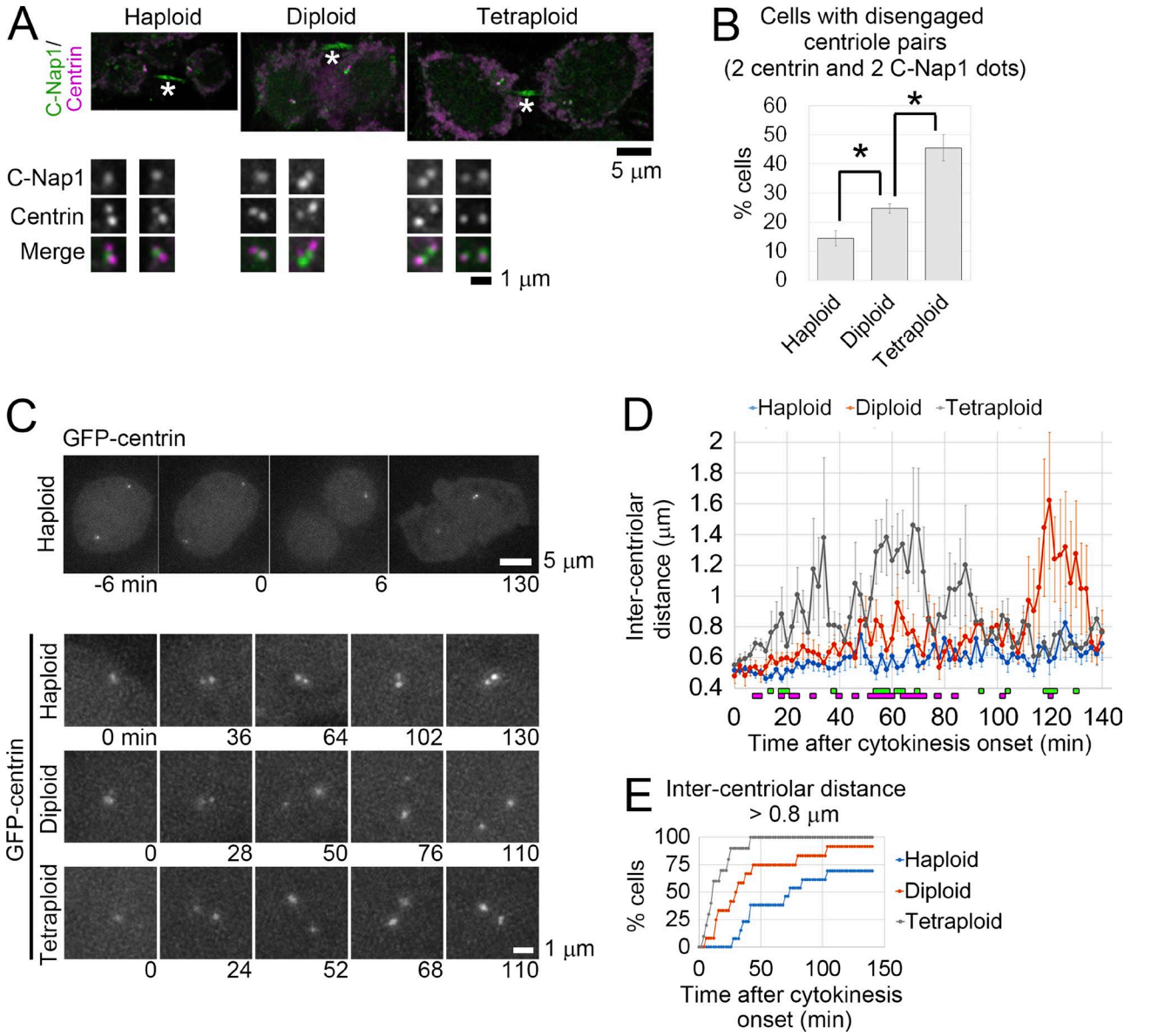

Figure 6. **The efficiency of centriole disengagement scales to ploidy level. (A)** Immunostaining of centrin and C-Nap1 in haploid, diploid, and tetraploid cells at mitotic exit. Whole-cell images (top) and 3× enlarged images of the centrioles (bottom). Asterisks indicate nonspecific staining of the intercellular bridge. **(B)** Frequencies of cells with disengaged centriole pairs (with two centrin and two C-Nap1 dots) in A. Values represent means ± SE of three independent experiments (*, $P < 0.05$, *t* test). At least 144 cells were analyzed for each condition. **(C)** Live imaging of GFP-centrin cells taken at 2-min intervals. Cytokinesis onset was set as 0 min. Whole-cell images of a haploid cell (top) and enlarged images of the centrioles in cells with different ploidies (bottom). **(D)** Time course of intercentriolar distance in C. Values represent means ± SE of at least nine cells from at least two independent experiments for each data point (at least 10 cells were analyzed for each condition). Green or magenta markers at the bottom of the graph indicate statistically significant differences between haploid and diploid or diploid and tetraploid cells, respectively ($P < 0.05$, *t* test). **(E)** Cumulative frequency of cells in which intercentriolar distance had reached 0.8 µm in C. At least 10 cells from at least two independent experiments were analyzed for each condition.

aforementioned results indicate that the extent of astral MT development is a critical determinant of the efficiency of the centriole licensing process and subsequent centriole duplication and that inefficient centriole duplication cycle in haploid cells can be largely attributed to the poor organization of astral MTs during mitosis. Although we also wished to investigate the effect of astral MT enhancement on the stability of the haploid state, severe cell division failure and cell death caused by augmin depletion precluded us from testing its effect on haploid stability over weeks.

Haploid-specific centrosome loss in mouse parthenogenetic embryos

Finally, to assess whether the ploidy-linked change in centrosome homeostasis is also seen in systems other than human cultured cells, we investigated mitotic spindle organization in haploid and diploid mouse parthenogenetic embryos at embryonic day 4.5 (E4.5), a stage by which de novo centrosome generation is complete (Gueth-Hallonet et al., 1993; Latham et al., 2002; Liu et al., 2002; Courtois et al., 2012). As previously reported, morphological abnormalities were frequently observed specifically in

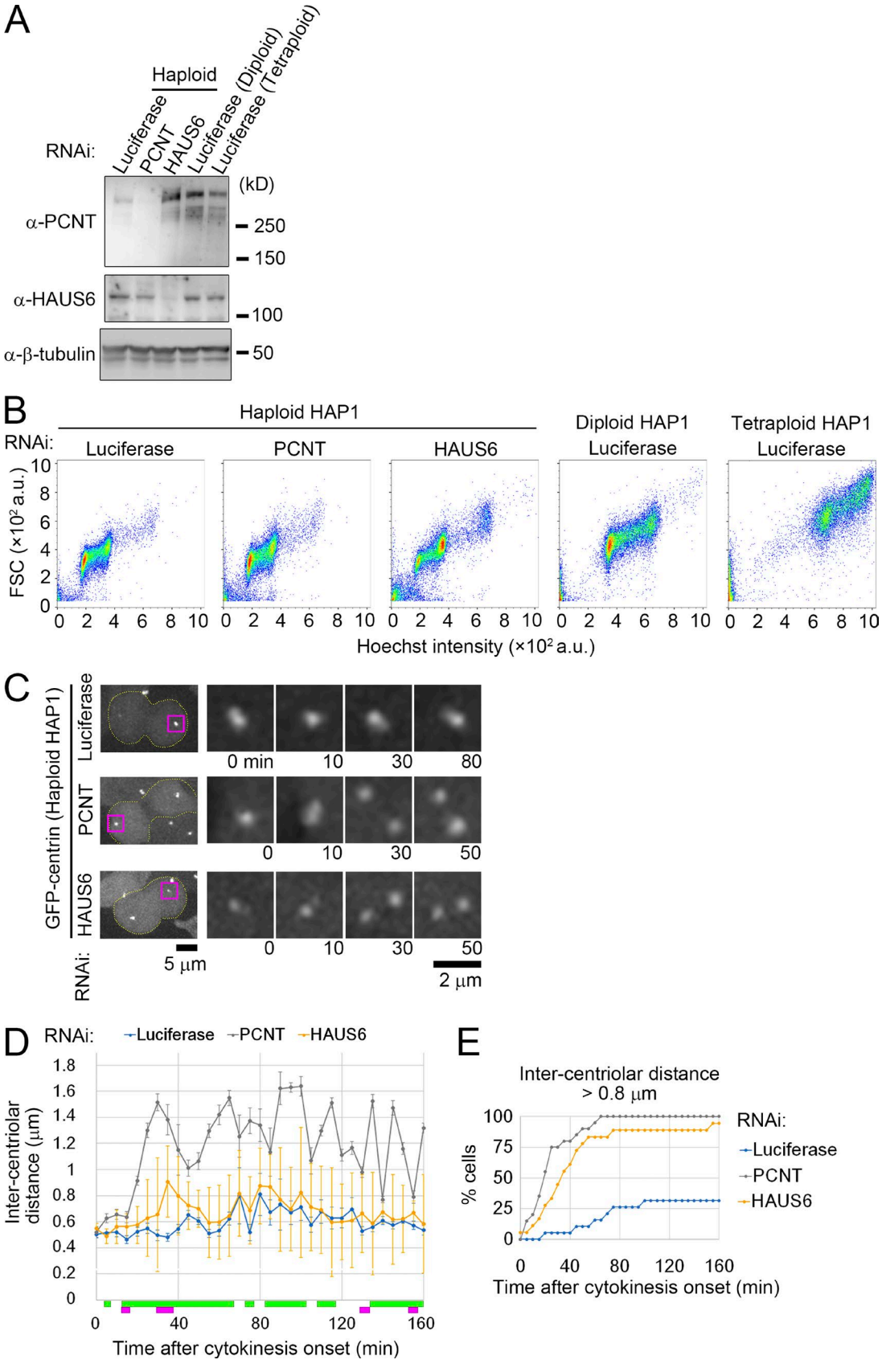

Figure 7. **Depletion of PCNT or augmin accelerates centriole separation in haploid cells. (A)** IB of PCNT, HAUS6 in RNAi-treated haploid, diploid, and tetraploid HAP1 cells. β-Tubulin was detected as a loading control. **(B)** Flow cytometric analysis of FSC and DNA content in RNAi-treated haploid, diploid, and tetraploid HAP1 cells stained by Hoechst. Representative data from two independent experiments are shown in A and B. **(C)** Live imaging of RNAi-treated haploid GFP-centrin cells taken at 5-min intervals. Cytokinesis onset was set as 0 min. Broken lines mark cell boundaries. Centrioles (indicated by magenta

haploid embryos (Latham et al., 2002; Liu et al., 2002; Fig. 10, A and B; and Fig. S5, A and B). A substantial proportion of mitotic cells in haploid embryos (46 out of 114 cells) had monopolar spindles with less than two centrosomes, whereas the majority of mitotic cells had bipolar spindles in diploid embryos (Fig. 10, C–E). The haploid-specific centrosome loss was also observed in embryos from another mouse strain (Fig. S5, C and D). Forced diploidization of haploid embryos through inhibition of the second cleavage at E1.5 stage fully restored the subsequent formation of normal number of centrosomes and bipolar spindles at E4.5 embryos, eliminating the possibility that the experimental procedure of haploid parthenogenesis has deleterious effects on centrosome biogenesis during the subsequent developmental stages (Fig. S5, E–G). These results suggest conservation of the ploidy-centrosome link among mammalian organisms.

Discussion

The unstable nature of somatic haploidy in animals has been recognized for decades, but the fundamental problems in maintaining the genomic integrity of somatic cells brought about by ploidy difference are poorly understood. Through side-by-side comparison of isogenic cell lines with different ploidies, we found a linear relationship between ploidy level and efficiency of the centrosome cycle. This relationship seems to stem from the ploidy-linked scaling of astral MT development during mitosis, which promotes centriole disengagement in a ploidy-dependent manner (Fig. 10 F). This ploidy-centrosome link impairs temporal coordination between the centrosome duplication cycle and the chromosome replication cycle in non-diploid states, which would account at least in part for the relatively low tolerance of animal cells to ploidy variance compared with acentrosomal organisms such as land plants.

Ploidy-linked scaling of centrosomal protein accumulation and astral MT development

Compared with the diploid control, haploid HAP1 cells showed severe delay in multiple key processes of the centrosome cycle such as centrosome disengagement, recruitment of duplication factors to mother centrioles, and daughter centriole formation. Because the enhancement of astral MTs by augmin depletion resolved the delay in all these processes, the poor astral MT formation appears to be the primary cause of all the observed centrosomal defects in haploid cells. In contrast, tetraploid HAP1 cells formed more robust asters than their diploid counterparts and showed up-regulation of all the above processes of the centrosome cycle, suggesting linearity of the astral MT-mediated change in centrosome duplication efficiency among different ploidies. Because γ-tubulin provides templates for astral MT nucleation (Oakley et al., 2015), the ploidy-linked scaling of astral MT development in HAP1 cells might result from the ploidy-dependent accumulation of γ-tubulin at the spindle poles. The ploidy-dependent accumulation of γ-tubulin and up-regulation of centriole disengagement/duplication were also prominent in DLD-1 cells, but not in RPE-1 cells. This suggests that the ploidy–centrosome link is conserved among human cells with different tissue origins, whereas it may be absent in certain cell types. Considering the potential contribution of γ-tubulin to the astral MT-mediated centriole licensing process, the ploidy dependency of the centrosome cycle in specific cell types may be determined by the presence or absence of the ploidy-dependent scaling of γ-tubulin accumulation at the mitotic centrosomes. However, the determinants of ploidy dependent accumulation of γ-tubulin in different cell types remain unknown. In early *Caenorhabditis elegans* embryos, centrosome size gradually decreases with progress of the cell division cycle because of the reduction in cell size and the available pool of centrosomal proteins (Decker et al., 2011). Similar centrosome scaling may occur if protein production and/or cell size drastically changes upon ploidy conversion. Indeed, we observed that the levels of total protein or several centrosomal proteins per cell, as well as cell size, increased proportionally with ploidy level (Fig. S1 C; and Fig. S4, E–H). However, because the ploidy-dependent increase in centrosomal protein was also observed in RPE-1 cells, another unidentified layer of regulation that determines ploidy dependency of centrosomal protein accumulation in different cell types might exist.

Besides centrosomal protein accumulation at the spindle poles during mitosis, the accumulation of some key centriole duplication factors, such as Cep152 and Plk4, also changed in a ploidy-dependent manner during G1/S phase. The general reduction in the amounts of centriole duplication factors at the centrosomes potentially endangers centrosome homeostasis in haploid states, especially considering that some important duplication factors such as Plk4 or NDC1 in yeast cells show haploinsufficiency (Chial et al., 1999; Ko et al., 2005). However, we found that augmin depletion singly restored the efficiency of SAS-6 recruitment and centriole duplication in haploid cells. These results indicate that that single-gene copies of centriole duplication factors are sufficient to support the normal progression of centriole duplication in a haploid background. However, we cannot rule out the possibility that ploidy-dependent accumulation of centriole duplication factors influences the efficiency of centriole duplication in hyperploidy states. It is also important that future studies examine whether ploidy-dependent changes in centrosomal protein enrichment have any influence on the ultrastructure of the centriole throughout the centrosome duplication cycle.

Generality of the ploidy–centrosome link among animal organisms

Although the ploidy–centrosome link seems preserved between human cultured cells and mouse embryonic cells, it remains to

boxes) are enlarged in the right panels. **(D)** Time course of intercentriolar distance in C. Values represent means ± SE of at least 14 cells from two independent experiments for each data point (at least 18 cells were analyzed for each condition). Green or magenta markers at the bottom of the graph indicate statistically significant differences between mock-depleted and PCNT-depleted, or HAUS6-depleted haploid cells, respectively ($P < 0.05$, *t* test). **(E)** Cumulative frequency of cells in which intercentriolar distance had reached 0.8 µm in C. At least 18 cells from two independent experiments were analyzed for each condition.

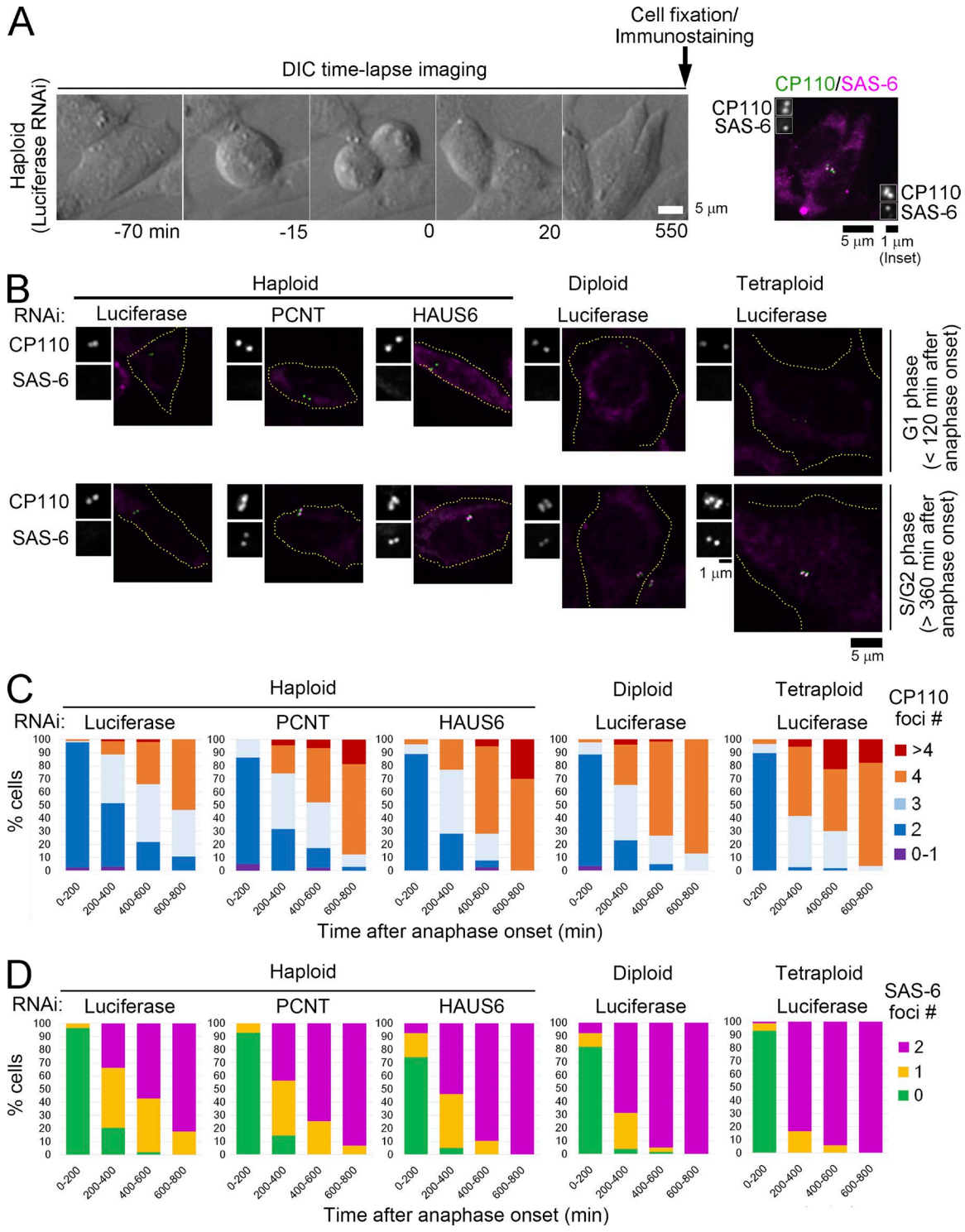

Figure 8. **Depletion of PCNT or augmin accelerates centriole duplication in haploid cells. (A)** Correlative live- and fixed-cell imaging. RNAi-treated HAP1 cells were live imaged by DIC microscopy every 5 min for 16 h (left) and then fixed and subjected to immunostaining against CP110 and SAS-6. The cells that passed the mitotic phase during time-lapse imaging were identified using grid patterns on the culture dish and observed using fluorescence microscopy (right). Anaphase onset was set as 0 min. **(B)** Immunostaining of CP110 and SAS-6 in RNAi-treated HAP1 cells in the correlative live and fixed cell imaging. Insets show 2× enlarged images of the centrioles in A and B. Broken lines mark cell boundaries. **(C and D)** Percentages of cells with indicated numbers of CP110 foci (C) or SAS-6 foci (D) at each time window after anaphase onset in B. At least 114 cells from two independent experiments were analyzed for each condition (at least 10 cells for each data point). Note that percentage of the cells that possessed three or four centrin foci increased in PCNT- or HAUS6-depleted haploid cells compared with control haploid cells in a 200- to 400-min time window, indicating that the initiation of centriole duplication was accelerated in these cells.

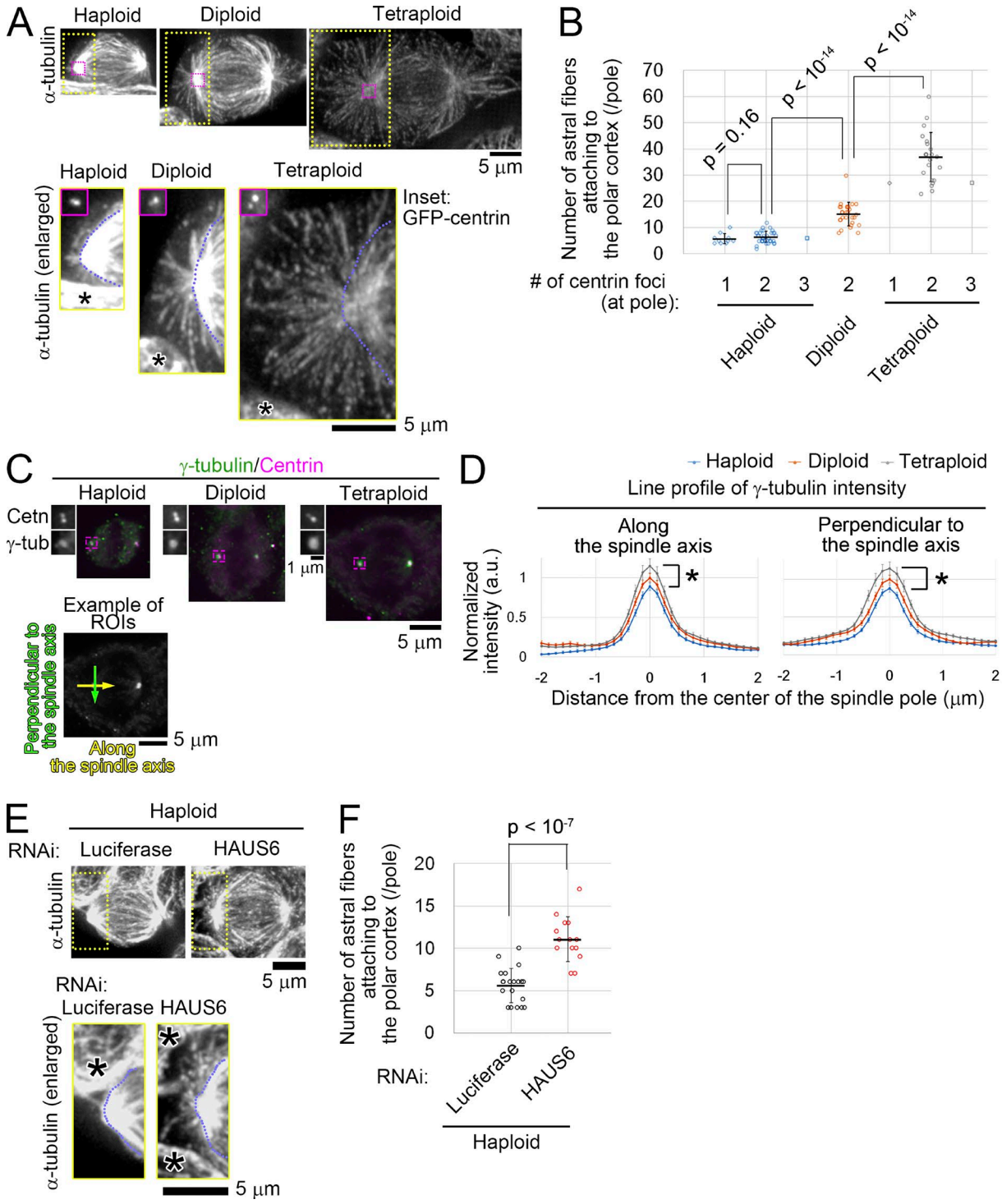

Figure 9. **Development of astral MTs scales to ploidy level. (A and E)** Immunostaining of α-tubulin during anaphase in GFP-centrin HAP1 cells with different ploidies (A) or in RNAi-treated haploid HAP1 cells (E). Enlarged images of the astral MTs at the polar region (yellow boxes) and GFP-centrin at the spindle pole (magenta boxes in A) are shown in the bottom panels. Asterisks: neighboring interphase cells. Blue broken lines: spindle regions. **(B and F)** Number of astral fibers attached to the polar cortex in A or E. Values represent means ± SD of at least 10 spindle poles from three independent experiments (B) or at least 14 poles from two independent experiments (F; p-values calculated using *t* tests are shown). Spindle poles with different numbers of GFP-centrin foci were separately categorized in B. Examples of MT tracking are shown in Video 7. **(C)** Immunostaining of γ-tubulin and centrin in preanaphase cells with different ploidies. Insets show 2× enlarged images of the spindle poles indicated by magenta boxes. Bottom: An example of regions of interest (ROIs) for the quantification in D. **(D)** Line profiles of γ-tubulin at the spindle poles in C. Spindle poles with two centrioles were analyzed. Values represent means ± SE of at least 24 spindle poles from two independent experiments. Asterisks indicate statistically significant differences between haploid and tetraploid cells at the center of the spindle pole (*, P < 0.05, one-way ANOVA with Tukey post-hoc test).

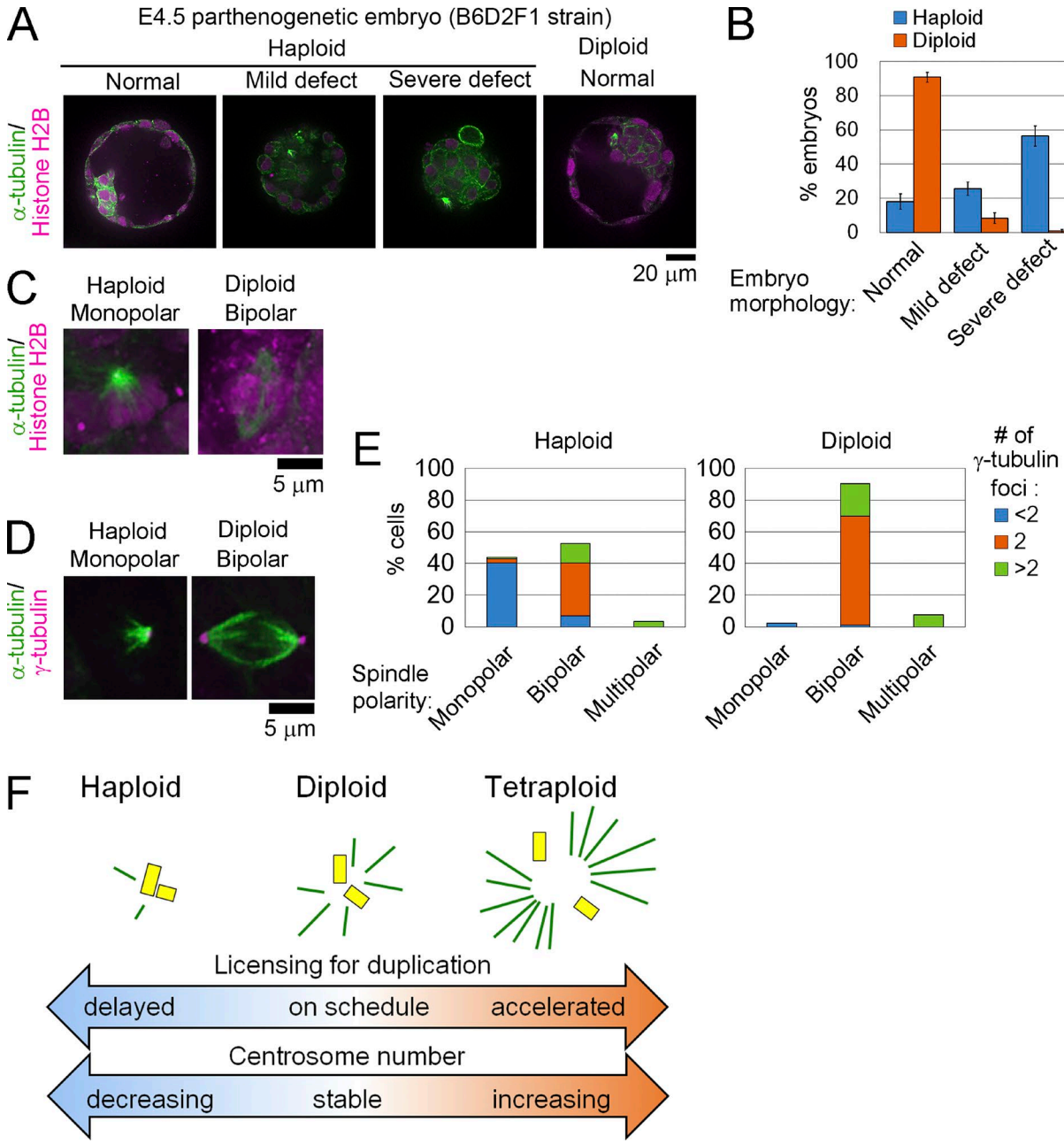

Figure 10. **Centrosome reduction and monopolar spindle formation in haploid mouse embryos. (A, C, and D)** Immunostaining of α-tubulin and histone H2B (A and C), or γ-tubulin (D) in B6D2F1 mouse parthenogenetic embryos at E4.5. Mitotic cells are shown in C and D. **(B)** Frequencies of morphological abnormalities in A. Values represent means ± SE of four independent experiments. At least 109 embryos were analyzed per condition. **(E)** Spindle polarities and numbers of γ-tubulin foci in D. At least 93 cells from 71 embryos from 11 independent experiments were analyzed per condition. **(F)** A model for the ploidy–centrosome link. During mitosis, astral MTs (lines) develop in a ploidy-linked manner. Inadequate or excess amounts of asters lead to deceleration or acceleration of centriole disengagement (and subsequent duplication), respectively, in haploid or tetraploid cells, respectively. As a result, the efficiency of the entire centriole duplication cycle scales proportionally to ploidy level, which drives uncoupling of centriole duplication and DNA replication in non-diploid states.

be elucidated whether it is also conserved among nonmammalian animal species. Of interest, however, is that in different fish species, haploid embryos develop abnormally small brains and eyes (Araki et al., 2001; Patton and Zon, 2001; Luo and Li, 2003), which are very similar to morphological defects reported in zebrafish embryos depleted of several centrosomal genes (Kim et al., 2011; Novorol et al., 2013). Therefore, it is intriguing to speculate that these developmental defects observed in haploid fishes are caused by haploidy-driven centrosome loss. Another hint on the generality of the ploidy–centrosome link is that cell lines derived from haploid lethal embryos of a *Drosophila melanogaster* mutant are devoid of centrioles (Debec, 1978, 1984; Szöllösi et al., 1986; Debec and Abbadie, 1989). Although in the original articles, the centrosome loss in these cell lines was attributed to an unidentified mutation in the original embryos, it is also possible that their haploid state by itself drove the centrosome

loss. Further analyses using nonmammalian organisms would improve our understanding of the general impact of ploidy difference on centrosome homeostasis.

Attenuation of centrosome-independent pathway in haploid cells

Our results indicate that the frequent mitotic failure in haploid cells and subsequent diploidization are caused by combinational effect of haploidy-linked centrosome loss and attenuation of the centrosome-independent pathway. Currently, the reason behind the poor efficiency of centrosome-independent spindle formation in the haploid state is not known. However, as chromosome number potentially affects Ran-GTP gradient formation (Hasegawa et al., 2013), the lesser number of chromosomes in haploid cells may attenuate the Ran-GTP–dependent pathway and suppress centrosome-independent spindle formation. Ran-GTP may also be involved in ploidy-linked scaling of mitotic centrosomes through its downstream factors involved in centrosome maturation (Petretti et al., 2006; Yokoyama et al., 2008).

Potential importance of the hyperploidy-driven centriole overduplication

The ploidy-dependent up-regulation of centriole duplication suggests a new route to centrosome amplification in hyperploid tumor cells. Hyperploid tumor cells often possess extra centrosomes, which conceivably arise from cell division failure in ancestor cells (Godinho and Pellman, 2014). The extra centrosomes are normally purged from the progeny cell population because of the disadvantages associated with multipolar spindle formation, but they are sustained in some populations through an adaptation mechanism that promotes centrosome clustering or selection owing to their invasive qualities (Ganem et al., 2009; Godinho et al., 2014; Rhys et al., 2018). In addition to these mechanisms, the hyperploid state itself may promote chronic deregulation of centrosome number control as observed in HAP1 or DLD-1 cells and thus may contribute significantly to the maintenance of extra centrosomes in hyperploid tumor cells. Future investigations on the contribution of hyperploidy-driven centrosome overduplication to genome instability during cancer development using in vivo models are required.

Materials and methods

Cell culture and flow cytometry

The HAP1 cell line (Haplogen) was cultured in Iscove's modified Dulbecco's medium (IMDM; Wako) or DMEM (Wako; for cell viability assay) supplemented with 10% FBS and 1× antibiotic-antimycotic (1× AA; Sigma-Aldrich) on culture dishes coated with rat tail type-I collagen (Corning). hTERT-RPE-1, DLD-1, and HeLa cell lines were cultured in DMEM supplemented with 10% FBS and 1× AA. Haploid HAP1 cells were purified by sorting based on forward scatter (FSC) intensity using a JSAN desktop cell sorter (Bay bioscience). For each sorting, ∼10^6 cells were collected. Sorted cells were cultured for a further 6–7 d to reach subconfluence on 15-cm dishes (Nippon Genetics) and then stored in freezing medium (Bambanker; Lymphotec) as 5–6 aliquots in vials (Corning) at −80°C or −196°C. Every cell culture lot was checked for DNA content as described below. Haploid-enriched cells were used within 7 d after recovery from frozen stocks for all experiments to minimize the effects of spontaneous diploidization. For long-term culture experiments, the point at which haploid-enriched HAP1 cell stocks were freshly thawed was set as "day 0," and cells were cultured for several weeks, with passaging every 1–3 d. To obtain diploid HAP1 cells, haploid-enriched cells were cultured for a few weeks, and the spontaneously diploidized cell population purified by FSC-based sorting. To obtain tetraploid HAP1 or DLD-1 cells, diploid cells were treated with 2.5 µM cytochalasin D for 16 h to induce cytokinesis failure, washed three times with cell culture medium, and then subjected to limiting dilution. After 10 d, colonies containing cells that were uniform in size and larger than diploid cells were picked and cultured, and their ploidy states were tested by DNA content analyses using flow cytometry to select tetraploid clones. To obtain tetraploid RPE-1 cells, cytokinesis failure was induced in diploid cells as described above, and the tetraploidized cell population was purified by sequential cell sorting based on Hoechst 33342 signal intensities. The HAP1 EGFP-α-tubulin or GFP-centrin cell line was established by transfecting HAP1 cells with pEGFP-α-tubulin vector (Uehara and Goshima, 2010) or pEGFP-centrin2 vector (Kleylein-Sohn et al., 2007; plasmid 41147; Addgene), respectively, and selecting positive cells that grew in the presence of 500 µg/ml G418 (Wako). For DNA content analyses, cells were cultured until they reached subconfluence on 10-cm dishes and then trypsinized, washed once with Dulbecco's PBS (DPBS; Wako), suspended in 1 ml DPBS at a density of 2 × 10^6 cells/ml, stained with 10 µg/ml Hoechst 33342 (Dojindo) for 15 min at 37°C, and washed once with DPBS, and their DNA content was analyzed using a JSAN desktop cell sorter. In each DNA content analysis, 2 × 10^4 cells were counted. For viability assay of centrinone B–treated cells, the cell counting kit-8 (CCK-8; Dojindo) was used following the manufacturer's instructions. Absorbance of each well at 450 nm was measured using the Sunrise plate reader (Tecan).

RNAi

For siRNA transfection, Lipofectamine RNAiMAX (Thermo Fisher Scientific) was used following the manufacturer's instructions. The siRNAs used in this study were 5′-CGUACGCGGAAU ACUUCGATT-3′ (luciferase), 5′-CAGUUAAGCAGGUACGAAATT-3′ (HAUS6; Uehara et al., 2009), and 5′-UGGACGUCAUCCAAUGAG ATT-3′ (PCNT; Kim et al., 2015). Cells were subjected to live cell imaging or flow cytometry analyses 48 h after siRNA transfection.

Immunofluorescence (IF) staining

For IF staining of centrosomal proteins and mitotic spindles, cells or embryos were fixed with 100% methanol at −20°C for 10 min. For IF of astral MTs, cells were fixed with 3.2% PFA and 2% sucrose in DPBS for 10 min at 37°C and permeabilized with 0.5% Triton X-100 in DPBS supplemented with 100 mM glycine (DPBS-G) on ice for 5 min. For IF of incorporated BrdU, cells were prefixed with 100% methanol at −20°C for 10 min, postfixed with 3.7% PFA in DPBS for 15 min at 25°C, and treated with 1% Triton X-100 in 4 N HCl for 5 min at 25°C. Fixed samples were treated with BSA blocking buffer (150 mM NaCl, 10 mM Tris-HCl, pH

7.5, 5% BSA, and 0.1% Tween 20) for 30 min at 25°C, incubated with primary antibodies overnight at 4°C, and incubated with secondary antibodies for 1 h at 37°C or overnight at 4°C. After each treatment, cells were washed two to three times with DPBS or DPBS-G. Stained cells were mounted with mounting medium (90% [vol/vol] glycerol; 100 mM Tris-HCl, pH 8.0, and 0.5% [wt/vol] *N*-propyl gallate). Stained mouse embryos were embedded in 0.5% PrimeGel Agarose LMT (Takara Bio) dissolved in DPBS.

SDS-PAGE and immunoblotting (IB)

For SDS-PAGE, cells were lysed in SDS-PAGE sample buffer, and boiled for 5 min. For quantification of the total protein amount per cell, aliquots of cell lysate corresponding to 2.5–5 × 10^4 cells were loaded into each well of gels. Separated proteins were stained using Coomassie brilliant blue, and the total protein amount in each lane quantified using BSA as a standard. For IB, proteins separated by SDS-PAGE were transferred to Immun-Blot PVDF membrane (Bio-Rad). Membranes were then blocked with 0.3% skim milk in TTBS (50 mM Tris, 138 mM NaCl, 2.7 mM KCl, and 0.1% Tween 20) incubated with primary antibodies overnight at 4°C or for 1 h at 37°C and with secondary antibodies for 30 min at 37°C. Each step was followed by three washes with TTBS. Signal detection used the ezWestLumi plus ECL Substrate (ATTO) and a LuminoGraph II chemiluminescent imaging system (ATTO).

Antibodies

Antibodies were purchased from suppliers and used at the following dilutions: rat monoclonal anti–α-tubulin (1:1,000 for IF and 1:500 for IB; YOL1/34; EMD Millipore); mouse monoclonal anti–β-tubulin (1:1,000 for IB; 10G10; Wako); goat polyclonal anti–Histone H2B (1:50 for IF; sc-8650; Santa Cruz Biotechnology); mouse monoclonal anti-centrin (1:1,000 for IF and 1:200 for IB; 20H5; EMD Millipore); rabbit polyclonal anti–centrin 2 (1:50 for IF; sc-27793; Santa Cruz Biotechnology); mouse monoclonal anti–γ-tubulin (1:200 or 1:100 for IF in HAP1 cells, 1:100 for IF in mouse embryos, and 1:1,000 for IB; GTU88; Sigma-Aldrich); rabbit polyclonal anti-Cep152 (1:1,000 for IF and 1:500 for IB; ab183911; Abcam); mouse monoclonal anti-Plk4 (1:500 for IF; 6H5; EMD Millipore); rabbit polyclonal anti-CP110 (1:500 for IF; A301-343A; Bethyl Laboratories); mouse monoclonal anti-SAS-6 (1:50 for IF and 1:200 for IB; sc-81431; Santa Cruz Biotechnology); rabbit polyclonal anti–C-Nap1 (1:200 for IF; 14498-1-AP; Proteintech); rabbit polyclonal anti-PCNT (1:200 for IB; ab4448; Abcam); rabbit polyclonal anti–hDgt6/HAUS6 (1:500 for IB; Uehara et al., 2009); rat monoclonal anti-BrdU (1:50 for IF; sc-56258; Santa Cruz Biotechnology); and fluorescence (Alexa Fluor 488, Rhodamine Red-X, or Alexa Fluor 594) or horseradish peroxidase–conjugated secondaries (1:1,000 for IF and IB; Jackson ImmunoResearch Laboratories).

Microscopy

Fixed or living cells were observed at 25°C or 37°C with 5% CO_2, respectively, under a TE2000 microscope (Nikon) equipped with a 100× 1.4 NA Plan-Apochromatic, a 60× 1.4 NA Plan-Apochromatic, or a 40× 1.3 NA Plan Fluor oil immersion objective lens (Nikon), a CSU-X1 confocal unit (Yokogawa), and an iXon3 electron multiplier-charge–coupled device camera (Andor) or an ORCA-ER CCD camera (Hamamatsu Photonics). Image acquisition was controlled by μManager software (Open Imaging). Long-term live imaging for cell cycle analyses was performed using a LCV110 microscope (Olympus) equipped with a 40× 0.95 NA UPLSAPO dry lens (Olympus). Because we found that 488-nm light irradiation severely interfered the progression of cell cycle and mitosis in HAP1 cells, we used bright-field microscope for long-term live imaging for cell cycle analyses (Figs. 1, 8, and S3). For live imaging, cells were cultured in phenol red–free IMDM (Thermo Fisher Scientific) supplemented with 10% FBS and 1× AA.

Cell cycle synchronization

Asynchronous HAP1 cell cultures were treated with 20 ng/ml nocodazole (Wako) for 4 h or with 3 μM MG132 (Peptide Institute) for 1 h and then washed with IMDM supplemented with 10% FBS and 1× AA three times. Mitotic cells were dislodged from the culture dishes by tapping and then transferred to collagen-coated 8-well coverglass chambers (ZelKontakt) or 6-well dishes (Nippon Genetics) and synchronized cells sampled at each time point indicated. To arrest cells in early S phase, the nocodazole-released cells were treated with 4 mM thymidine (Wako).

Correlative live- and fixed-cell imaging

To compare the progression of centriole duplication and SAS-6 recruitment among isogenic cells with different ploidies in asynchronous culture condition, cells were cultured on dishes with grid patterns (AGC Techno Glass), subjected to differential interference contrast (DIC) time-lapse imaging for 16–24 h to identify the cells that passed the mitotic phase. Cells were then fixed and subjected to immunostaining against centrin and SAS-6 to quantify centriole number in the live-monitored cells that were identified by grid patterns on the dishes. By quantifying the distribution of centriole numbers in respective time windows after mitotic exit, we were able to monitor and compare the progression of centriole duplication among cells with different ploidies or with different RNAi conditions.

Exogenous expression of GFP-Plk4 in HAP1 cells

Full-length cDNA of human Plk4 (GenBank accession no. NM014264.4) was obtained from the RPE-1 cell cDNA pool by PCR using primers 5′-ATCTCGAGCACCATGGCGACCTGCATC GGGGAGAAG-3′, and 5′-ATGGATCCCGATGAAAATTAGGAGTCG GATTAG-3′, and subcloned into the XhoI and BamHI sites of pEGFP-C1 (Takara Bio). Mitotic cells were collected by shake-off, transfected with the plasmid using Nucleofector 2b (Lonza), and then arrested in the early S phase by 16-h thymidine treatment. Centriole overduplication was monitored by centrin immunostaining. Under this condition, the overduplicated daughter centrioles were connected to their mother centrioles, enabling the quantification of daughter centriole generated from each mother centriole (Habedanck et al., 2005).

Theoretical modeling of the progression of diploidization

To theoretically assess the impact of haploid-specific mitotic defects and cell cycle delay on the stability of the haploid state in HAP1 cells, we constructed a mathematical model based on the following simple assumptions: (1) haploid and diploid populations proliferate exponentially with characteristic doubling times

corresponding to their cell cycle lengths (Fig. 1 D); (2) haploid cells die or convert into diploids through mitotic death or mitotic slippage, respectively, with the observed frequencies (Fig. 1 F); and (3) the proportion of cells in G1 phase remains unchanged in haploid populations throughout long-term culture. The basic time-dependent growth of a cell population can be modeled as

$$N(t) = 2^{\frac{t}{\tau}} \times N(0),$$

where N is the number of cells at time point, t, and τ is the mean cell cycle length in the cell population.

Assuming ergodicity in the processes of the cell cycle, mitosis, and cell proliferation, the probability of the occurrence of mitotic death in a haploid cell population during unit time length, p_{death}, is derived as

$$p_{death} = \frac{q_{death}}{\tau_{haploid}},$$

and mitotic slippage in a haploid cell population during unit time length, $p_{slippage}$, as

$$p_{slippage} = \frac{q_{slippage}}{\tau_{haploid}},$$

where $q_{slippage}$ and q_{death} are the rate of incidence of mitotic slippage and mitotic death per mitotic event, respectively, and $\tau_{haploid}$ is the mean cell cycle length of a haploid cell population. The time-dependent growth of a haploid cell population is then modeled as

$$N_{haploid}(t) = \left[2\left(1 - p_{slippage} - p_{death}\right)\right]^{\frac{t}{\tau_{haploid}}} \times N_{haploid}(0),$$

where $N_{haploid}$ is the number of haploid cells at the time point, t. A haploid cell that converts to diploid through mitotic slippage at any point during the simulation will thereafter proliferate with the characteristic doubling time of diploid cells. The time-dependent growth of a diploid cell population is, therefore, modeled as

$$N_{diploid}(t) = 2^{\frac{t}{\tau_{diploid}}} \times N_{diploid}(0) + \sum_{i=1}^{t} 2^{\frac{t-i}{\tau_{diploid}}} \times N_{haploid}(i-1) \times p_{slippage},$$

where $N_{diploid}$ is the number of diploid cells at time point, t, and $\tau_{diploid}$ is the mean cell cycle length of a diploid cell population. Finally, the time-dependent change in the percentage of haploid cells in G1, $P_{haploid,G1}$, in a cell culture is modeled as

$$P_{haploid,G1} = F_{haploid,G1} \times \left(\frac{100 \times N_{haploid}}{N_{haploid} + N_{diploid}} \right),$$

where $F_{haploid,G1}$ is the fraction of cells in G1 phase within a haploid cell population.

Computer programs were written using MATLAB (MathWorks). Parameters used in simulations are listed in Table S1.

Image analyses

To estimate the sizes of HAP1 cells with different ploidy levels, the areas of trypsinized round-shaped cells were measured using the ROI tool in ImageJ software (National Institutes of Health), and the cell radius, r, was calculated using the equation $r = \sqrt{A/\pi}$, where A is the measured cell area.

The fluorescence intensities of centrosome-associated IF signals were measured using plot profile or round-shaped ROIs with diameters of 0.53 µm (ImageJ), with subtraction of background signals in the areas outside the cells or the cytoplasmic areas, respectively. Measurement of intercentriolar distance in GFP-centrin cells or counting of astral fibers in fixed anaphase cells was performed using the Line tool or the Manual tracking tool in ImageJ, respectively.

Statistical analysis

Analyses for significant differences between two groups were conducted using the one-tailed Student's t test in Excel software (Microsoft). Multiple group analysis in Fig. 9 D was conducted using the one-way ANOVA with Tukey post-hoc test in R software (The R Foundation). Statistical significance was set at $P < 0.05$. p-values are indicated in figures or the corresponding figure legends. Data distribution was assumed to be normal, but this was not formally tested. The plus/minus sign in the main text indicates standard deviation.

Parthenogenesis and embryo culture

C57BL/6 and DBA/2 mice were purchased from Japan SLC, and CBA mice were from Charles River Laboratories Japan. For mouse embryo experiments, 8- to 12-wk-old female B6D2F1 (C57BL/6 × DBA/2) or BCF1 mice (C57BL/6 × CBA) were injected with 5 IU pregnant mare serum gonadotropin (ASKA Animal Health) followed by injection with 5 IU human chorionic gonadotropin (ASKA Pharmaceutical) 46–48 h later, and matured oocytes were obtained from oviducts 16 h later. Haploid and diploid parthenogenetic embryos were produced as described previously, with slight modifications (Latham et al., 2002; Kishigami and Wakayama, 2007). Oocytes were treated with 0.1% hyaluronidase (Sigma-Aldrich) in M2 medium (Sigma-Aldrich) for 30 s to remove cumulus cells, washed with M2 medium and M16 medium (Sigma-Aldrich) three times each, and incubated in M16 medium supplemented with 2 mM EGTA (EGTA-M16) for 20 min. To produce haploid parthenogenetic embryos, these oocytes were treated with 5 mM $SrCl_2$ in EGTA-M16 for 2.5 h. Diploid parthenogenetic embryos were produced by treating the oocytes with 5 mM $SrCl_2$ in EGTA-M16 in the presence of 5 µg/ml cytochalasin B (Wako) for 2.5 h and then incubating them in KSOM medium (MTI-GlobalStem) in the presence of the same concentration of cytochalasin B for 3.5 h. Activated haploid and diploid parthenogenetic embryos were then washed with KSOM three times and cultured in the same medium at 37°C with 5% CO_2. In case haploid embryos were converted to diploid after parthenogenesis, E1.5 embryos were treated with 5 µg/ml cytochalasin B for 12 h to block the second cleavage and washed three times with KSOM.

Ethics statement

The maintenance and handling of mice for all embryo experiments were performed in the animal facility of the Platform for Research on Biofunctional Molecules of Hokkaido University under the guidelines and with the permission of the committee on animal experiments of Hokkaido University (permission number 16-0038).

Online supplemental material

Fig. S1 shows additional analyses of isogenic HAP1 cells with different ploidies. Fig. S2 shows ploidy-dependent changes in

centriole duplication in HAP1 cells. Fig. S3 shows ploidy-dependent changes in centrosome cycle in RPE-1 and DLD-1 cells. Fig. S4 shows comparison of PCNT degradation, spindle positioning, and protein expression among different ploidy states. Fig. S5 shows additional data on centrosome loss in haploid mouse embryos. Table S1 shows parameters used in the simulation. Source code files used in the simulation for modeling dynamics of haploid cell population (haploid.txt) and for drawing plots (plot_hap.txt) are also provided.

Acknowledgments

We are grateful to M. Mishra, S. Bulchand, T. Kamasaki, and G. Goshima for valuable comments on the draft of this paper, M.F. Tsou for GFP-centrin live imaging advice, and the members of the Faculty of Advanced Life Science and the Open Facility (Hokkaido University) for the use of their equipment.

This work was supported by the Akiyama Life Science Foundation, the Inamori Foundation, the Mochida Memorial Foundation, the Naito Foundation, the Nakajima Foundation, the Noastec Foundation (grant T-3-9), the SGH Foundation, the Suhara Memorial Foundation, the Sumitomo Foundation (grant 150105), the Takeda Science Foundation, the Uehara Memorial Foundation (grant G15118), and Ministry of Education, Culture, Sports, Science and Technology-Japan/Japan Society for the Promotion of Science KAKENHI (grants 15K14501 and 17K15111) to R. Uehara.

The authors declare no competing financial interests.

Author contributions: Conceptualization, K. Yaguchi, and R. Uehara; Methodology, K. Yaguchi, T. Yamamoto, R. Matsui, A. Shibanuma, K. Kamimura, T. Koda, and R. Uehara; Software, T. Yamamoto, R. Matsui, Y. Tsukada, and R. Uehara; Investigation, K. Yaguchi, T. Yamamoto, R. Matsui, and R. Uehara; Formal Analysis, K. Yaguchi, T. Yamamoto, R. Matsui, and R. Uehara; Resources, T. Koda, and R. Uehara; Writing – Original Draft, R. Uehara; Writing – Review & Editing, Y. Tsukada, T. Koda, and R. Uehara; Funding Acquisition, T. Koda, and R. Uehara.

Submitted: 29 January 2017
Revised: 27 September 2017
Accepted: 9 April 2018

References

Araki, K., H. Okamoto, A.C. Graveson, I. Nakayama, and H. Nagoya. 2001. Analysis of haploid development based on expression patterns of developmental genes in the medaka Oryzias latipes. *Dev. Growth Differ.* 43:591–599. https://doi.org/10.1046/j.1440-169X.2001.00601.x

Bettencourt-Dias, M., A. Rodrigues-Martins, L. Carpenter, M. Riparbelli, L. Lehmann, M.K. Gatt, N. Carmo, F. Balloux, G. Callaini, and D.M. Glover. 2005. SAK/PLK4 is required for centriole duplication and flagella development. *Curr. Biol.* 15:2199–2207. https://doi.org/10.1016/j.cub.2005.11.042

Cabral, G., S.S. Sans, C.R. Cowan, and A. Dammermann. 2013. Multiple mechanisms contribute to centriole separation in C. elegans. *Curr. Biol.* 23:1380–1387. https://doi.org/10.1016/j.cub.2013.06.043

Carette, J.E., M. Raaben, A.C. Wong, A.S. Herbert, G. Obernosterer, N. Mulherkar, A.I. Kuehne, P.J. Kranzusch, A.M. Griffin, G. Ruthel, et al. 2011. Ebola virus entry requires the cholesterol transporter Niemann-Pick C1. *Nature.* 477:340–343. https://doi.org/10.1038/nature10348

Chial, H.J., T.H. Giddings Jr., E.A. Siewert, M.A. Hoyt, and M. Winey. 1999. Altered dosage of the Saccharomyces cerevisiae spindle pole body duplication gene, NDC1, leads to aneuploidy and polyploidy. *Proc. Natl. Acad. Sci. USA.* 96:10200–10205. https://doi.org/10.1073/pnas.96.18.10200

Cizmecioglu, O., M. Arnold, R. Bahtz, F. Settele, L. Ehret, U. Haselmann-Weiss, C. Antony, and I. Hoffmann. 2010. Cep152 acts as a scaffold for recruitment of Plk4 and CPAP to the centrosome. *J. Cell Biol.* 191:731–739. https://doi.org/10.1083/jcb.201007107

Courtois, A., M. Schuh, J. Ellenberg, and T. Hiiragi. 2012. The transition from meiotic to mitotic spindle assembly is gradual during early mammalian development. *J. Cell Biol.* 198:357–370. https://doi.org/10.1083/jcb.201202135

Coverley, D., H. Laman, and R.A. Laskey. 2002. Distinct roles for cyclins E and A during DNA replication complex assembly and activation. *Nat. Cell Biol.* 4:523–528. https://doi.org/10.1038/ncb813

Debec, A. 1978. Haploid cell cultures of Drosophila melanogaster. *Nature.* 274:255–256. https://doi.org/10.1038/274255a0

Debec, A. 1984. Evolution of karyotype in haploid cell lines of Drosophila melanogaster. *Exp. Cell Res.* 151:236–246. https://doi.org/10.1016/0014-4827(84)90371-9

Debec, A., and C. Abbadie. 1989. The acentriolar state of the Drosophila cell lines 1182. *Biol. Cell.* 67:307–311. https://doi.org/10.1111/j.1768-322X.1989.tb00876.x

Decker, M., S. Jaensch, A. Pozniakovsky, A. Zinke, K.F. O'Connell, W. Zachariae, E. Myers, and A.A. Hyman. 2011. Limiting amounts of centrosome material set centrosome size in C. elegans embryos. *Curr. Biol.* 21:1259–1267. https://doi.org/10.1016/j.cub.2011.06.002

Dzhindzhev, N.S., Q.D. Yu, K. Weiskopf, G. Tzolovsky, I. Cunha-Ferreira, M. Riparbelli, A. Rodrigues-Martins, M. Bettencourt-Dias, G. Callaini, and D.M. Glover. 2010. Asterless is a scaffold for the onset of centriole assembly. *Nature.* 467:714–718. https://doi.org/10.1038/nature09445

Dzhindzhev, N.S., G. Tzolovsky, Z. Lipinszki, S. Schneider, R. Lattao, J. Fu, J. Debski, M. Dadlez, and D.M. Glover. 2014. Plk4 phosphorylates Ana2 to trigger Sas6 recruitment and procentriole formation. *Curr. Biol.* 24:2526–2532. https://doi.org/10.1016/j.cub.2014.08.061

Elling, U., J. Taubenschmid, G. Wirnsberger, R. O'Malley, S.P. Demers, Q. Vanhaelen, A.I. Shukalyuk, G. Schmauss, D. Schramek, F. Schnuetgen, et al. 2011. Forward and reverse genetics through derivation of haploid mouse embryonic stem cells. *Cell Stem Cell.* 9:563–574. https://doi.org/10.1016/j.stem.2011.10.012

Essletzbichler, P., T. Konopka, F. Santoro, D. Chen, B.V. Gapp, R. Kralovics, T.R. Brummelkamp, S.M. Nijman, and T. Bürckstümmer. 2014. Megabase-scale deletion using CRISPR/Cas9 to generate a fully haploid human cell line. *Genome Res.* 24:2059–2065. https://doi.org/10.1101/gr.177220.114

Fong, C.S., M. Kim, T.T. Yang, J.C. Liao, and M.F.B. Tsou. 2014. SAS-6 assembly templated by the lumen of cartwheel-less centrioles precedes centriole duplication. *Dev. Cell.* 30:238–245. https://doi.org/10.1016/j.devcel.2014.05.008

Forster, B.P., E. Heberle-Bors, K.J. Kasha, and A. Touraev. 2007. The resurgence of haploids in higher plants. *Trends Plant Sci.* 12:368–375. https://doi.org/10.1016/j.tplants.2007.06.007

Freed, J.J. 1962. Continuous cultivation of cells derived from haploid Rana pipiens embryos. *Exp. Cell Res.* 26:327–333. https://doi.org/10.1016/0014-4827(62)90185-4

Fu, J., Z. Lipinszki, H. Rangone, M. Min, C. Mykura, J. Chao-Chu, S. Schneider, N.S. Dzhindzhev, M. Gottardo, M.G. Riparbelli, et al. 2016. Conserved molecular interactions in centriole-to-centrosome conversion. *Nat. Cell Biol.* 18:87–99. https://doi.org/10.1038/ncb3274

Ganem, N.J., S.A. Godinho, and D. Pellman. 2009. A mechanism linking extra centrosomes to chromosomal instability. *Nature.* 460:278–282. https://doi.org/10.1038/nature08136

Godinho, S.A., and D. Pellman. 2014. Causes and consequences of centrosome abnormalities in cancer. *Philos. Trans. R. Soc. Lond. B Biol. Sci.* 369:20130467. https://doi.org/10.1098/rstb.2013.0467

Godinho, S.A., R. Picone, M. Burute, R. Dagher, Y. Su, C.T. Leung, K. Polyak, J.S. Brugge, M. Théry, and D. Pellman. 2014. Oncogene-like induction of cellular invasion from centrosome amplification. *Nature.* 510:167–171. https://doi.org/10.1038/nature13277

Gönczy, P. 2015. Centrosomes and cancer: revisiting a long-standing relationship. *Nat. Rev. Cancer.* 15:639–652. https://doi.org/10.1038/nrc3995

Gueth-Hallonet, C., C. Antony, J. Aghion, A. Santa-Maria, I. Lajoie-Mazenc, M. Wright, and B. Maro. 1993. gamma-Tubulin is present in acentriolar MTOCs during early mouse development. *J. Cell Sci.* 105:157–166.

Habedanck, R., Y.D. Stierhof, C.J. Wilkinson, and E.A. Nigg. 2005. The Polo kinase Plk4 functions in centriole duplication. *Nat. Cell Biol.* 7:1140–1146. https://doi.org/10.1038/ncb1320

Hasegawa, K., S.J. Ryu, and P. Kaláb. 2013. Chromosomal gain promotes formation of a steep RanGTP gradient that drives mitosis in aneuploid cells. *J. Cell Biol.* 200:151–161. https://doi.org/10.1083/jcb.201206142

Hatch, E.M., A. Kulukian, A.J. Holland, D.W. Cleveland, and T. Stearns. 2010. Cep152 interacts with Plk4 and is required for centriole duplication. *J. Cell Biol.* 191:721–729. https://doi.org/10.1083/jcb.201006049

Kaufman, M.H. 1978. Chromosome analysis of early postimplantation presumptive haploid parthenogenetic mouse embryos. *J. Embryol. Exp. Morphol.* 45:85–91.

Khodjakov, A., and C.L. Rieder. 2001. Centrosomes enhance the fidelity of cytokinesis in vertebrates and are required for cell cycle progression. *J. Cell Biol.* 153:237–242. https://doi.org/10.1083/jcb.153.1.237

Khodjakov, A., R.W. Cole, B.R. Oakley, and C.L. Rieder. 2000. Centrosome-independent mitotic spindle formation in vertebrates. *Curr. Biol.* 10:59–67. https://doi.org/10.1016/S0960-9822(99)00276-6

Kim, H.-T., M.-S. Lee, J.-H. Choi, J.-Y. Jung, D.-G. Ahn, S.-Y. Yeo, D.-K. Choi, and C.-H. Kim. 2011. The microcephaly gene aspm is involved in brain development in zebrafish. *Biochem. Biophys. Res. Commun.* 409:640–644. https://doi.org/10.1016/j.bbrc.2011.05.056

Kim, J., K. Lee, and K. Rhee. 2015. PLK1 regulation of PCNT cleavage ensures fidelity of centriole separation during mitotic exit. *Nat. Commun.* 6:10076. https://doi.org/10.1038/ncomms10076

Kim, T.S., J.E. Park, A. Shukla, S. Choi, R.N. Murugan, J.H. Lee, M. Ahn, K. Rhee, J.K. Bang, B.Y. Kim, et al. 2013. Hierarchical recruitment of Plk4 and regulation of centriole biogenesis by two centrosomal scaffolds, Cep192 and Cep152. *Proc. Natl. Acad. Sci. USA.* 110:E4849–E4857. https://doi.org/10.1073/pnas.1319656110

Kishigami, S., and T. Wakayama. 2007. Efficient strontium-induced activation of mouse oocytes in standard culture media by chelating calcium. *J. Reprod. Dev.* 53:1207–1215. https://doi.org/10.1262/jrd.19067

Kleylein-Sohn, J., J. Westendorf, M. Le Clech, R. Habedanck, Y.D. Stierhof, and E.A. Nigg. 2007. Plk4-induced centriole biogenesis in human cells. *Dev. Cell.* 13:190–202. https://doi.org/10.1016/j.devcel.2007.07.002

Ko, M.A., C.O. Rosario, J.W. Hudson, S. Kulkarni, A. Pollett, J.W. Dennis, and C.J. Swallow. 2005. Plk4 haploinsufficiency causes mitotic infidelity and carcinogenesis. *Nat. Genet.* 37:883–888. https://doi.org/10.1038/ng1605

Kotecki, M., P.S. Reddy, and B.H. Cochran. 1999. Isolation and characterization of a near-haploid human cell line. *Exp. Cell Res.* 252:273–280. https://doi.org/10.1006/excr.1999.4656

Kuriyama, R., and G.G. Borisy. 1981. Centriole cycle in Chinese hamster ovary cells as determined by whole-mount electron microscopy. *J. Cell Biol.* 91:814–821. https://doi.org/10.1083/jcb.91.3.814

Latham, K.E., H. Akutsu, B. Patel, and R. Yanagimachi. 2002. Comparison of gene expression during preimplantation development between diploid and haploid mouse embryos. *Biol. Reprod.* 67:386–392. https://doi.org/10.1095/biolreprod67.2.386

Lee, K., and K. Rhee. 2012. Separase-dependent cleavage of pericentrin B is necessary and sufficient for centriole disengagement during mitosis. *Cell Cycle.* 11:2476–2485. https://doi.org/10.4161/cc.20878

Leeb, M., and A. Wutz. 2011. Derivation of haploid embryonic stem cells from mouse embryos. *Nature.* 479:131–134. https://doi.org/10.1038/nature10448

Leidel, S., M. Delattre, L. Cerutti, K. Baumer, and P. Gönczy. 2005. SAS-6 defines a protein family required for centrosome duplication in C. elegans and in human cells. *Nat. Cell Biol.* 7:115–125. https://doi.org/10.1038/ncb1220

Li, W., X. Li, T. Li, M.G. Jiang, H. Wan, G.Z. Luo, C. Feng, X. Cui, F. Teng, Y. Yuan, et al. 2014. Genetic modification and screening in rat using haploid embryonic stem cells. *Cell Stem Cell.* 14:404–414. https://doi.org/10.1016/j.stem.2013.11.016

Liu, L., J.R. Trimarchi, and D.L. Keefe. 2002. Haploidy but not parthenogenetic activation leads to increased incidence of apoptosis in mouse embryos. *Biol. Reprod.* 66:204–210. https://doi.org/10.1095/biolreprod66.1.204

Loncarek, J., and M. Bettencourt-Dias. 2018. Building the right centriole for each cell type. *J. Cell Biol.* 217:823–835.

Luo, C., and B. Li. 2003. Diploid-dependent regulation of gene expression: a genetic cause of abnormal development in fish haploid embryos. *Heredity (Edinb).* 90:405–409. https://doi.org/10.1038/sj.hdy.6800263

Mable, B.K., and S.P. Otto. 1998. The evolution of life cycles with haploid and diploid phases. *BioEssays.* 20:453–462. https://doi.org/10.1002/(SICI)1521-1878(199806)20:6%3C453::AID-BIES3%3E3.0.CO;2-N

Matsumoto, Y., K. Hayashi, and E. Nishida. 1999. Cyclin-dependent kinase 2 (Cdk2) is required for centrosome duplication in mammalian cells. *Curr. Biol.* 9:429–432. https://doi.org/10.1016/S0960-9822(99)80191-2

Matsuo, K., K. Ohsumi, M. Iwabuchi, T. Kawamata, Y. Ono, and M. Takahashi. 2012. Kendrin is a novel substrate for separase involved in the licensing of centriole duplication. *Curr. Biol.* 22:915–921. https://doi.org/10.1016/j.cub.2012.03.048

McNally, F.J. 2013. Mechanisms of spindle positioning. *J. Cell Biol.* 200:131–140. https://doi.org/10.1083/jcb.201210007

Meraldi, P., J. Lukas, A.M. Fry, J. Bartek, and E.A. Nigg. 1999. Centrosome duplication in mammalian somatic cells requires E2F and Cdk2-cyclin A. *Nat. Cell Biol.* 1:88–93. https://doi.org/10.1038/10054

Moyer, T.C., K.M. Clutario, B.G. Lambrus, V. Daggubati, and A.J. Holland. 2015. Binding of STIL to Plk4 activates kinase activity to promote centriole assembly. *J. Cell Biol.* 209:863–878. https://doi.org/10.1083/jcb.201502088

Nakazawa, Y., M. Hiraki, R. Kamiya, and M. Hirono. 2007. SAS-6 is a cartwheel protein that establishes the 9-fold symmetry of the centriole. *Curr. Biol.* 17:2169–2174. https://doi.org/10.1016/j.cub.2007.11.046

Nasmyth, K. 2002. Segregating sister genomes: the molecular biology of chromosome separation. *Science.* 297:559–565. https://doi.org/10.1126/science.1074757

Novorol, C., J. Burkhardt, K.J. Wood, A. Iqbal, C. Roque, N. Coutts, A.D. Almeida, J. He, C.J. Wilkinson, and W.A. Harris. 2013. Microcephaly models in the developing zebrafish retinal neuroepithelium point to an underlying defect in metaphase progression. *Open Biol.* 3:130065. https://doi.org/10.1098/rsob.130065

Oakley, B.R., V. Paolillo, and Y. Zheng. 2015. γ-Tubulin complexes in microtubule nucleation and beyond. *Mol. Biol. Cell.* 26:2957–2962. https://doi.org/10.1091/mbc.E14-11-1514

Ohta, M., T. Ashikawa, Y. Nozaki, H. Kozuka-Hata, H. Goto, M. Inagaki, M. Oyama, and D. Kitagawa. 2014. Direct interaction of Plk4 with STIL ensures formation of a single procentriole per parental centriole. *Nat. Commun.* 5:5267. https://doi.org/10.1038/ncomms6267

Pagan, J.K., A. Marzio, M.J. Jones, A. Saraf, P.V. Jallepalli, L. Florens, M.P. Washburn, and M. Pagano. 2015. Degradation of Cep68 and PCNT cleavage mediate Cep215 removal from the PCM to allow centriole separation, disengagement and licensing. *Nat. Cell Biol.* 17:31–43. https://doi.org/10.1038/ncb3076

Park, S.-Y., J.-E. Park, T.-S. Kim, J.H. Kim, M.-J. Kwak, B. Ku, L. Tian, R.N. Murugan, M. Ahn, S. Komiya, et al. 2014. Molecular basis for unidirectional scaffold switching of human Plk4 in centriole biogenesis. *Nat. Struct. Mol. Biol.* 21:696–703. https://doi.org/10.1038/nsmb.2846

Patton, E.E., and L.I. Zon. 2001. The art and design of genetic screens: zebrafish. *Nat. Rev. Genet.* 2:956–966. https://doi.org/10.1038/35103567

Peel, N., N.R. Stevens, R. Basto, and J.W. Raff. 2007. Overexpressing centriole-replication proteins in vivo induces centriole overduplication and de novo formation. *Curr. Biol.* 17:834–843. https://doi.org/10.1016/j.cub.2007.04.036

Petretti, C., M. Savoian, E. Montembault, D.M. Glover, C. Prigent, and R. Giet. 2006. The PITSLRE/CDK11p58 protein kinase promotes centrosome maturation and bipolar spindle formation. *EMBO Rep.* 7:418–424.

Piel, M., P. Meyer, A. Khodjakov, C.L. Rieder, and M. Bornens. 2000. The respective contributions of the mother and daughter centrioles to centrosome activity and behavior in vertebrate cells. *J. Cell Biol.* 149:317–330. https://doi.org/10.1083/jcb.149.2.317

Potapova, T.A., C.W. Seidel, A.C. Box, G. Rancati, and R. Li. 2016. Transcriptome analysis of tetraploid cells identifies cyclin D2 as a facilitator of adaptation to genome doubling in the presence of p53. *Mol. Biol. Cell.* 27:3065–3084. https://doi.org/10.1091/mbc.E16-05-0268

Rhys, A.D., P. Monteiro, C. Smith, M. Vaghela, T. Arnandis, T. Kato, B. Leitinger, E. Sahai, A. McAinsh, G. Charras, and S.A. Godinho. 2018. Loss of E-cadherin provides tolerance to centrosome amplification in epithelial cancer cells. *J. Cell Biol.* 217:195–209. https://doi.org/10.1083/jcb.201704102

Sagi, I., G. Chia, T. Golan-Lev, M. Peretz, U. Weissbein, L. Sui, M.V. Sauer, O. Yanuka, D. Egli, and N. Benvenisty. 2016. Derivation and differentiation of haploid human embryonic stem cells. *Nature.* 532:107–111. https://doi.org/10.1038/nature17408

Seo, M.Y., W. Jang, and K. Rhee. 2015. Integrity of the Pericentriolar Material Is Essential for Maintaining Centriole Association during M Phase. *PLoS One.* 10:e0138905. https://doi.org/10.1371/journal.pone.0138905

Sir, J.H., M. Pütz, O. Daly, C.G. Morrison, M. Dunning, J.V. Kilmartin, and F. Gergely. 2013. Loss of centrioles causes chromosomal instability in

vertebrate somatic cells. *J. Cell Biol.* 203:747–756. https://doi.org/10.1083/jcb.201309038

Sonnen, K.F., A.M. Gabryjonczyk, E. Anselm, Y.D. Stierhof, and E.A. Nigg. 2013. Human Cep192 and Cep152 cooperate in Plk4 recruitment and centriole duplication. *J. Cell Sci.* 126:3223–3233. https://doi.org/10.1242/jcs.129502

Sumara, I., E. Vorlaufer, P.T. Stukenberg, O. Kelm, N. Redemann, E.A. Nigg, and J.M. Peters. 2002. The dissociation of cohesin from chromosomes in prophase is regulated by Polo-like kinase. *Mol. Cell.* 9:515–525. https://doi.org/10.1016/S1097-2765(02)00473-2

Szöllösi, A., H. Ris, D. Szöllösi, and A. Debec. 1986. A centriole-free Drosophila cell line. A high voltage EM study. *Eur. J. Cell Biol.* 40:100–104.

Tsou, M.F., and T. Stearns. 2006. Mechanism limiting centrosome duplication to once per cell cycle. *Nature.* 442:947–951. https://doi.org/10.1038/nature04985

Tsou, M.F., W.J. Wang, K.A. George, K. Uryu, T. Stearns, and P.V. Jallepalli. 2009. Polo kinase and separase regulate the mitotic licensing of centriole duplication in human cells. *Dev. Cell.* 17:344–354. https://doi.org/10.1016/j.devcel.2009.07.015

Uehara, R., and G. Goshima. 2010. Functional central spindle assembly requires de novo microtubule generation in the interchromosomal region during anaphase. *J. Cell Biol.* 191:259–267. https://doi.org/10.1083/jcb.201004150

Uehara, R., R.S. Nozawa, A. Tomioka, S. Petry, R.D. Vale, C. Obuse, and G. Goshima. 2009. The augmin complex plays a critical role in spindle microtubule generation for mitotic progression and cytokinesis in human cells. *Proc. Natl. Acad. Sci. USA.* 106:6998–7003. https://doi.org/10.1073/pnas.0901587106

Uehara, R., T. Kamasaki, S. Hiruma, I. Poser, K. Yoda, J. Yajima, D.W. Gerlich, and G. Goshima. 2016. Augmin shapes the anaphase spindle for efficient cytokinetic furrow ingression and abscission. *Mol. Biol. Cell.* 27:812–827. https://doi.org/10.1091/mbc.E15-02-0101

Uetake, Y., and G. Sluder. 2010. Prolonged prometaphase blocks daughter cell proliferation despite normal completion of mitosis. *Curr. Biol.* 20:1666–1671. https://doi.org/10.1016/j.cub.2010.08.018

Wong, Y.L., J.V. Anzola, R.L. Davis, M. Yoon, A. Motamedi, A. Kroll, C.P. Seo, J.E. Hsia, S.K. Kim, J.W. Mitchell, et al. 2015. Cell biology. Reversible centriole depletion with an inhibitor of Polo-like kinase 4. *Science.* 348:1155–1160. https://doi.org/10.1126/science.aaa5111

Wutz, A. 2014. Haploid animal cells. *Development.* 141:1423–1426. https://doi.org/10.1242/dev.102202

Yang, H., Z. Liu, Y. Ma, C. Zhong, Q. Yin, C. Zhou, L. Shi, Y. Cai, H. Zhao, H. Wang, et al. 2013. Generation of haploid embryonic stem cells from Macaca fascicularis monkey parthenotes. *Cell Res.* 23:1187–1200. https://doi.org/10.1038/cr.2013.93

Yokoyama, H., O.J. Gruss, S. Rybina, M. Caudron, M. Schelder, M. Wilm, I.W. Mattaj, and E. Karsenti. 2008. Cdk11 is a RanGTP-dependent microtubule stabilization factor that regulates spindle assembly rate. *J. Cell Biol.* 180:867–875. https://doi.org/10.1083/jcb.200706189

Biochemical and Biophysical Research Communications 504 (2018) 231–237

Contents lists available at ScienceDirect

Biochemical and Biophysical Research Communications

journal homepage: www.elsevier.com/locate/ybbrc

Ploidy-dependent change in cyclin D2 expression and sensitization to cdk4/6 inhibition in human somatic haploid cells☆

Kan Yaguchi [a], Takahiro Yamamoto [a], Masaya Shimada [a], Rina Sugimoto [a], Kiminori Nakamura [a], Tokiyoshi Ayabe [a, b], Ryota Uehara [a, b, *]

[a] Graduate School of Life Science, Hokkaido University, Japan
[b] Faculty of Advanced Life Science, Hokkaido University, Japan

ARTICLE INFO

Article history:
Received 9 August 2018
Accepted 26 August 2018
Available online 5 September 2018

Keywords:
Ploidy
Cyclin D

ABSTRACT

Near-haploidy is observed in certain cancer types, but ploidy-dependent alterations in gene regulation in the haploid state remain elusive. Here, by comparative transcriptome analysis between human isogenic haploid and diploid cell lines, we found lowering of cyclin D2 level in haploids. Acute genome duplication in haploids restored cyclin D2 expression to diploid level, indicating that the regulation of cyclin D2 expression is directly linked to ploidy. Downstream pathways of cyclin D2, such as Rb phosphorylation and p27 sequestration remained intact in haploids, suggesting that they adapt to lowered cyclin D level. Interestingly, however, haploid cells were more susceptible to cdk4/6 inhibition compared to diploids. Our finding indicates feasibility of selective growth suppression of haploid cells based on ploidy-linked gene regulation.

1. Introduction

Alterations in chromosome number are hallmark of cancer cells. Tetraploidy, the doubling of the whole chromosome sets of normal diploid cells, is observed in broad spectrum of cancers [1–5]. Artificially-induced tetraploidization has been demonstrated to promote tumorigenesis in rodents, indicating important pathological contribution of tetraploid cells to malignancy [6,7]. On the other hand, albeit with much lower frequency compared to tetraploidy, near-haploidy is also observed in certain types of blood and solid cancers, being regarded as signs of poor prognosis [8–17]. Near haploid somatic cells are generally very unstable and easily convert to diploids both in vitro and in vivo [18,19]. Once diploidized, they are nearly indistinguishable from canonical diploid cells by conventional chromosome diagnoses [8,20]. Therefore, it is possible that much more cancer cell types than those currently recognized have passed through “near-haploid phase” in their history.

A comprehensive understanding of ploidy-dependent alteration in gene regulation would provide important information for developing new cancer therapeutic strategies that enable selectively targeting of cancer cells with abnormal ploidy states. Recent comparative transcriptome and proteome analyses between human isogenic diploid and tetraploid cells revealed that expression of G1/S cyclin, cyclin D is commonly upregulated in several tetraploid cell lines [21,22]. Cyclin D mediates entry into the cell cycle through activation of its binding partners cyclin-dependent kinase 4/6 (cdk4/6) [23], and was proposed to be required for overriding p53-mediated suppression of proliferation upon tetraploidization. Another proteome study reported tetraploidy-linked activation of mitotic regulatory pathways, which was proposed to overcome mitotic stresses arose from increased number of chromosomes upon tetraploidization [24]. Moreover, several comparative pharmacological studies between diploid and tetraploid cell lines have revealed selective growth suppression of tetraploid cells by mitosis- or cell cycle-related cytotoxic compounds [25–27]. On the other hand, while recent studies revealed haploidy-linked p53 upregulation or mitotic stress arising from haploidy-specific centrosome loss, it remains largely unknown how haploidy effects global gene regulation [28,29]. It also remains to be determined whether there are any molecular targets with which near-haploid cancer cells are selectively affected. In this study, we performed comparative transcriptome analyses between isogenic haploid and diploid human cells, through which we identified

☆ Kan Yaguchi, Takahiro Yamamoto, Masaya Shimada and Rina Sugimoto equally contributed to this work.

* Corresponding author. Faculty of Advanced Life Science, Hokkaido University, Kita 21, Nishi 11, Kita-ku, Sapporo, 001-0021, Japan.
E-mail address: ruehara@sci.hokudai.ac.jp (R. Uehara).

https://doi.org/10.1016/j.bbrc.2018.08.160
0006-291X/

haploidy-linked alterations in expression of several genes including reduction of cyclin D2. Based on these results, we found haploid cells are more susceptible to cdk4/6 inhibition compared to their diploid counterparts.

2. Materials and methods

2.1. Cell culture, and flow cytometry

The haploid HAP1 cells were maintained as previously described [28]. Diploid and tetraploid HAP1 cell lines were established as previously described [28]. For DNA content analyses, 2×10^6 cells were stained with 10 μg/mL Hoechst 33342 (Dojindo) for 15 min at 37 °C, and fluorescence intensity was analyzed using a JSAN desktop cell sorter (Bay bioscience). Cell synchronization was performed as previously described with modifications [30]. Shortly, asynchronous cells were treated with 20 ng/mL nocodazole for 4 h, and washed with culture medium three times. Mitotic cells were shaken off and subjected to immunoblotting at each time point indicated.

2.2. Cell proliferation assay

For cell proliferation assay, cells were seeded on 96-well plates at 9,000, 4,500, or 2250 cells/well (for haploid, diploid, or tetraploid HAP1 cells, respectively). After 24 h, cells were treated with different concentrations of PD0332991 (PZ0199, Sigma-Aldrich), LY2835219 (HY-16297, MedChemExpress) or doxorubicin hydrochloride (040–21521, Wako). Forty-eight h after addition of the compounds, 5% Cell Counting Kit-8 (Dojindo) was added to culture medium, incubated for 4 h, and absorbance at 450 nm was measured using the Sunrise plate reader (Tecan).

2.3. RNAi

The siRNA sequences used in this study are 5′-CGAUGCCUCUUUGAAUAAA-3' (Anillin) [31], and 5′-CGUACGCGGAAUACUUCGA-3' (Luciferase). siRNA transfection was performed using Lipofectamine RNAiMAX (Thermo Fisher Scientific).

2.4. Immunoprecipitation and immunoblotting

Immunoprecipitation and immunoblotting were performed as previously described [32]. For signal detection, the ezWestLumi plus ECL Substrate (ATTO) and a LuminoGraph II chemiluminescent imaging system (ATTO) were used. Quantification of CBB staining or immunoblotting signals was performed using the Gels tool in ImageJ software (National Institutes of Health).

2.5. RNA-seq and differentially expressed gene (DEG) analysis

Total RNA was isolated from asynchronous cell culture using NucleoSpin RNA kit (Macherey-Nagel) according to the manufacturer's instruction. Library preparation, sequencing and analysis were performed by Macrogen Inc. (Seoul Korea) as previously described [33]. Briefly, integrity of total RNA was checked using an Agilent 2100 Bioanalyzer. cDNA libraries were constructed using TruSeq RNA Sample Prep Kit v2 (Illumina), and quantified using 2100 Bioanalyzer. One hundred-base paired end sequencing was conducted on the Illumina HiSeq 2000. Overall reads' quality, total bases, total reads, GC (%) and basic statistics were calculated by FastQC program version 0.10.0, and adapter sequences and low quality reads removed by Trimmomatic program version 0.32. The trimmed reads were mapped to UCSC hg19 human genome with HopHat version 2.0.13. Then, -G option of Cufflinks version 2.2.1 was used to assemble transcripts from aligned reads and calculate expression profiles of assembled transcripts. Expression profiles were expressed as the fragments per kilobase of transcript per million mapped reads (FPKM). To facilitate the statistical analysis with a balanced data distribution, 1 was added to the raw signals (FPKMs) and transformed the data to log 2. After log transformation, in order to reduce systematic bias, quantile normalization was used with preprocessCore' R library. Statistical analysis was performed using fold change per comparison pair. The significant results were selected on conditions of $|fc| \geq 2$.

2.6. Quantitative real-time PCR

Reverse transcription reactions were conducted using 1500 ng of total RNA template in 60 μl of total volume reactions using SuperScript VILO master mix (Thermo Fisher). The reaction solutions were diluted 5 time in nuclease-free water, and real-time PCR was performed on the Light Cycler 480 (Roche) in 20 μl reaction mixture containing 5 μl cDNA template, 500 nM forward and reverse primers, and 100 nM universal probe (Roche). Primers used for qRT-PCR were listed in Table S1.

2.7. Bromodeoxyuridine (BrdU) incorporation assay

BrdU incorporation was conducted as previously described [28]. Chromosomes were stained using 1.0 μg/mL DAPI (Dojindo). Fixed cells were observed under a TE2000 microscope (Nikon) equipped with a × 40 0.95 NA Plan Apo objective lens (Nikon), and an ORCA-ER CCD camera (Hamamatsu Photonics). Image acquisition was controlled by μManager software (Open Imaging).

2.8. Antibodies

Antibodies used in this study were listed in Table S2. Fluorescence- or horseradish peroxidase-conjugated secondary antibodies were purchased from Jackson ImmunoResearch Laboratories and used at dilution of 1:1000 for IF and IB.

3. Results and discussion

3.1. Ploidy-dependent changes in gene expression between haploid and diploid HAP1 cells

To gain insight into haploidy-linked changes in gene expression profiles, we performed comprehensive next generation RNA-seq using near-haploid human somatic cell line, HAP1 and its isogenic diploid counterpart (Fig. 1A) [28,34]. Among ~70 genes indicated to be up- or downregulated in haploid cells compared to diploids in differentially expressed gene analysis (Fig. 1B, and Table S3), we confirmed the ploidy-dependent changes in transcriptional and translational levels of several genes by quantitative RT-PCR (for GPC3/glypican3, IGFBP5, CCND2/Cyclin D2, ANXA1, and LAMB1) and immunoblotting (for glypican3, and cyclin D2), respectively (Fig. 1C and D). Of interest, glypican3 or cyclin D2, whose expression is reportedly downregulated or upregulated, respectively, in the tetraploid state compared to diploid counterparts in different types of cells [21,35], was found to be upregulated or downregulated, respectively, in haploid HAP1 cells. These results indicate general linearity in ploidy-dependent changes in regulation of certain genes across hypo- and hyperdiploid states. Cell cycle distribution was similar between asynchronous haploid and diploid cells (Fig. 1A), ruling out the possibility that the ploidy-dependent change in cyclin D2 expression is merely an indirect consequence of altered cell cycle distribution between different ploidies. Moreover, the ploidy-dependent change in cyclin D2

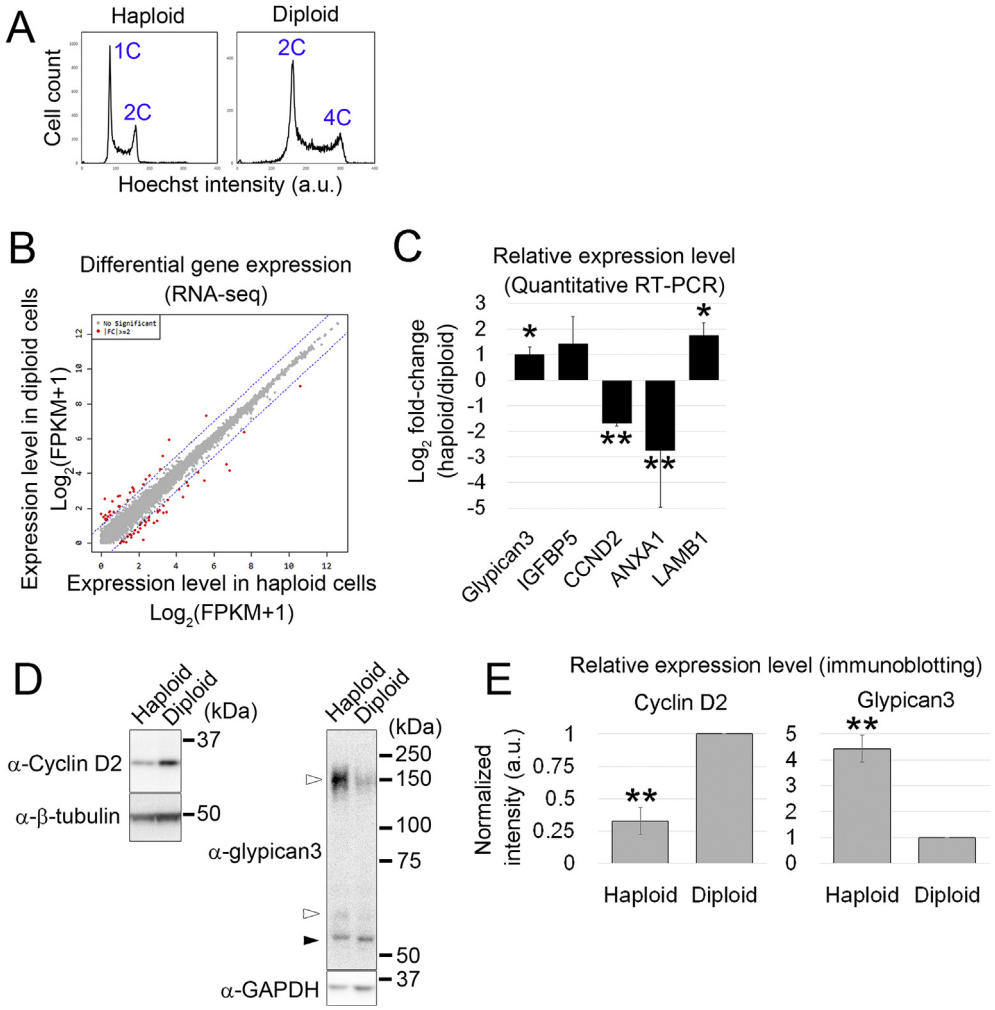

Fig. 1. Ploidy-dependent change in gene expression between haploid and diploid HAP1 cells
(**A**) Flow cytometric analysis of DNA content in Hoechst-stained haploid and diploid HAP1 cells. (**B**) Scatter plot of gene expression level between haploid and diploid HAP1 cells in differentially expressed gene analysis. Genes with more than 2 fold differences in $\log_2$ (FPKM+1) values were indicated in red. (**C**) Quantification of relative expression levels of several genes between haploid and diploid cells by quantitative real-time PCR. Expression level of each gene was normalized to that of GAPDH. Mean ± SE of 3 independent experiments (*p < 0.05, **p < 0.01, *t*-test). (**D**) Immunoblotting of cyclin D2 and glypican3 in haploid and diploid cells. Solid and open arrowheads correspond to unglycosylated and glycosylated forms of glypican3, respectively. Equal total protein amount of sample was loaded to each lane. β-tubulin or GAPDH was detected as a loading control. (**E**) Quantification of immunoblotting signals in D. Signal intensities were normalized to those of the loading control. Mean ± SE of 3 independent experiments (**p < 0.01, *t*-test). (For interpretation of the references to colour in this figure legend, the reader is referred to the Web version of this article.)

expression was also observed in G1/S-synchronized cell populations (Fig. 2A and B). Ploidy dependent altered expression of G1/S cyclin has been also observed in budding yeasts, but in that case, expression level of cln3, a yeast G1/S cyclin is in inverse proportion to the ploidy level [36]. Since G1/S cyclins are key regulators of cell proliferation and viability, we decided to investigate the physiological impact of the change in cyclin D2 expression in haploid cells in further detail.

Changes in the expression of cyclin D potentially affects cell cycle regulatory events including the induction of S phase cyclins [37,38]. To test this possibility, we compared time-dependent patterns of the expressions of cyclin D2 and other cyclins (cyclin D1, D3, E1 and A2) during G1 and S phases between haploid and diploid cells that were synchronized by nocodazole shake-off (Fig. 2A and B). There was no obvious time-dependent change in expression levels of cyclin D1 and D2 both in haploid and diploid cells, and expression of these cyclins was lowered in haploid cells compared to diploids throughout G1/S phase. On the other hand, cyclin D3 was expressed slightly higher in haploid cells than in diploid ones around 4 h after nocodazole release, which corresponds to late G1 in these cell lines [28]. Expression level of cyclin E1 and A2, which govern the initiation and the progression of S phase [39], was roughly equivalent between haploid and diploid cells throughout G1/S phase. These results indicate that the haploidy-linked reduction in cyclin D2 expression during G1 phase has minimal effect on regulation of the subsequent cell cycle control. Supporting this idea, we found that the level of retinoblastoma protein (Rb) phosphorylation and the amount of p27 bound to cdk2, which are reportedly under control of cyclin D-cdk4/6 remained unchanged between haploid and diploid cells during G1/S phase (Fig. 2D–F) [37,40–42]. These results indicate that haploid cells adapt to the low cyclin D level and can promote G1/S progression as efficiently as diploid cells.

3.2. Acute increase in cyclin D expression upon diploidization after cell division failure

Next, we wished to gain insight into the mechanism underlying

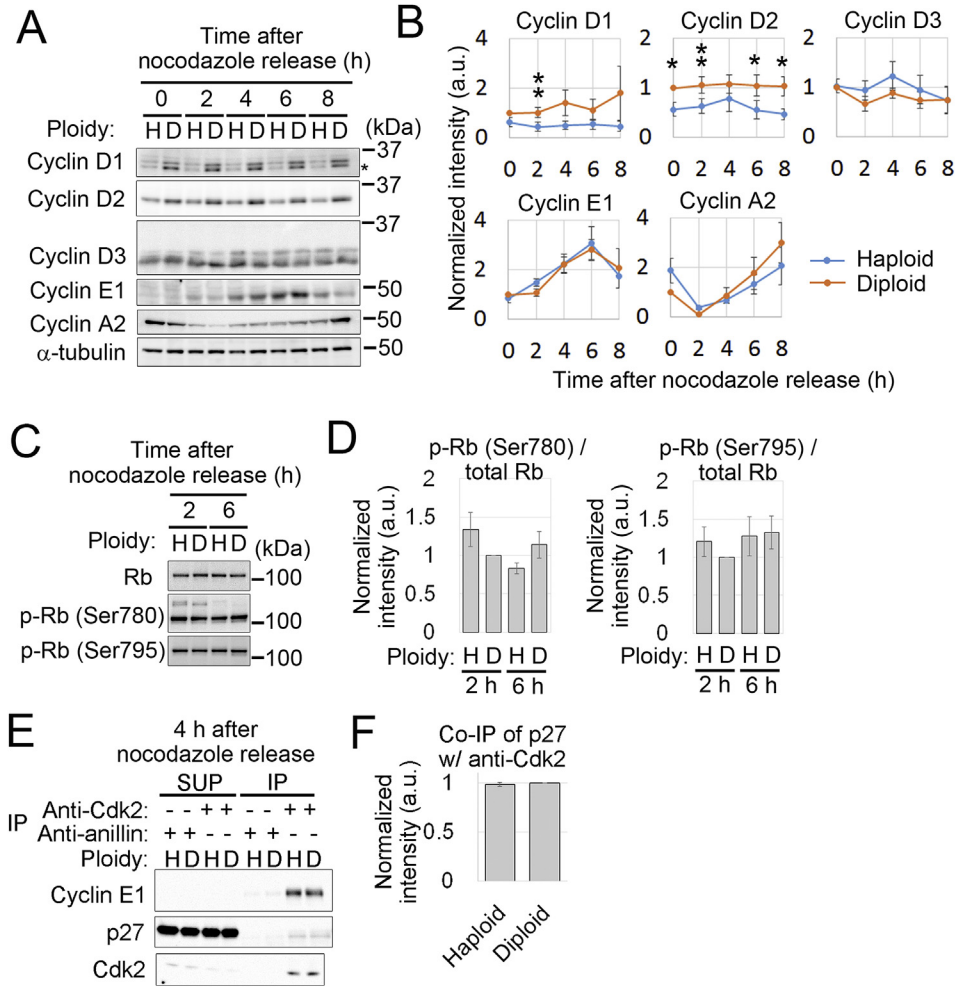

Fig. 2. Expression of G1/S cyclins in synchronized haploid and diploid cells
(**A**, **C**) Immunoblotting of G1/S cyclins (A) or phosphorylated Rb (C) in synchronized haploid or diploid cells. Equal total protein amount of sample was loaded to each lane. α-tubulin was detected as a loading control in A. Asterisk in A indicates cross-reaction of anti-cyclin D1 antibody to cyclin D2. (**B**, **D**) Quantification of immunostaining signals in A or C. Signal intensities were normalized to those of the loading control, and then to that of diploid cells at 0 h (B) or 2 h (D) after nocodazole release. Mean ± SE of 3 independent experiments (*$p < 0.05$, **$p < 0.01$, *t*-test). (**E**) Immunoblotting of cyclin E1, p27, and cdk2 in immunoprecipitant obtained using anti-cdk2 antibody from synchronized haploid or diploid cells. Anti-anillin antibody was used as negative control. (**F**) Quantification of p27 co-immunoprecipitated with cdk2 in F. Mean ± SE of 3 independent experiments.

the ploidy-dependent change in cyclin D expression between haploid and diploid cells. Previous studies have proposed that elevated expression of cyclin D in tetraploid cells is a result of cyclin D-overexpressing cells that spontaneously arise and override tetraploidy-associated induction of p53-dependent cell cycle arrest [21,22]. Supporting this idea, it was found that elevation of cyclin D expression commonly takes place in clonal tetraploid cells established through long-term culture, but not in the cells acutely tetraploidized by cell division failure [21]. To test whether ploidy-dependent difference in cyclin D2 expression between haploids and diploids also arises from a similar selective mechanism, we investigated the impact of acute diploidization of haploid cells on cyclin D2 expression (Fig. 3A–D). For that purpose, an essential cytokinesis regulator anillin was depleted to induce whole genome duplication through cell division failure in haploid and diploid cells (Fig. 3A and B) [43]. Depletion of anillin resulted in doubling of DNA contents with binucleation in a substantial population of haploid cells (Fig. 3A and D), and importantly, lead to a substantial increase in expression of cyclin D2 compared to mock-depleted control haploid cells (Fig. 3B and C). Upon binucleation in anillin-depleted cells, a proportion of BrdU-positive cells remained unchanged from controls, suggesting that diploidization of haploid HAP1 cells did not induce cell cycle arrest. This rules out the possibility that the change in cyclin D2 expression arose from cell cycle arrest upon cell division failure (Fig. 3D). The fact that cyclin D2 expression changes within a few days upon diploidization indicates that ploidy conversion *per se*, rather than selection or adaptive processes accompanying ploidy conversion, drives the change in cyclin D2 expression in our experimental condition. These results suggest a new mechanism that directly controls cyclin D2 expression depending on ploidy state.

3.3. Haploid cells are more susceptible to cdk4/6 inhibition than diploids

Cyclin D is often deregulated in broad spectrum of tumor cells and is an attractive therapeutic target for cancer treatment [23]. Based on the finding of ploidy-dependent difference in cyclin D expression, we next determined whether the efficacy of selective inhibitors of cdk4/6 differs among cells with different ploidies. For this, viability of haploid, diploid, and tetraploid (previously established from diploid [28]) HAP1 cells was compared after treating various concentrations of two different cdk4/6 inhibitors, PD-0332991 and LY-2835219 (Fig. 4A and B). Consistent with a

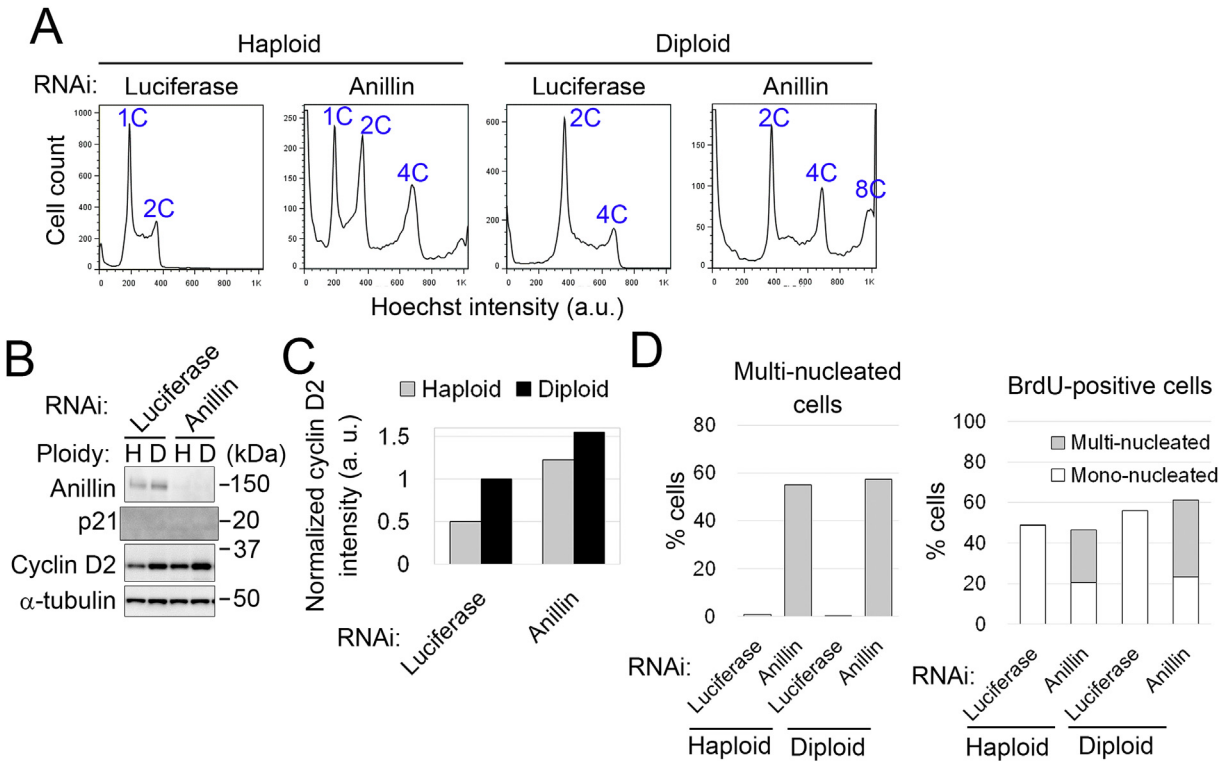

Fig. 3. Acute diploidization results in upregulation of cyclin D expression
(**A**) Flow cytometric analysis of DNA content in RNAi-treated Hoechst-stained haploid and diploid cells. (**B**) Immunoblotting of anillin, p21 and cyclin D in control or anillin-depleted haploid or diploid HAP1 cells. α-tubulin was detected as a loading control. (**C**) Quantification of immunostaining signals in B. Signal intensities were normalized to those of the loading control, and then to that of diploid mock-depleted cells. Mean of 2 independent experiments. (**D**) Frequency of multi-nucleated cells (left) or BrdU-incorporated cell population (right) in RNAi-treated haploid or diploid cells. Mean of 2 independent experiments. At least 393 cells were analysed for each condition.

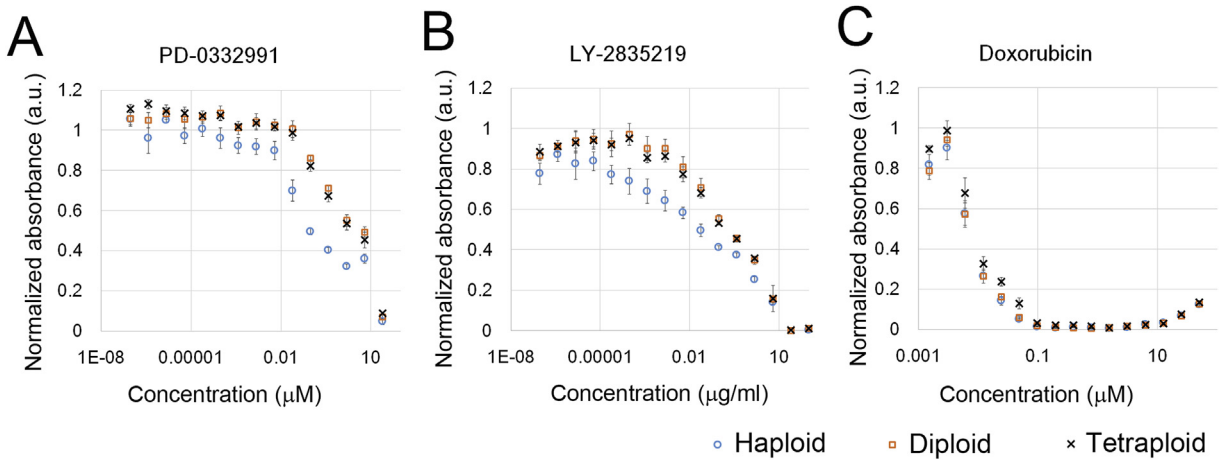

Fig. 4. Haploid cells are more susceptible to cdk4/6 inhibitors
(**A-C**) Effect of PD-0332991 (A), LY-2835219 (B), and Doxorubicin (C) on growth of haploid, diploid, and tetraploid HAP1 cells. Cells were treated with each compounds for 48 h, and their growth was quantified by the CCK-8 assay. Absorbance at 450 nm measured of each sample was normalized to that of non-treated control with the corresponding ploidy. Mean ± SE of 4 samples from 2 independent experiments.

previous report in different cell lines, we did not observe a difference in efficacy of these reagents between diploid and tetraploid HAP1 cells [22]. Interestingly, however, we found that both of these cdk4/6 inhibitors suppressed growth of haploid cells more efficiently than that of their diploid or tetraploid counterparts. The ploidy dependency was not observed with another cell toxic reagent doxorubicin, demonstrating that ploidy selectivity is a specific property of cdk4/6 inhibitors (Fig. 4C). These results indicate that cells are more susceptible to inhibition of cyclin D-cdk4/6 function in the haploid state than in diploid or higher ploidy states.

In this study, we found haploidy-associated attenuation of cyclin D1 and D2 expression in human somatic cells. Expression of Cyclin D is regulated at the transcriptional, translational, and post-translational levels [44,45]. Since a difference in ploidy affected the abundance of cyclin D2 mRNA (Fig. 1B and C), there seems to be a ploidy-dependent mechanism that controls cyclin D2 expression

at the transcriptional level. Transcription of cyclin D is regulated by various inputs such as signals from growth factors and the extracellular matrix [44]. Of interest, we recently found a substantial delay in post-mitotic cell spreading in haploid HAP1 cells compared to their diploid counterparts (Yaguchi and Uehara, unpublished), which may potentially affect cyclin D2 expression in haploid cells. However, since ploidy-dependent difference in cyclin D2 expression was observed even in mitotically arrested cells (Fig. 2A and B), there seems to be another layer of regulation than cell adhesion involved in the attenuation of cyclin D2 in haploid cells.

Despite lowered cyclin D2 expression, its downstream pathways remained intact in haploid cells, suggesting that they adapt to the low cyclin D2 level. It might be possible that the halving of the cell contents from diploid cells reduces the cellular requirement for cyclin D function in haploid cells. However, haploid cells showed substantially higher sensitivity to cdk4/6 inhibitors (Fig. 4). Though further analyses are required to understand the mechanisms underlying the sensitization of haploid cells to cdk4/6 inhibition, one possible explanation is that the haploidy-linked reduction in cyclin D2 level reduces the active pool of cyclin D-cdk4/6 which can buffer cytotoxicity of low-dose cdk4/6 inhibitors. Our finding of the selective effect of cdk4/6 inhibitors on haploid cell growth indicates the feasibility of specific growth suppression of cancer cells with abnormal ploidies by targeting genes whose abundance or functionality changes depending on ploidy states.

Acknowledgement

We are grateful to Mithilesh Mishra and Sarada Bulchand, for valuable comments on the draft of this paper, Kimino Sato, and Eva Margittai for technical assistance, and Gohta Goshima for sharing reagents. This work was supported by the Orange Foundation, the SGH Foundation, the Smoking Research Foundation, the Suhara Memorial Foundation, and MEXT/JSPS KAKENHI (Grants Numbers 15K14501, and 17K15111) to R. U.

Appendix A. Supplementary data

Supplementary data related to this article can be found at https://doi.org/10.1016/j.bbrc.2018.08.160.

References

[1] S.M. Dewhurst, N. McGranahan, R.A. Burrell, et al., Tolerance of whole-genome doubling propagates chromosomal instability and accelerates cancer genome evolution, Canc. Discov. 4 (2014) 175–185.
[2] P.C. Galipeau, D.S. Cowan, C.A. Sanchez, M.T. Barrett, M.J. Emond, D.S. Levine, P.S. Rabinovitch, B.J. Reid, 17p (p53) allelic losses, 4N (G2/tetraploid) populations, and progression to aneuploidy in Barrett's esophagus, Proc. Natl. Acad. Sci. U. S. A. 93 (1996) 7081–7084.
[3] A.J. Olaharski, R. Sotelo, G. Solorza-Luna, M.E. Gonsebatt, P. Guzman, A. Mohar, D.A. Eastmond, Tetraploidy and chromosomal instability are early events during cervical carcinogenesis, Carcinogenesis 27 (2006) 337–343.
[4] S.L. Carter, K. Cibulskis, E. Helman, et al., Absolute quantification of somatic DNA alterations in human cancer, Nat. Biotechnol. 30 (2012) 413–421.
[5] I. Vitale, L. Galluzzi, L. Senovilla, A. Criollo, M. Jemaa, M. Castedo, G. Kroemer, Illicit survival of cancer cells during polyploidization and depolyploidization, Cell Death Differ. 18 (2011) 1403–1413.
[6] T. Fujiwara, M. Bandi, M. Nitta, E.V. Ivanova, R.T. Bronson, D. Pellman, Cytokinesis failure generating tetraploids promotes tumorigenesis in p53-null cells, Nature 437 (2005) 1043–1047.
[7] A. Castillo, H.C. Morse 3rd, V.L. Godfrey, R. Naeem, M.J. Justice, Overexpression of Eg5 causes genomic instability and tumor formation in mice, Canc. Res. 67 (2007) 10138–10147.
[8] S. Safavi, K. Paulsson, Near-haploid and low-hypodiploid acute lymphoblastic leukemia: two distinct subtypes with consistently poor prognosis, Blood 129 (2017) 420–423.
[9] G.M. Brodeur, D.L. Williams, A.T. Look, W.P. Bowman, D.K. Kalwinsky, Near-haploid acute lymphoblastic leukemia: a unique subgroup with a poor prognosis? Blood 58 (1981) 14–19.
[10] S. Kohno, J. Minowada, A.A. Sandberg, Chromosome evolution of near-haploid clones in an established human acute lymphoblastic leukemia cell line (NALM-16), J. Natl. Cancer Inst. 64 (1980) 485–493.
[11] Y. Kaneko, M. Sakurai, Acute lymphocytic leukemia (ALL) with near-haploidy—a unique subgroup of ALL? Canc. Genet. Cytogenet. 2 (1980) 13–18.
[12] L. Holmfeldt, L. Wei, E. Diaz-Flores, et al., The genomic landscape of hypodiploid acute lymphoblastic leukemia, Nat. Genet. 45 (2013) 242–252.
[13] B. Gibbons, P. MacCallum, E. Watts, A.Z. Rohatiner, D. Webb, F.E. Katz, L.M. Secker-Walker, I.J. Temperley, C.J. Harrison, R.H. Campbell, et al., Near haploid acute lymphoblastic leukemia: seven new cases and a review of the literature, Leukemia 5 (1991) 738–743.
[14] D.F. Callen, K. Raphael, P.M. Michael, O.M. Garson, Acute lymphoblastic leukemia with a hypodiploid karyotype with less than 40 chromosomes: the basis for division into two subgroups, Leukemia 3 (1989) 749–752.
[15] J.V. Bovee, A.M. Cleton-Jansen, N.J. Kuipers-Dijkshoorn, et al., Loss of heterozygosity and DNA ploidy point to a diverging genetic mechanism in the origin of peripheral and central chondrosarcoma, Gene Chromosome Canc. 26 (1999) 237–246.
[16] W.R. Sukov, R.P. Ketterling, S. Wei, et al., Nearly identical near-haploid karyotype in a peritoneal mesothelioma and a retroperitoneal malignant peripheral nerve sheath tumor, Canc. Genet. Cytogenet. 202 (2010) 123–128.
[17] M. Oshimura, A.I. Freeman, A.A. Sandberg, Chromosomes and causation of human cancer and leukemia. XXIII. Near-haploidy in acute leukemia, Cancer 40 (1977) 1143–1148.
[18] M. Kotecki, P.S. Reddy, B.H. Cochran, Isolation and characterization of a near-haploid human cell line, Exp. Cell Res. 252 (1999) 273–280.
[19] I. Sagi, G. Chia, T. Golan-Lev, M. Peretz, U. Weissbein, L. Sui, M.V. Sauer, O. Yanuka, D. Egli, N. Benvenisty, Derivation and differentiation of haploid human embryonic stem cells, Nature 532 (2016) 107–111.
[20] B. Stark, M. Jeison, R. Gobuzov, H. Krug, L. Glaser-Gabay, D. Luria, R. El-Hasid, M.B. Harush, G. Avrahami, S. Fisher, J. Stein, R. Zaizov, I. Yaniv, Near haploid childhood acute lymphoblastic leukemia masked by hyperdiploid line: detection by fluorescence in situ hybridization, Canc. Genet. Cytogenet. 128 (2001) 108–113.
[21] T.A. Potapova, C.W. Seidel, A.C. Box, G. Rancati, R. Li, Transcriptome analysis of tetraploid cells identifies cyclin D2 as a facilitator of adaptation to genome doubling in the presence of p53, Mol. Biol. Cell 27 (2016) 3065–3084.
[22] A. Crockford, L.P. Zalmas, E. Gronroos, et al., Cyclin D mediates tolerance of genome-doubling in cancers with functional p53, Ann. Oncol. official. Eur. Soc. Med. Oncol. 28 (2017) 149–156.
[23] E.A. Musgrove, C.E. Caldon, J. Barraclough, A. Stone, R.L. Sutherland, Cyclin D as a therapeutic target in cancer, Nat. Rev. Canc. 11 (2011) 558–572.
[24] C. Vigano, C. von Schubert, E. Ahrne, A. Schmidt, T. Lorber, L. Bubendorf, J.R.F. De Vetter, G.J.R. Zaman, Z. Storchova, E.A. Nigg, Quantitative proteomic and phosphoproteomic comparison of human colon cancer DLD-1 cells differing in ploidy and chromosome stability, Mol. Biol. Cell 29 (2018) 1031–1047.
[25] I. Vitale, L. Galluzzi, S. Vivet, L. Nanty, P. Dessen, L. Senovilla, K.A. Olaussen, V. Lazar, M. Prudhomme, R.M. Golsteyn, M. Castedo, G. Kroemer, Inhibition of Chk1 kills tetraploid tumor cells through a p53-dependent pathway, PLoS One 2 (2007), e1337.
[26] S. Rello-Varona, I. Vitale, O. Kepp, L. Senovilla, M. Jemaa, D. Metivier, M. Castedo, G. Kroemer, Preferential killing of tetraploid tumor cells by targeting the mitotic kinesin Eg5, Cell Cycle (Georgetown, Tex.) 8 (2009) 1030–1035.
[27] M. Jemaa, G. Manic, G. Lledo, D. Lissa, C. Reynes, N. Morin, F. Chibon, A. Sistigu, M. Castedo, I. Vitale, G. Kroemer, A. Abrieu, Whole-genome duplication increases tumor cell sensitivity to MPS1 inhibition, Oncotarget 7 (2016) 885–901.
[28] K. Yaguchi, T. Yamamoto, R. Matsui, Y. Tsukada, A. Shibanuma, K. Kamimura, T. Koda, R. Uehara, Uncoordinated centrosome cycle underlies the instability of non-diploid somatic cells in mammals, J. Cell Biol. 217 (2018) 2463–2483.
[29] T. Olbrich, C. Mayor-Ruiz, M. Vega-Sendino, C. Gomez, S. Ortega, S. Ruiz, O. Fernandez-Capetillo, A p53-dependent response limits the viability of mammalian haploid cells, Proc. Natl. Acad. Sci. U. S. A. 114 (2017) 9367–9372.
[30] R. Uehara, G. Goshima, Functional central spindle assembly requires de novo microtubule generation in the interchromosomal region during anaphase, J. Cell Biol. 191 (2010) 259–267.
[31] A.J. Piekny, M. Glotzer, Anillin is a scaffold protein that links RhoA, actin, and myosin during cytokinesis, Curr. Biol. CB (Curr. Biol.) 18 (2008) 30–36.
[32] R. Uehara, Y. Tsukada, T. Kamasaki, I. Poser, K. Yoda, D.W. Gerlich, G. Goshima, Aurora B and Kif2A control microtubule length for assembly of a functional central spindle during anaphase, J. Cell Biol. 202 (2013) 623–636.
[33] J.A. Martin, Z. Wang, Next-generation transcriptome assembly, Nat. Rev. Genet. 12 (2011) 671–682.
[34] J.E. Carette, M. Raaben, A.C. Wong, A.S. Herbert, G. Obernosterer, N. Mulherkar, A.I. Kuehne, P.J. Kranzusch, A.M. Griffin, G. Ruthel, P. Dal Cin, J.M. Dye, S.P. Whelan, K. Chandran, T.R. Brummelkamp, Ebola virus entry requires the cholesterol transporter Niemann-Pick C1, Nature 477 (2011) 340–343.
[35] M.R. Jones, K. Ravid, Vascular smooth muscle polyploidization as a biomarker for aging and its impact on differential gene expression, J. Biol. Chem. 279 (2004) 5306–5313.
[36] T. Galitski, A.J. Saldanha, C.A. Styles, E.S. Lander, G.R. Fink, Ploidy regulation of gene expression, Science 285 (1999) 251–254.
[37] C.J. Sherr, J.M. Roberts, CDK inhibitors: positive and negative regulators of G1-phase progression, Genes Dev. 13 (1999) 1501–1512.

[38] Y.J. Choi, L. Anders, Signaling through cyclin D-dependent kinases, Oncogene 33 (2013) 1890.
[39] X. Grana, E.P. Reddy, Cell cycle control in mammalian cells: role of cyclins, cyclin dependent kinases (CDKs), growth suppressor genes and cyclin-dependent kinase inhibitors (CKIs), Oncogene 11 (1995) 211–219.
[40] H. Matsushime, M.E. Ewen, D.K. Strom, J.Y. Kato, S.K. Hanks, M.F. Roussel, C.J. Sherr, Identification and properties of an atypical catalytic subunit (p34PSK-J3/cdk4) for mammalian D type G1 cyclins, Cell 71 (1992) 323–334.
[41] J. Kato, H. Matsushime, S.W. Hiebert, M.E. Ewen, C.J. Sherr, Direct binding of cyclin D to the retinoblastoma gene product (pRb) and pRb phosphorylation by the cyclin D-dependent kinase CDK4, Genes Dev. 7 (1993) 331–342.
[42] H. Jiang, H.S. Chou, L. Zhu, Requirement of cyclin E-cdk2 inhibition in p16 INK4a -mediated growth suppression, Mol. Cell Biol. 18 (1998) 5284–5290.
[43] K. Oegema, M.S. Savoian, T.J. Mitchison, C.M. Field, Functional analysis of a human homologue of the Drosophila actin binding protein anillin suggests a role in cytokinesis, J. Cell Biol. 150 (2000) 539–552.
[44] E.A. Klein, R.K. Assoian, Transcriptional regulation of the cyclin D1 gene at a glance, J. Cell Sci. 121 (2008) 3853–3857.
[45] W.-Y. Tarn, M.-C. Lai, Translational control of cyclins, Cell Div. 6 (2011) 5.

CELL STRUCTURE AND FUNCTION 46: 1–??? (2021)

Short Communication

Mevalonate Pathway-mediated ER Homeostasis Is Required for Haploid Stability in Human Somatic Cells

Kan Yaguchi[1], Kimino Sato[1], Koya Yoshizawa[1], Daisuke Mikami[2], Kohei Yuyama[2], Yasuyuki Igarashi[2], Gabor Banhegyi[3], Eva Margittai[4], and Ryota Uehara[1,5]*

[1]*Graduate School of Life Science, Hokkaido University, Japan,* [2]*Lipid Biofunction Section, Faculty of Advanced Life Science, Hokkaido University, Japan,* [3]*Institute of Biochemistry and Molecular Biology, Semmelweis University, Hungary,* [4]*Institute of Translational Medicine, Semmelweis University, Hungary,* [5]*Faculty of Advanced Life Science, Hokkaido University, Japan*

ABSTRACT. **The somatic haploidy is unstable in diplontic animals, but cellular processes determining haploid stability remain elusive. Here, we found that inhibition of mevalonate pathway by pitavastatin, a widely used cholesterol-lowering drug, drastically destabilized the haploid state in HAP1 cells. Interestingly, cholesterol supplementation did not restore haploid stability in pitavastatin-treated cells, and cholesterol inhibitor U18666A did not phenocopy haploid destabilization. These results ruled out the involvement of cholesterol in haploid stability. Besides cholesterol perturbation, pitavastatin induced endoplasmic reticulum (ER) stress, the suppression of which by a chemical chaperon significantly restored haploid stability in pitavastatin-treated cells. Our data demonstrate the involvement of the mevalonate pathway in the stability of the haploid state in human somatic cells through managing ER stress, highlighting a novel link between ploidy and ER homeostatic control.**

Key words: Haploid, ER stress, Mevalonate pathway

Introduction

In diplontic animal organisms, somatic haploidy is generally unstable, causing frequent autodiploidization at the cellular level and severe developmental abnormalities at the organismal level (Sagi and Benvenisty, 2017; Wutz, 2014). The halving of genome copy from the normal diploid state potentially has pleiotropic effects on cellular homeostasis in haploid cells. An apparent feature of haploid cells is their halved cellular volume to diploids with the halving of total protein content (Yaguchi *et al.*, 2018). Though these features possibly have profound influence on intracellular processes—such as the metabolic control—in haploid state, it remains elusive what aspects of the metabolism alter and characterize cellular phenotypes of haploid cells.

The mevalonate pathway metabolizes acetyl-CoA to produce sterol isoprenoids, and non-sterol isoprenoids that mediate diverse biosynthetic processes essential for cell construction and proliferation (Buhaescu and Izzedine, 2007; Mullen *et al.*, 2016). Among mevalonate-derived metabolites, cholesterol serves as a structural component of cell membranes and a precursor of fundamental biomolecules, such as steroid hormones. Mevalonate-derived polyisoprenols, such as dolichol phosphates are essential components of glycoprotein synthesis and endoplasmic reticulum (ER) homeostasis participating in protein N-glycosylation, C- and O-mannosylation, and GPI-anchor production (Carlberg *et al.*, 1996; Chojnacki and Dallner, 1988; Doucey *et al.*, 1998). Mevalonate-derived isoprenoids are also used for the prenylation of small GTPases, which mediates signal transduction for dynamic processes such as cytoskeletal reorganization and vesicular trafficking (Leung *et al.*, 2006; Wang and Casey, 2016). Mevalonate pathway controls cell size by optimizing mitochondrial functionality through protein prenylation (Miettinen and Björklund, 2015, 2016; Miettinen *et al.*, 2014). Inhibition of the rate-limiting enzyme of mevalonate pathway, 3-hydroxy-3-methylglutaryl-coenzyme A reductase (HMGCR) by statins perturbs this homeostatic control, leading to increased cell size in cultured cells (Miettinen and Björklund, 2015).

In this study, in an attempt to modulate cell size by an HMGCR inhibitor pitavastatin in human haploid HAP1 cells (Carette *et al.*, 2011), we found that the inhibitor compromised the stability of the haploid state in these cells.

*To whom correspondence should be addressed: Ryota Uehara, Faculty of Advanced Life Science, Hokkaido University, Kita 21, Nishi 11, Kita-ku, Sapporo 001-0021, Japan.
Tel: +81–11–706–9238
E-mail: ruehara@sci.hokudai.ac.jp

Interestingly, a recent chemical screen searching for compounds that stabilize haploid state has also identified statins leading to the selective loss of haploid cells (Olbrich *et al.*, 2019). However, whether the mevalonate pathway is indeed involved in promoting haploid stability, and how the inhibition of the pathway may lead to destabilization of haploid state is still unknown. Using a pharmacological approach, we specified that statin-induced ER stress as a process responsible for the destabilization of the haploid state.

Materials and Methods

Cell culture and flow cytometry

HAP1 cells were purchased from Haplogen and cultured in Iscove's Modified Dulbecco's Medium (IMDM; Wako) supplemented with 10% fetal bovine serum and 1× antibiotic-antimycotic (Sigma-Aldrich). Haploid cells were regularly maintained by size-based cell sorting, as previously described (Yaguchi *et al.*, 2018). For DNA content analysis, cells were stained with 10 μg/ml Hoechst 33342 (Dojindo) for 15 min at 37°C, and fluorescence intensity was analyzed using a JSAN desktop cell sorter (Bay bioscience). For the long-term passage experiments, freshly purified haploid cells were cultured, with passage typically once two days, in the presence of different compounds at final concentrations described elsewhere.

Cholesterol measurement

Details on the cholesterol measurement are described in Supplemental Materials and methods.

Chemical compounds

Compounds were purchased from suppliers as follows: Pitavastatin (163-24861, Wako); U18666A (10009085, Cayman Chemical); Cholesterol (SLBZ0657, Sigma-Aldrich); FTI-277 (S7465, Selleck); GGTI-298 (S7466, Selleck); tauroursodeoxycholic acid (TUDCA, T1567, Tokyo Chemical Industry); and mevalonate (mevalonolactone, M4667, Sigma-Aldrich).

Antibodies and immunoblotting

Antibodies used in this study are listed in Table S1. Phos-tag SDS-PAGE for PERK immunoblotting was conducted as previously described (Yang *et al.*, 2010). We used the ezWestLumi plus ECL Substrate (ATTO) and a LuminoGraph II chemiluminescent imaging system (ATTO) for immunoblotting signal detection. We used the Gels tool in ImageJ (NIH) for signal quantification.

Results

Mevalonate production is required for the stability of the haploid state in HAP1 cells

To test the effects of inhibition of the mevalonate pathway on cell size control, we treated human haploid cell HAP1 with a competitive HMGCR inhibitor pitavastatin, which has been reported to increase the size of human cell lines such as Jurkat (Miettinen and Björklund, 2015). Although we did not observe the increase of cell size in HAP1 cells upon pitavastatin treatment (Fig. S1), we unexpectedly found that the inhibitor destabilized the haploid state of HAP1 cells in flow cytometric DNA content analysis (Fig. 1A–D). Freshly purified, non-treated haploid HAP1 cells gradually diploidized during ~3-weeks continuous passages, resulting in the reduction in haploid G1 proportion (1C peak) from 37.4±1.0% to 28.0±1.7% (mean±standard error, n=3; Fig. 1A–D) (Yaguchi *et al.*, 2018). Diploid G2/M proportion (4C peak) concomitantly increased during the continuous passages from 1.5±0.4% to 10.4±1.5% (Fig. 1A–D). However, when treated with 0.5 μM pitavastatin, which allowed long-term culture without blocking cell proliferation, haploid G1 proportion became significantly less than non-treated control (17.1±1.2%; Fig. 1C and D). Diploid G2/M proportion concomitantly became substantially more in pitavastatin-treated culture than in non-treated control (18.2±1.3%; Fig. 1C and D). Since this result indicates the importance of statin-targeted processes in haploid stability, we further investigated the mechanism underlying the statin-mediated destabilization of haploid state. First, we tested whether co-treatment with mevalonate ameliorates haploid stability in the presence of pitavastatin (Fig. 1C and D). Mevalonate supplementation significantly preserved the haploid population in pitavastatin-treated culture (haploid G1 or diploid G2/M proportion of 30.2±1.0% or 9.4±0.9%, respectively; Fig. 1C and D), demonstrating the requirement for a sufficient amount of mevalonate for haploid stability in HAP1 cells.

Cholesterol perturbation is not the cause of haploid destabilization by pitavastatin

Next, we determined downstream branches of the mevalonate pathway crucial for the maintenance of haploid state. Because statins are widely used cholesterol-lowering drugs (Adhyaru and Jacobson, 2018), we addressed the possible involvement of the cholesterol branch in haploid stability. For this, we compared the content of total cholesterol extracted from control and pitavastatin-treated HAP1 cells using a colorimetric method (Fig. 2A; Materials and methods). In this assay, we did not observe a significant difference in cholesterol content between control and pitavastatin-treated cells. This suggests that, at such a low concentration as 0.5 μM, pitavastatin does not drastically

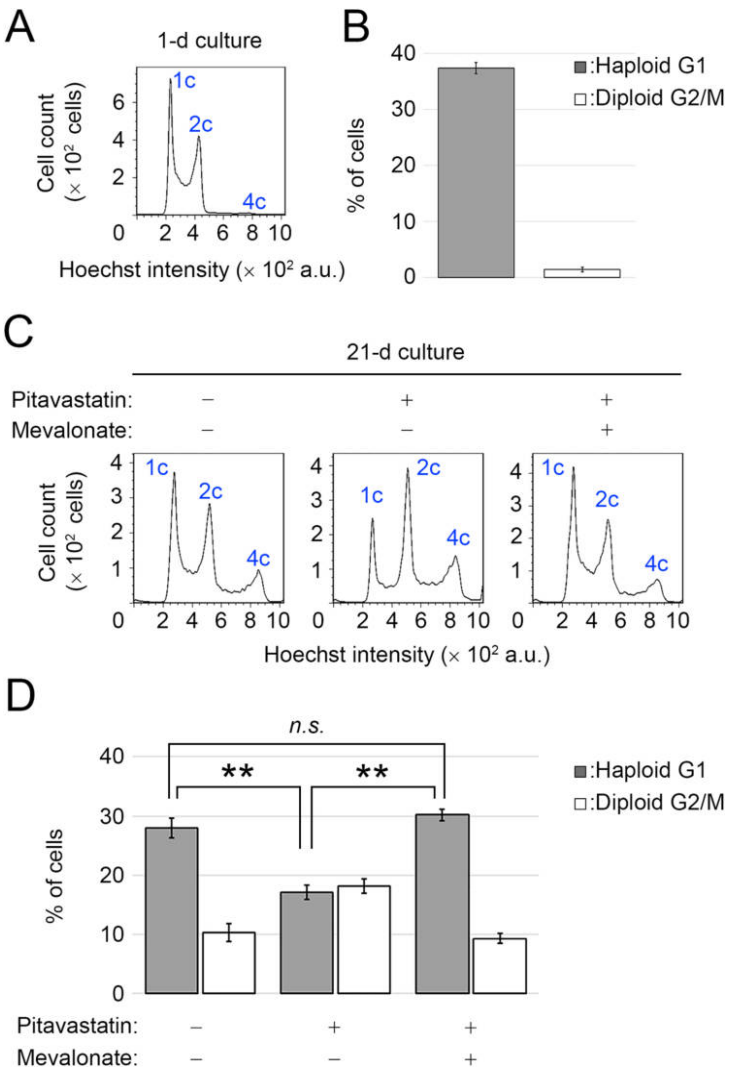

Fig. 1. Destabilization of the haploid state by inhibition of the mevalonate pathway in HAP1 cells. (A, C) Flow cytometric analysis of DNA content in Hoechst-stained cells. Cells were analyzed one day after cell thawing (A), or after 21-d culture in the absence or presence of 0.5 μM pitavastatin with or without 20 μM mevalonate supplementation (C). (B, D) The proportion of the haploid G1 (1 c peak) or diploid G2/M (4 c peak) population in A or C. Means±standard error (SE) of three independent experiments (day 1 in B and day 20 or 21 in D, $^{**}p<0.01$, n.s.: not significant, one-way ANOVA with Tukey post-hoc test).

block cholesterol synthesis. We next visualized intracellular distribution and the content of cholesterol at the single-cell level using a cholesterol-binding fluorescent compound filipin (Fig. 2B) (Drabikowski *et al.*, 1973). In control cells, filipin fluorescence signal distributed throughout the plasma- and intracellular membrane structures, and 0.5 μM pitavastatin modestly reduced the filipin staining intensity (Fig. 2B–D). Next, we addressed whether cholesterol supplementation is sufficient to restore haploid stability in pitavastatin-treated cells. The addition of 10 μM cholesterol to the pitavastatin-treated cell culture fully restored cholesterol level (Fig. 2A–D). However, cholesterol supplementation did not change haploid G1 or diploid G2/M proportion in statin-treated culture (Fig. 2E and F). On the other hand, mevalonate supplementation, which fully restored haploid stability in statin-treated cells (Fig. 1), did not increase the cholesterol level in statin-treated cells (Fig. 2A and D). These data demonstrated that lowered cholesterol level was not the cause of haploid destabilization by pitavastatin.

Next, we tested the effect of perturbation of cholesterol homeostasis by a non-statin cholesterol inhibitor on haploid stability. An amphipathic steroid U18666A perturbs the cholesterol-mediated bioprocesses by inhibiting both synthesis and intracellular transport of cholesterol (Cenedella, 2009). Treatment with 2.5 μM U18666A resulted in the accumulation of cholesterol in intracellular vesicles, a typi-

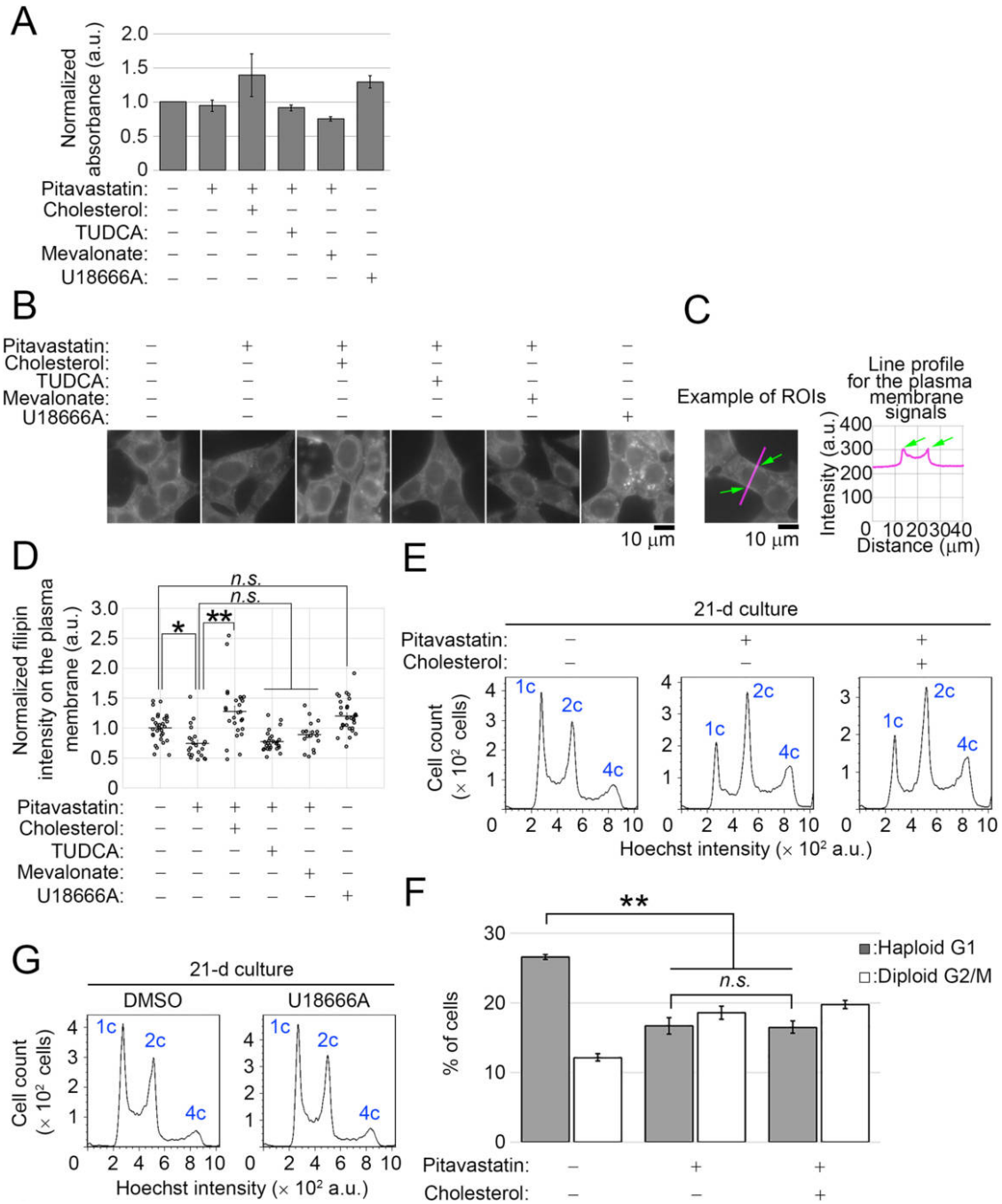

Fig. 2. Either supplementation or perturbation of cholesterol does not affect haploid stability. (A) Measurement of cholesterol extracted from the cells treated with the compounds for 1 d. Means±SE of three independent experiments. There was no significant difference among these samples (one-way ANOVA with Tukey post-hoc test). (B) Fluorescence microscopy of HAP1 cells stained by filipin after treating with the compounds for 1 d. (C, D) Quantification of filipin fluorescence intensity on the plasma membrane in B. The fluorescence signals on the plasma membrane were quantified from line profiles taken across the cells, as shown in C. Means±SE of at least 18 cells from two independent experiments (*p<0.05, **p<0.01, one-way ANOVA with Tukey post-hoc test). (E) DNA content analysis after 21-d culture. Cells were cultured in the absence or presence of 0.5 μM pitavastatin with or without 10 μM cholesterol supplementation. (F) The proportion of the haploid G1 or diploid G2/M population in E. Means±SE of three independent experiments (day 21 in the long-term passages, **p<0.01, one-way ANOVA with Tukey post-hoc test). (G) DNA content analysis after 21-d culture. Cells were cultured in the absence or presence of 2.5 μM U18666A. Representative data from two independent experiments.

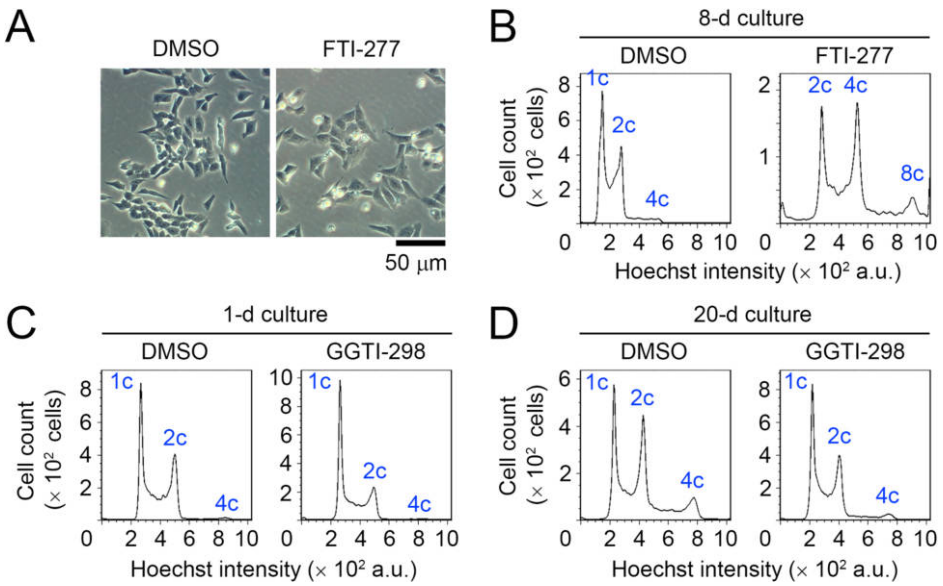

Fig. 3. Inhibition of protein prenylation does not phenocopy the statin-induced haploid destabilization. (A) Transparent microscopy of HAP1 cells treated with or without 20 μM FTI-277 for 2 d. Representative data from two independent experiments. (B–D) DNA content analysis after 8-d (B), 1-d (C), or 20-d culture (D). Cells were cultured with or without 20 μM FTI-277 (B) or 2 μM GGTI-298 (C, D). Representative data from two independent experiments.

cal defect caused by the compound (Fig. 2B) (Reiners *et al.*, 2011; Underwood *et al.*, 1998). HAP1 cell proliferation was not severely affected by 2.5 μM U18666A, allowing us to test its effect on the long-term haploid stability. In the long-term passages, DNA content profile was equivalent between non-treated control and 2.5 μM U18666A-treated culture (Fig. 2G). This result further ruled out the possible involvement of cholesterol homeostatic control in haploid stability in HAP1 cells.

Inhibition of protein prenylation does not phenocopy haploid destabilization by pitavastatin

Among the mevalonate-derived metabolites, farnesyl pyrophosphate and geranylgeranyl pyrophosphate are used for the posttranslational prenylation of small GTPases that play crucial roles in the regulation of cell cycle and proliferation, as well as cell size control (Berndt *et al.*, 2011; Miettinen and Björklund, 2015, 2016). Therefore, we tested the effects of FTI-277 or GGTI-298, which inhibits protein farnesylation or geranylgeranylation, respectively, on the stability of the haploid state in HAP1 cells. Twenty μM FTI-277 treatment caused mitotic progression defects marked by the round-shaped mitotically-arrested cells and abnormally enlarged cells in culture (Fig. 3A). Similar FTI-277-induced mitotic defects have been reported in different cell lines (Holland *et al.*, 2015; Morgan *et al.*, 2001; Moudgil *et al.*, 2015). Consistent with the microscopic observation, FTI-277-treated HAP1 cells were drastically polyploidized within several days with the prominent accumulation of 2, 4, and 8 c peaks in flow cytometric analysis (Fig. 3B). This result suggests that FTI-277 induces whole-genome duplication in HAP1 cells regardless of the ploidy state, which was in contrast to the specific destabilization of haploid state by pitavastatin. The drastic polyploidization and subsequent cell death precluded us from testing the effects of FTI-277 on ploidy dynamics in a more extended period.

On the other hand, treatment with 2 μM GGTI-298 mildly arrested haploid HAP1 cells at the G1 phase within 24 h (Fig. 3C), consistent with a previous report in several cell types (Sun *et al.*, 1999). In prolonged culture for 20 d in the presence of 2 μM GGTI-298, haploid G1 proportion was considerably conserved with smaller diploid G2/M proportion than non-treated control, presumably because of the moderate G1 arrest (Fig. 3D). Therefore, the suppression of either protein farnesylation or geranylgeranylation did not phenocopy the pitavastatin-induced haploid destabilization in our long-term experiment.

Pitavastatin destabilizes the haploid state by evoking ER stress

Since statins potentially induce ER stress by suppressing dolichol phosphates biosynthesis and inhibiting protein N-glycosylation (Chojnacki and Dallner, 1988), we next tested the possibility that pitavastatin destabilizes the haploid state through perturbing ER homeostasis. For this, we tested the effect of pitavastatin on ER stress in HAP1 cells using immunoblot analysis of several components in three signaling branches (i.e., the ATF6, IRE1α, and PERK pathways) of the unfolded protein response (UPR) (Kaufman,

1999; Mori, 2000; Patil and Walter, 2001; Urano *et al.*, 2000). We observed a consistent trend of a modest increase in the active cleaved form of ATF6 (Haze *et al.*, 1999; Yoshida *et al.*, 2000) and IRE1α expression (Tsuru *et al.*, 2016) upon 3-d treatment with 0.5 μM pitavastatin treatment (Fig. 4A and B) in agreement with the previous studies in simvastatin-treated human cultured cells (Ghavami *et al.*, 2014, 2012). The pitavastatin-treated cells also showed a trend of mild mobility shift of PERK in Phos-tag SDS-PAGE gels (Fig. 4C), suggesting a mild increase in PERK phosphorylation (Harding *et al.*, 1999). Consistent with this, pitavastatin treatment also resulted in a significant increase in the expression of ATF4 and CHOP, downstream components of the PERK pathway and multiple UPR branches, respectively (Fig. 4A and B) (Harding *et al.*, 2000; Marciniak *et al.*, 2004; Oyadomari and Mori, 2004). Mevalonate supplementation mostly canceled all of these changes in the UPR markers in pitavastatin-treated cells (Fig. 4A–C), demonstrating that pitavastatin evoked ER stress specifically through blocking mevalonate metabolism.

Finally, we determined whether ER stress induction is the cause of pitavastatin-mediated destabilization of haploid state in HAP1 cells. For this, we tested the effect of an ER stress-reducing chemical chaperone, tauroursodeoxycholic acid (TUDCA) (Ozcan *et al.*, 2006; Yoon *et al.*, 2016) on the haploid stability of HAP1 cells. Co-treatment with TUDCA did not affect ATF4 expression or PERK phosphorylation but substantially canceled the cleavage of ATF6 and the upregulation of IRE1α and CHOP in pitavastatin-treated cells (Fig. 4A–C), presumably reflecting the complex effects of chemical chaperones on different factors in the UPR pathways (Uppala *et al.*, 2017). In contrast, TUDCA did not change the cholesterol level in pitavastatin-treated cells (Fig. 2A–D). In long-term passages, co-treatment of TUDCA significantly preserved haploid G1 proportion in pitavastatin-treated cells (Fig. 4D and E). Therefore, restoration of ER homeostasis by TUDCA substantially improved the stability of the haploid state in the presence of pitavastatin, demonstrating that haploid destabilization by pitavastatin is caused, at least in part, through the induction of ER stress.

Discussion

It is assumed that ploidy differences have pleiotropic effects on intracellular biosynthetic processes and that the altered biosynthesis, in turn, affects cellular physiology at different ploidy states. However, it remains mostly elusive what biosynthetic processes have influences on ploidy-linked cellular phenotypes. In this study, we found that an HMGCR inhibitor pitavastatin destabilized haploid state in human HAP1 cells. This result is consistent with the recent compound screen that identified statins to efficiently promote the expansion of diploidized population over haploids in HAP1 cell culture (Olbrich *et al.*, 2019). As statins are widely used cholesterol-lowering drugs, the possible involvement of cholesterol metabolism in haploid stability has been suggested in the previous study (Olbrich *et al.*, 2019). Interestingly, however, our results in the current study exclude this possibility for three reasons; 1) full restoration of cholesterol level by cholesterol supplementation did not improve haploid stability in statin-treated cells, 2) mevalonate supplementation fully restored haploid stability without restoring cholesterol level in statin-treated cells, and 3) cholesterol perturbation by a non-statin compound did not affect haploid stability.

Our data further specified the perturbation of mevalonate-mediated ER homeostatic control as a critical cause of the statin-induced haploid destabilization. Interestingly, pitavastatin-induced ER stress caused a drastic transition from haploid to diploid state without affecting the stability of diploid state in HAP1 cells. It remains unknown why the effect of pitavastatin on genome stability was specific to the haploid state. However, a possible reason might be a ploidy-dependent difference in tolerance to ER stress. Haploid cells are half in cell volume than diploid cells (Yaguchi *et al.*, 2018), which presumably restricts intracellular spatial capacity for organelle structures. It has been demonstrated that the expansion of the ER lumen serves as a mechanism to increase ER capacity to ameliorate ER stress upon the accumulation of unfolded proteins (Bernales *et al.*, 2006; Schuck *et al.*, 2009; Shaffer *et al.*, 2004; Sriburi *et al.*, 2004). The lower availability of intracellular space may limit stress-responding ER expansion in haploid cells, hence lower tolerance to unfolded protein accumulation.

Mevalonate metabolism is an essential process that supports diverse biosynthetic pathways. Though we specified the preservation of ER homeostasis as a critical process underlying statin-mediate haploid destabilization, we cannot rule out other mevalonate-derived biosynthetic processes in haploid stability. For example, we cannot exclude the possibility that specific targets of protein farnesylation play roles in haploid stability, which might have been masked by the gross polyploidization upon the treatment with FTI-277. Comparative metabolome analysis would be a powerful approach to elucidate other biosynthetic processes playing critical roles in determining the physiology of cells at different ploidy states.

Acknowledgments. We thank the Global Facility Center at Hokkaido Univ for the flow cytometer. This work was supported by JSPS KAKENHI (Grant #19J12210 to K.Ya., 19H03219, 19H05413, and 19KK0181 to R.U), the Hungarian National Research, Development and Innovation Office (NKFIH grant #FK124442) and János Bolyai Research Scholarship from HAS to E.M., the Princess Takamatsu Cancer Research Fund, the Kato Memorial Bioscience Foundation, the Orange Foundation, the Smoking Research Foundation, the Suhara Memorial Foundation, and the Nakatani Foundation to R.U., and Bilateral Joint Research Projects of JSPS and HAS (JPJSBP120193801) to G.B., E.M., and R.U.

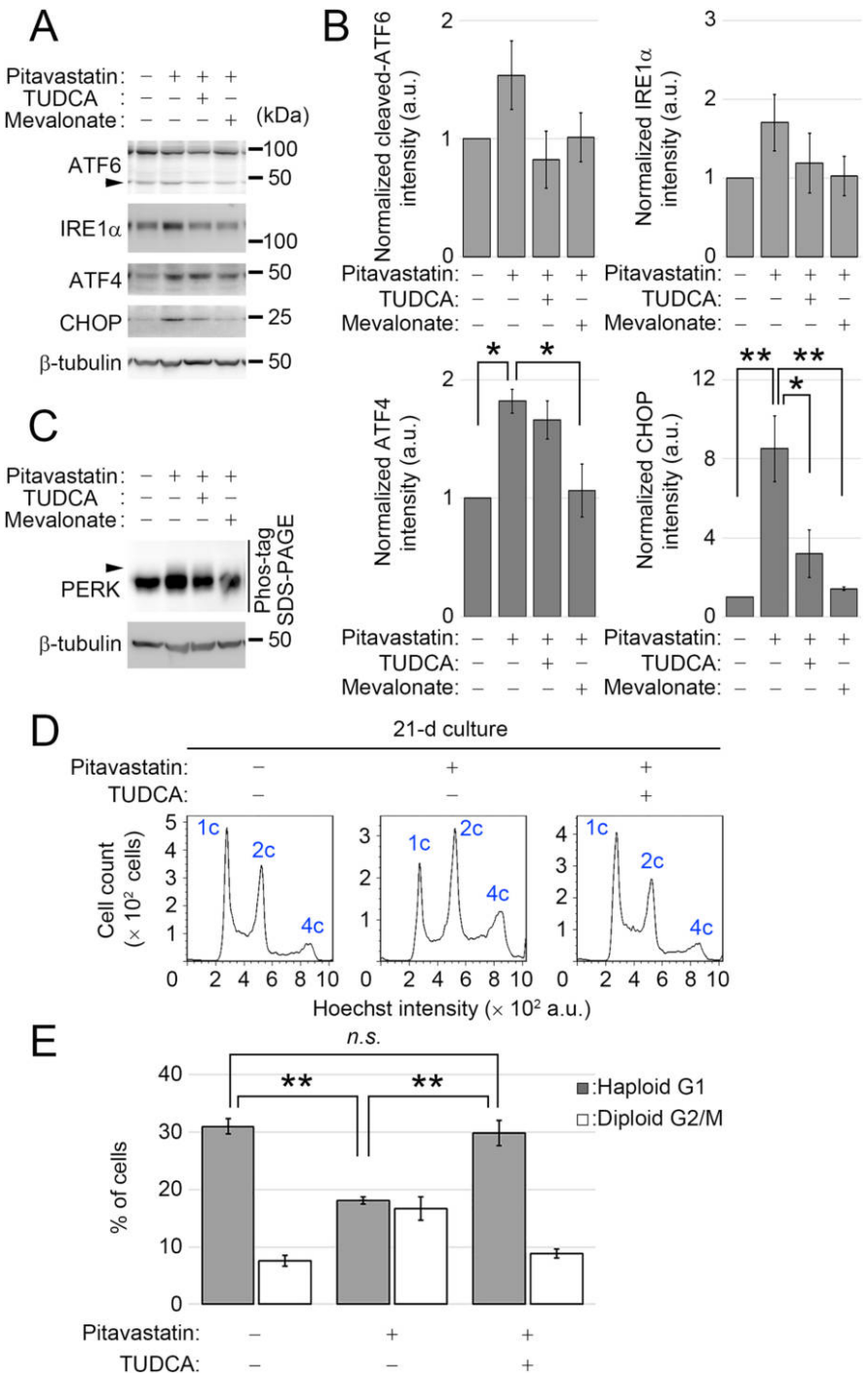

Fig. 4. Amelioration of ER stress improves haploid stability in pitavastatin-treated cells. (A, C) Immunoblotting of UPR components in HAP1 cells treated with the compounds for 3 d. Cleaved ATF6 is indicated by the arrowhead. Immunoblotting of PERK was conducted using Phos-tag SDS-PAGE to detect phosphorylation-dependent band shift in C (the arrowhead). β-tubulin was detected as a loading control. Representative results from three independent experiments are shown. (B) Quantification of relative expression of UPR regulators/components in A. Means±SE of three independent experiments (*p<0.05, **p<0.01, one-way ANOVA with Tukey post-hoc test). (D) DNA content analysis after 21-d culture. Cells were cultured in the absence or presence of 0.5 μM pitavastatin with or without 2.5 mM TUDCA. (E) The proportion of the haploid G1 or diploid G2/M population in D. Means±SE of three independent experiments (day 21 in the long-term passages, **p<0.01, one-way ANOVA with Tukey post-hoc test).

Author Contributions

Conceptualization, K.Ya., and R.U.; Methodology, K.Ya., K. S., D.M., K.Yu., Y.I., G.B., E.M., and R.U.; Investigation, K.Ya, K.S. K.Yo., E.M., and R.U.; Formal Analysis, K.Ya., K.S., and R.U.; Resources, G.B., E.M., and R.U.; Writing—Original Draft, K.Ya., and R.U.; Writing—Review & Editing, K.Ya., D.M., K.Yu., E.M., and R.U.; Funding Acquisition, K.Ya., G.B., E.M., and R.U.

References

Adhyaru, B.B. and Jacobson, T.A. 2018. Safety and efficacy of statin therapy. *Nat. Rev. Cardiol.*, **15**: 757–769.

Bernales, S., McDonald, K.L., and Walter, P. 2006. Autophagy counterbalances endoplasmic reticulum expansion during the unfolded protein response. *PLoS Biol.*, **4**: e423.

Berndt, N., Hamilton, A.D., and Sebti, S.M. 2011. Targeting protein prenylation for cancer therapy. *Nat. Rev. Cancer*, **11**: 775–791.

Buhaescu, I. and Izzedine, H. 2007. Mevalonate pathway: A review of clinical and therapeutical implications. *Clin. Biochem.*, **40**: 575–584.

Carette, J.E., Raaben, M., Wong, A.C., Herbert, A.S., Obernosterer, G., Mulherkar, N., Kuehne, A.I., Kranzusch, P.J., Griffin, A.M., Ruthel, G., Dal Cin, P., Dye, J.M., Whelan, S.P., Chandran, K., and Brummelkamp, T.R. 2011. Ebola virus entry requires the cholesterol transporter Niemann-Pick C1. *Nature*, **477**: 340–343.

Carlberg, M., Dricu, A., Blegen, H., Wang, M., Hjertman, M., Zickert, P., Höög, A., and Larsson, O. 1996. Mevalonic Acid Is Limiting for N-Linked Glycosylation and Translocation of the Insulin-like Growth Factor-1 Receptor to the Cell Surface: EVIDENCE FOR A NEW LINK BETWEEN 3-HYDROXY-3-METHYLGLUTARYL-COENZYME A REDUCTASE AND CELL GROWTH. *J. Biol. Chem.*, **271**: 17453–17462.

Cenedella, R.J. 2009. Cholesterol synthesis inhibitor U18666A and the role of sterol metabolism and trafficking in numerous pathophysiological processes. *Lipids*, **44**: 477–487.

Chojnacki, T. and Dallner, G. 1988. The biological role of dolichol. *Biochem. J.*, **251**: 1–9.

Doucey, M.A., Hess, D., Cacan, R., and Hofsteenge, J. 1998. Protein C-mannosylation is enzyme-catalysed and uses dolichyl-phosphate-mannose as a precursor. *Mol. Biol. Cell*, **9**: 291–300.

Drabikowski, W., Lagwińska, E., and Sarzala, M.G. 1973. Filipin as a fluorescent probe for the location of cholesterol in the membranes of fragmented sarcoplasmic reticulum. *Biochim. Biophys. Acta*, **291**: 61–70.

Ghavami, S., Yeganeh, B., Stelmack, G.L., Kashani, H.H., Sharma, P., Cunnington, R., Rattan, S., Bathe, K., Klonisch, T., Dixon, I.M., Freed, D.H., and Halayko, A.J. 2012. Apoptosis, autophagy and ER stress in mevalonate cascade inhibition-induced cell death of human atrial fibroblasts. *Cell Death Dis.*, **3**: e330.

Ghavami, S., Sharma, P., Yeganeh, B., Ojo, O.O., Jha, A., Mutawe, M.M., Kashani, H.H., Los, M.J., Klonisch, T., Unruh, H., and Halayko, A.J. 2014. Airway mesenchymal cell death by mevalonate cascade inhibition: integration of autophagy, unfolded protein response and apoptosis focusing on Bcl2 family proteins. *Biochim. Biophys. Acta*, **1843**: 1259–1271.

Harding, H.P., Zhang, Y., and Ron, D. 1999. Protein translation and folding are coupled by an endoplasmic-reticulum-resident kinase. *Nature*, **397**: 271–274.

Harding, H.P., Novoa, I., Zhang, Y., Zeng, H., Wek, R., Schapira, M., and Ron, D. 2000. Regulated translation initiation controls stress-induced gene expression in mammalian cells. *Mol. Cell*, **6**: 1099–1108.

Haze, K., Yoshida, H., Yanagi, H., Yura, T., and Mori, K. 1999. Mammalian transcription factor ATF6 is synthesized as a transmembrane protein and activated by proteolysis in response to endoplasmic reticulum stress. *Mol. Biol. Cell*, **10**: 3787–3799.

Holland, A.J., Reis, R.M., Niessen, S., Pereira, C., Andres, D.A., Spielmann, H.P., Cleveland, D.W., Desai, A., and Gassmann, R. 2015. Preventing farnesylation of the dynein adaptor Spindly contributes to the mitotic defects caused by farnesyltransferase inhibitors. *Mol. Biol. Cell*, **26**: 1845–1856.

Kaufman, R.J. 1999. Stress signaling from the lumen of the endoplasmic reticulum: coordination of gene transcriptional and translational controls. *Genes Dev.*, **13**: 1211–1233.

Leung, K.F., Baron, R., and Seabra, M.C. 2006. Thematic review series: lipid posttranslational modifications. geranylgeranylation of Rab GTPases. *J. Lipid Res.*, **47**: 467–475.

Marciniak, S.J., Yun, C.Y., Oyadomari, S., Novoa, I., Zhang, Y., Jungreis, R., Nagata, K., Harding, H.P., and Ron, D. 2004. CHOP induces death by promoting protein synthesis and oxidation in the stressed endoplasmic reticulum. *Genes Dev.*, **18**: 3066–3077.

Miettinen, Teemu P., Pessa, Heli K.J., Caldez, Matias J., Fuhrer, T., Diril, M.K., Sauer, U., Kaldis, P., and Björklund, M. 2014. Identification of Transcriptional and Metabolic Programs Related to Mammalian Cell Size. *Curr. Biol.*, **24**: 598–608.

Miettinen, T.P. and Björklund, M. 2015. Mevalonate Pathway Regulates Cell Size Homeostasis and Proteostasis through Autophagy. *Cell Reports*, **13**: 2610–2620.

Miettinen, T.P. and Björklund, M. 2016. Cellular Allometry of Mitochondrial Functionality Establishes the Optimal Cell Size. *Dev. Cell*, **39**: 370–382.

Morgan, M.A., Dolp, O., and Reuter, C.W.M. 2001. Cell-cycle–dependent activation of mitogen-activated protein kinase kinase (MEK-1/2) in myeloid leukemia cell lines and induction of growth inhibition and apoptosis by inhibitors of RAS signaling. *Blood*, **97**: 1823–1834.

Mori, K. 2000. Tripartite management of unfolded proteins in the endoplasmic reticulum. *Cell*, **101**: 451–454.

Moudgil, D.K., Westcott, N., Famulski, J.K., Patel, K., Macdonald, D., Hang, H., and Chan, G.K. 2015. A novel role of farnesylation in targeting a mitotic checkpoint protein, human Spindly, to kinetochores. *J. Cell Biol.*, **208**: 881–896.

Mullen, P.J., Yu, R., Longo, J., Archer, M.C., and Penn, L.Z. 2016. The interplay between cell signalling and the mevalonate pathway in cancer. *Nat. Rev. Cancer*, **16**: 718–731.

Olbrich, T., Vega-Sendino, M., Murga, M., de Carcer, G., Malumbres, M., Ortega, S., Ruiz, S., and Fernandez-Capetillo, O. 2019. A Chemical Screen Identifies Compounds Capable of Selecting for Haploidy in Mammalian Cells. *Cell Reports*, **28**: 597–604.e594.

Oyadomari, S. and Mori, M. 2004. Roles of CHOP/GADD153 in endoplasmic reticulum stress. *Cell Death Differ.*, **11**: 381–389.

Ozcan, U., Yilmaz, E., Ozcan, L., Furuhashi, M., Vaillancourt, E., Smith, R.O., Görgün, C.Z., and Hotamisligil, G.S. 2006. Chemical chaperones reduce ER stress and restore glucose homeostasis in a mouse model of type 2 diabetes. *Science*, **313**: 1137–1140.

Patil, C. and Walter, P. 2001. Intracellular signaling from the endoplasmic reticulum to the nucleus: the unfolded protein response in yeast and mammals. *Curr. Opin. Cell Biol.*, **13**: 349–355.

Reiners, J.J., Jr., Kleinman, M., Kessel, D., Mathieu, P.A., and Caruso, J.A. 2011. Nonesterified cholesterol content of lysosomes modulates susceptibility to oxidant-induced permeabilization. *Free Radic. Biol. Med.*, **50**: 281–294.

Sagi, I. and Benvenisty, N. 2017. Haploidy in Humans: An Evolutionary and Developmental Perspective. *Dev. Cell*, **41**: 581–589.

Schuck, S., Prinz, W.A., Thorn, K.S., Voss, C., and Walter, P. 2009. Membrane expansion alleviates endoplasmic reticulum stress independently of the unfolded protein response. *J. Cell Biol.*, **187**: 525–536.

Shaffer, A.L., Shapiro-Shelef, M., Iwakoshi, N.N., Lee, A.-H., Qian, S.-B., Zhao, H., Yu, X., Yang, L., Tan, B.K., Rosenwald, A., Hurt, E.M., Petroulakis, E., Sonenberg, N., Yewdell, J.W., Calame, K., Glimcher, L.H., and Staudt, L.M. 2004. XBP1, Downstream of Blimp-1, Expands the Secretory Apparatus and Other Organelles, and Increases Protein Synthesis in Plasma Cell Differentiation. *Immunity*, **21**: 81–93.

Sriburi, R., Jackowski, S., Mori, K., and Brewer, J.W. 2004. XBP1: a link between the unfolded protein response, lipid biosynthesis, and biogenesis of the endoplasmic reticulum. *J. Cell Biol.*, **167**: 35–41.

Sun, J., Qian, Y., Chen, Z., Marfurt, J., Hamilton, A.D., and Sebti, S.M. 1999. The geranylgeranyltransferase I inhibitor GGTI-298 induces hypophosphorylation of retinoblastoma and partner switching of cyclin-dependent kinase inhibitors. A potential mechanism for GGTI-298 antitumor activity. *J. Biol. Chem.*, **274**: 6930–6934.

Tsuru, A., Imai, Y., Saito, M., and Kohno, K. 2016. Novel mechanism of enhancing IRE1α-XBP1 signalling via the PERK-ATF4 pathway. *Sci. Rep.*, **6**: 24217.

Underwood, K.W., Jacobs, N.L., Howley, A., and Liscum, L. 1998. Evidence for a cholesterol transport pathway from lysosomes to endoplasmic reticulum that is independent of the plasma membrane. *J. Biol. Chem.*, **273**: 4266–4274.

Uppala, J.K., Gani, A.R., and Ramaiah, K.V.A. 2017. Chemical chaperone, TUDCA unlike PBA, mitigates protein aggregation efficiently and resists ER and non-ER stress induced HepG2 cell death. *Sci. Rep.*, **7**: 3831.

Urano, F., Bertolotti, A., and Ron, D. 2000. IRE1 and efferent signaling from the endoplasmic reticulum. *J. Cell Sci.*, **113 Pt 21**: 3697–3702.

Wang, M. and Casey, P.J. 2016. Protein prenylation: unique fats make their mark on biology. *Nat. Rev. Mol. Cell Biol.*, **17**: 110–122.

Wutz, A. 2014. Haploid animal cells. *Development*, **141**: 1423–1426.

Yaguchi, K., Yamamoto, T., Matsui, R., Tsukada, Y., Shibanuma, A., Kamimura, K., Koda, T., and Uehara, R. 2018. Uncoordinated centrosome cycle underlies the instability of non-diploid somatic cells in mammals. *J. Cell Biol.*, **217**: 2463–2483.

Yang, L., Xue, Z., He, Y., Sun, S., Chen, H., and Qi, L. 2010. A Phos-tag-based approach reveals the extent of physiological endoplasmic reticulum stress. *PLoS One*, **5**: e11621–e11621.

Yoon, Y.M., Lee, J.H., Yun, S.P., Han, Y.S., Yun, C.W., Lee, H.J., Noh, H., Lee, S.J., Han, H.J., and Lee, S.H. 2016. Tauroursodeoxycholic acid reduces ER stress by regulating of Akt-dependent cellular prion protein. *Sci. Rep.*, **6**: 39838.

Yoshida, H., Okada, T., Haze, K., Yanagi, H., Yura, T., Negishi, M., and Mori, K. 2000. ATF6 activated by proteolysis binds in the presence of NF-Y (CBF) directly to the cis-acting element responsible for the mammalian unfolded protein response. *Mol. Cell. Biol.*, **20**: 6755–6767.

(Received for publication, November 5, 2020, accepted, December 12, 2020 and published online, December 22, 2020)